GROWTH, STRUCTURE, AND PROPERTIES OF SELECTED TWO-DIMENSIONAL MATERIALS FROM DENSITY FUNCTIONAL THEORY INVESTIGATIONS

by

Abdulfattah Ab. Abdulslam

A thesis submitted to the Faculty and the Board of Trustees of the Colorado School of Mines in partial fulfillment of the requirements for the degree of Doctor of Philosophy (Mechanical Engineering).

Golden, Colorado

Date _____

Signed: _____
Abdulfattah Ab. Abdulslam

Signed: _____
Dr. Cristian V. Ciobanu
Thesis Advisor

Golden, Colorado

Date _____

Signed: _____
Dr. John Berger
Professor and Head
Department of Mechanical Engineering

ABSTRACT

After an initial decade of excitement brought by the successful isolation of graphene and discovery of its exotic properties, the attention of the scientific community turned to other 2-D materials that could provide diversity in terms of useful properties without relying on increasingly complex engineering of graphene-based 2-D layers or nanostructures. In this arena, a range of materials have been either experimentally synthesized or theoretically hypothesized, the most important currently being hexagonal boron nitride (hBN), molybdenum disulphide, silicene, phosphorene, and maxenes –among others. Some of the key issues of current importance in 2-D research are synthesis of specific 2-D materials, effects of the substrates on the morphology and properties of 2-D layers, and control of the properties through synthesizing different 2-D polymorphs: this thesis addresses particular problems falling under these three distinct themes. Specifically, parts of the thesis focus on phosphorene and hBN growth, morphology of hBN on palladium, and range of mechanical and electronic properties obtained from different 2-D silica polymorphs. For the phosphorene growth, the thesis advances the idea that the phosphorene can in fact grow by chemical vapor deposition on metals, provided that they are covered with hBN or graphene so as to prevent the formation of metal phosphides. For the multilayer hBN growth, results in this thesis support a recently proposed notion that adsorption of one precursor activates the adsorption and dehydrogenation of ammonia (the second precursor), which leads to the formation of second hBN layer and beyond when the metal substrate is already passivated by the firt hBN layer. Another chapter of this thesis shows a phenomenological model and density functional theory calculations explaining experimentally-observed novel morphologies of hBN on palladium. Lastly, this thesis shows examples of how polymorphs of 2-D silica can lead to diverse electronic properties ranging from insulating to metallic.

TABLE OF CONTENTS

LIST OF FIGURES

LIST OF TABLES

LIST OF ABBREVIATIONS

Density functional theory	DFT
Scanning tunneling microscopy	STM
Two-dimensional	2-D
van der Waals	vdW

ACKNOWLEDGMENTS

It is my great pleasure to express my gratitude and indebtedness to my advisor Prof. Cristian Ciobanu for the continuous support of my Ph.D. study and research, for his patience, motivation, enthusiasm, and immense knowledge. His guidance helped me in my research work. I would also like to thank my thesis committee members, Prof. John Berger, Prof. Anthony Petrella, and Prof. Dinesh Mehta, for their time and service on the committee. I also thank Prof. Graham Mustoe, previously a member of the thesis committee, and wish him a wonderful retirement. Big thanks to Dr. Branden Kappes and Dr. Badri Narayanan for taking time to share with me some of the skills necessary for this work. I also thank my friends, my brothers and sisters for their support, lastly I would like to thank my parents for their limitless love.

THIS THESIS IS DEDICATED TO MY BELOVED PARENTS.

CHAPTER 1

INTRODUCTION

Two-dimensional (2-D) materials have a thickness of a few Angstroms or less. They show unusual and novel properties, due to the rich and novel physical phenomena that occur when electronic and thermal conduction are limited to a plane. More that eighty years ago, Landau and Peierls showed theoretically that perfect 2D crystals could not exist [1–3]. Because of this rather general and fundamental result, numerous investigations of 2-D materials have been delayed until recently. In 2004, flakes of graphene (single layer of carbon atoms that makes graphite) have been successfully isolated by exfoliation from graphite. The key in reconciling Landau's theory with the recent isolation of graphene is understanding that the excitations required to bend a graphene layer out of its plane are infinitesimally small –hence, the graphene crystal is not strictly in 2-D but contains measurable ripples at any finite temperature. After this realization, 2-D materials became some of the most intensively investigated category of materials in recent years [4–7].

1.1 Brief overview

As mentioned, the starting point was the isolation of single-atomic layer of graphite, freely suspended in vacuum or air [8]. Graphene has several outstanding properties, such as very high thermal conductivity (3000 $W\ m^{-1}\ K^{-1}$) and a very high mechanical stiffness (1060 GPa) [9–12]. Furthermore, the monolayer of graphene showed a remarkable electronic transport properties [11, 13, 14]. From the point of view of electronic conduction, graphene is termed a semimetal with a zero bandgap. This is due to the contact of the valence and conduction band at a single point, the same point through which the Fermi level pases. Due to this small contact of the conduction and valence bands, the electronic structure and behavior of graphene displays high sensitivity to external electric fields, deformation, doping, and adsorbates, making the graphene an interesting candidate material for producing

sensors [15]. Furthermore, a very high thermal conductivity of a suspended single-layer graphene has been calculated, which makes graphene a candidate for thermal management of electronic devices [16]. These properties have not only theoretically and numerically have been predicted, but also experimentally confirmed [14, 17], thus starting a new field –that of 2-D materials.

Materials scientists and organic chemists are designing new synthetic methods to synthesize high-quality single layers, while engineers are fabricating innovative devices to utilize graphenes extraordinary properties. Due to high, dissipationless conduction, graphene has been hypothesized initialy as promising material for nanoelectronic applications. However, any electronic application would require graphene to be isolated from, e.g., metallic substrate onto which it grows. Furthemore, to use graphene as an active element in devices requires the presence of a bandgap –otherwise graphene could only be used lead connecting active elements and not as active element itself. Even if graphene is engineered as a smallbandgap semiconductor, it would have to be grown or transferred on an insulating substrate because if used on the metal substrate on which it has grown, then that metal substrate would significantly alter its properties.

Because of the need for engineered band gap and insulating substrate, soon after the inital excitement of synthesizing graphene and discovering its unusual properties [1], scientific efforts have turned towards other materials that could be used by themselves in various applications, or in conjunctions with graphene layers. For example, instead of trying to engineer the electronic properties of graphene, finding another 2-D material which already has a desired bandgap appears as good alternative especially if some of these materials are easier to obtain or to synthesize. For example, layered materials known as transition metal dichalcogenides (e.g., MoS_2) already have a semiconducting bandgap of 1.8 eV (Section 1.2 below). Several currently pursued 2-D materials are briefly described below.

1.1.1 Hexagonal boron nitride (hBN)

Growth of a large-area, single or bilayer graphene with a low cost, limited only by the size of the champer, and via ambient pressure CVD on Ni films had been reported [18]. The growth of graphene monolayers on metals substrates such as Ru, [19, 20],Pt [21, 22],Ni [23, 24] and Ir [25, 26] is well known. Hydrocarbon methane CH_4 is more stable than acetylene (C_2H_2) at high temperature (e.g. 800-1000°C) as precursors for graphene growth [27]. More than one layer of graphene can form on Ni substrate, while usually only one layer forms on Cu substrates [28]. Using similar substrates, hBN can also be grown using CVD on the entire Ni surface may be limited by the size of the Ni single crystal grains [29]. At low pressure and using CVD on the Cu substrate, and using Ammonia borane as BN precursor one can synthesize thin layers of hBN [30]. Boron nitride films were deposited on (001) silicon substrates using plasma CVD and using a $HeN_2BF_3H_2$ gas system as BN precursor [31].

Large area of h-BN films consisting of two to five atomic layers have been synthesised using CVD, using Cu substrates and ammonia borane precursors [32]. Hexagonal Boron nitride (BN) is structurally analog to graphene; one of the two C atoms in the primitive cell is replaced by B, and the other by N. An experimental study showed it is possible to segregate one or more layers of hexagonal h-BN [33]. The elastic modulus of BN is in the range of 200 - 500 N/m. hBN has high a optical band gap of 5.5 eV [32].

A high degree of control over the electronic properties of thin films is the key piece of know-how that allows the production of modern integrated circuitry [34]. By using the technique heterostructures of graphene and h-BN, we should be able to control the electrical properties, which could lead to novel thought-provoking electronic applications. Graphene and hBN have similar crystal structures with a nearly the same lattice constant. Nevertheless, pristine graphene is a zero-bandgap semimetal with curiously high carrier mobility at room temperature[1, 35, 36]. Research on combinations of 2-D layers can produce devices that have potential for high-frequency operation and large-scale integration [37].

1.1.2 Molybdenum disulfide (MoS_2)

A single layer of Molybdenum disulfide MoS_2 has been inspected by optical spectroscopy and found to have an intrinsic bandgap of 1.8 eV [38]. It has been mechanically exfoliated forming a nano-sheet, and used for making novel phototransistors with better photoresponsivity as compared with the graphene-based devices [39]. Large-area single crystalline monolayer sheets of MoS_2 have been manufactured on SiO_2, electrical [40]. The Youngs modulus for MoS_2 of a few (5 to 25) layers thick, freely suspended, has been measured to be 0.33 TPa, very high comparing to graphene oxide [41]. The electronic properties of MoS_2-graphene bilayer heterostructures have also been inspected and depend on the interlayer orientation of graphene with respect to MoS_2 [42]. The monolayer molybdenum disulfide (MoS_2) can be grown in a scalable manner, with the ability to control the atomic layer thickness on SiO_2 substrates [43]. Large-area MoS_2 atomic layers had been synthesized on SiO2 substrates by chemical vapor deposition using MoO_3 as a precursor. [40]. The MoS_2 grows on few-layer h-BN films by using CVD,confirming that there is strong interaction between the MoS_2 and underlying h-BN [44]. A large area with layer controlled (monolayer, bilayer, and trilayer) of MoS_2 films on SiO_2/Si substrates,using low pressure CVD can obtained [45].

1.1.3 Silicene (Si)

2-D silicon has been obtained by the synthesis of epitaxial silicene sheets on a silver (111) substrate [46, 47]. The elastic stiffness of silicene for the zigzag and armchair directions have been calculated from molecular dynamics simulations, and their values were 50.44 N/m and 62.31 N/m, respectively [48]. The electronic properties of silicene have been examined using the first principles simulations, and it was found that silicene is zero bandgap semimetal [49]. After the analysis of the chemical, magnetic and electronic properties of silicene were seen to display some of the same trends as graphene, which may allow silicen to become a viable candidate for 2-D materials-based electronic devices [50]. It has been reported that under increasing perpendicular electric field, the monolayer of silicene can drastically change its

electronic properties [51].

1.1.4 Germanene (Ge)

Germanene has been obtained by growth an atom-thin germanium layer on the gold (111) surface [52]. Also another growth of Germanene has been done on platinum (111) [53]. It has been reported that the germanane had much smaller in-plane stiffness than both graphene and boron nitride nanoribbons, which make germanene easier to stretch [54]. Its electronic properties have been inspected: germanene is a direct-gap material, with average gap of about 3.2 eV, so it is also material that has tremendous potential for novel optoelectronic applications [55, 56].

1.1.5 Phosphorene (P)

Phosphorene is a single or few layers of black phosphorus and is obtained by mechanical exfoliation only [57, 58]. Experimentally, the Young's modulus of few-layer black phosphorus have been have measured for both zigzag and armchair directions and found 58.6 ± 11.7 and 27.2 ± 4.1 GPa, respectively [59]. First-principles calculations show a significant band gap of 1-4 layers of phosphorene, with a direct band gap [60]. The effect number of layers on the band gap has been calculated, and observed that the band gap changes dramatically with the number of layers [61].

1.2 Key issues in 2-D materials and role of theoretical investigations

Synthesis and its mechanism. There are several key issues that generally appear when pursuing the investigation of 2-D materials beyond graphene. The first key issue is the synthesis of any new 2-D material, which would require either small changes to older methods, or new methods of growth altogether. In the examples given above, silicene as a single layer of Si atoms is highly reactive and cannot exist by itself: the metallic substrate is not only necessary for synthesis of Si from a precursor gas (usually silane) but also imparts stability to silicene: as such, silicene cannot be removed from the metallic substrate (with the purpose

of transferring it elsewhere) because it would be destroyed in the process. In other cases, for example the case of hBN, multiple layers can be grown on a metallic substrate and some of them can be removed and transferred on inert substrates. While sometimes synthesis techniques can be " borrowed" from other 2D materials, most of the times different 2D materials require different chemistry and/or thermodynamics to enable their growth. For example, it is rather straightforward to grow graphene on copper, but virtually impossible to grow phosphorene on copper. Chapter 2 and Chapter 3 deal with synthesis issues for different 2-D materials, phosphorene and multilayer hBN, respectively. A more subtle but important aspect of synthesis is also understanding how to control what particular polymorph would grow: for graphene and hBN, this is a non-issue since there is only one crystal structure in each case. However, for phosphorene or silica –both of which displaying several polymorphs, it is important to grow the polymorph with desired properties.

Effect of the substrate of structure and properties 2-D materials for high quality are usually grown on substrates, which are often metallic so as to enable their formation via catalyzed processes from precursor gases. Once grown, the 2-D materials certainly interact with the substrates, sometimes strongly (chemically) sometimes weakly (van der Waals, vdW) [62, 63]. The interaction with the substrate can give rise to significant large scale periodic patterns called moiré structures, can affect (usually deleteriously) the electronic properties of the 2D material grown on them (hBN, graphene), but can also impart chemical and mechanical stability to an otherwise unstable layer (silicene, germanene, 2-D silica) . In all cases, there is significant interest surrounding the effect of the substrate on the structure, properties, and stability of the 2-D materials. Representative of the issue of how substrates can affect structure and properties, Chapter 4 deals with the effect of the substrate on the morphology and electronic properties of an hBN monolayer.

Control of properties via synthesis of different polymorphs Graphene and boron nitride as 2-D materials have one single structure, the honeycomb lattice. However, it is conceivable that other materials (such as silica, phosphorene) can form in several different polymorphs

due to their richer phase diagram. Even though these phase diagrams are constructed and tabulated for 3-D phases, the presence of a multitude of 3-D phases often suggests that there could be multiple polymorphs for the 2-D phases as well. An important approach under the theme of controlling the properties via different polymorph structures (or designing the 2D material to have desired properties) is a high-throughput computation framework in which a large number of structures is created, optimized according to some protocol (usually global optimization methods), and then subject to computation of various properties (electronic, mechanical, piezoelectric, dielectric, magnetic, etc). Similar protocols have been pursued successfully for 3-D materials, but seem in infancy for 2-D materials. More commonly, heuristic structures are proposed and investigated with respect to desired properties, and we will show an example of this heuristic approach in Chapter 5.

The work in this thesis contains portions that fall under each of key issues mentioned above. In the very dynamic field of 2-D materials, the work here cannot be, and does not aim to be comprehensive, but rather addresses a few outstanding issues.

1.3 Research work in this thesis and specific contributions of the candidate

As mentioned, Chapter 2 and Chapter 3 deal with two current synthesis issues, Chapter 4 addresses one example of the effect of the metallic substrate on the structure and properties of the 2D hBN grown on it, and Chapter 5 shows examples of how different polymorphs of the same 2-D material determine vastly different properties.

1.3.1 Ch. 2: Necessary conditions for phosphorene growth on graphene- or boron-nitride-covered metals

In this chapter, it is hypothesized that phosphorene can be grown oh hBN- or graphene-covered metallic substrates. It is shown that these substrate can still bind the main molecular precursors that can lead to growth of phosphorene. Abdulfattah Abdulslam (AA) is the sole computational student or postdoc on this project. As such, he performed all the adsorption and reaction barrier calculations on the project. Chapter 2 is expected to become a theory-

lead publication soon, with the other authors contributing experimental insight or theoretical guidance.

1.3.2 Ch. 3: Growth of a bilayer hexagonal Boron-Nitride on Copper substrate

This chapter uses literature insight to initiate investigations of the hypothesis that B-containig precursors can adsorb first on the substrate, pyrolize, and activate the adsorption and dehydrogenation of the second precursor (ammonia). It is expected that this work could lead to a theory-only publication, provided that sufficient insight can be gained in regard to interaction of the different radicals on the substrate. AA is the sole computational student on this project, performing the adsorption calculations for precursors and their radicals, and comparing with recent literature.

1.3.3 Ch. 4: Corrugation of hexagonal Boron-Nitride monolayer on Palladium

This work was motivated by recent experimental work from collaborators at University of California Los Angeles dealing with scanning tunneling microscopy of hBN/Pd. The chapter shows a theoretical model for explaining the possibility well-oriented hBN layers on palladium can have both flat and corrugated structures due to the propensity of the layers to bend. AA was the only computational student or postdoc on the project, which resulted in an experimentally-led manuscript submitted to Nano Letters.

1.3.4 Ch. 5: Mechanical and electronic properties of 2D silica configurations

This chapter investigates several 2-D silica configurations and determined their mechanical and electronic properties. It is an example of how much the polymorphs can affect the electronic properties, going in this case from metallic to insulating behaviour depending on the 2-D polymorph. AA is the sole computational student on this theory-only project, which is expected to lead to a publication within the calendar year.

CHAPTER 2

NECESSARY CONDITIONS FOR PHOSPHORENE GROWTH ON METALLIC SUBSTRATES

Synopsis: Phosphorene has emerged as a highly sought-after new 2-D material, but its synthesis via chemical vapor deposition (CVD) on metals remains a major challenge. Although successful for the growth of graphene of high quality over large areas, the CVD synthesis route fails because all metals have a tendency to form stable phosphides, preventing the growth of phosphorene from gaseous precursors deposited on metal substrates. In this chapter, the possibility of using metal surfaces (covered with graphene or boron nitride) as substrates is explored: the passivation with boron nitride or graphene monolayers is proposed as a way to prevent the formation of phosphides. With these substrates, the phosphorene growth from three common precursors, P_2, P_4, and PH_3, is analyzed. Attachment of the precursors to the substrate is the first condition for a monolayer to form. Using DFT calculations, we find that these precursors and the radicals derived from them still attach to Cu(111) and Ni(111) when passivated with graphene or hBN, thereby suggesting potentially viable new substrates for growing phosphorene via CVD. Another condition is that the precursors decompose into radicals, which we show for the case of PH_3. Therefore, our computational results provide evidence that two necessary not sufficient- conditions for growth of phosphorene can be met, which should provide useful guidance for future experimental endeavors.

2.1 Introduction

Phosphorene –single or few layers of the black phosphorus (BP) allotrope, is an intriguing 2-D material exhibiting numerous exciting properties, similar to graphene [64, 65]. Unlike graphene, however, phosphorene is a semiconductor with a direct bandgap Figure 2.1 that varies strongly with the number of layers from 0.3 eV to about 2 eV [66, 67].

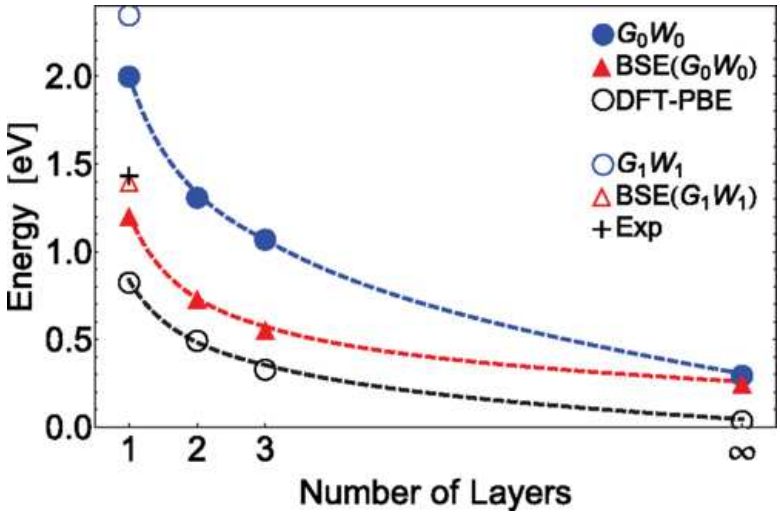

Figure 2.1: Dependence of the electronic bandgap on the number of layers in phosphorene. Reproduced from Ref. [68], with permission of the American Physical Society.

This range covers bandgap values between graphene (semimetal) and transition metal dichalcogenides (TMDs, bandgaps of 1.8 eV). The bandgap and its layer dependence,[68] along with the high carrier mobility large on/off ratio at room temperature, make phosphorene well suited for electronic, optoelectronic, and photovoltaic applications [69–72]. In order to access these and many other technological possibilities that could be open by using phosphorene in devices, it is necessary to synthesize high quality, large area phosphorene sheets, ideally with a controlled number of layers. Phosphorene sheets were first obtained by mechanical exfoliation of BP [58, 73] similar to graphene, solution methods for BP exfoliation have also been developed [74, 75].

Bottom-up approaches (e.g. chemical vapor deposition, CVD) while immensely successful for graphene on many metallic substrates [76–80], are only now emerging for phosphorene and involve formation of an intermediate phase (white or red phosphorus) that can subsequently be converted to BP in the presence of mineralizing agents and pressure [81, 82]. Because of the intermediate phase [58, 83], the CVD procedures for BP growth do not yield high-quality phosphorene sheets with controllable number of layers [84]. Analysis of the phase diagrams for metal-C and metal-P show a key difference with respect to graphene

Figure 2.2. For graphene, C is incorporated in the metal lattice as insterstitials during the CVD of hydrocarbons at high temperature: upon cooling, C atoms from the lattice segregate at the surface and form graphene because of the large stable graphite + fcc region in the phase diagram (Figure 2.2(a)). The phase separated region(s) in the metal-P phase diagram (Figure 2.2(b)) involve either pure Cu and a phosphide (Cu_3P), or two phosphides (Cu_3P and CuP_2: in either case, phosphorus is bound into the phosphide it is not thermodynamically feasible for it to segregate at the metal surface. As a result, the mechanism of CVD growth of phosphorene on metal using gaseous precursors is vastly different than that for graphene, and in fact unknown. This work proposes such a mechanism in which phosphorene could grow on passive Ni or Cu substrates, from gaseous precursors, by heterogeneous catalysis [85] similar to hBN on these substrates.

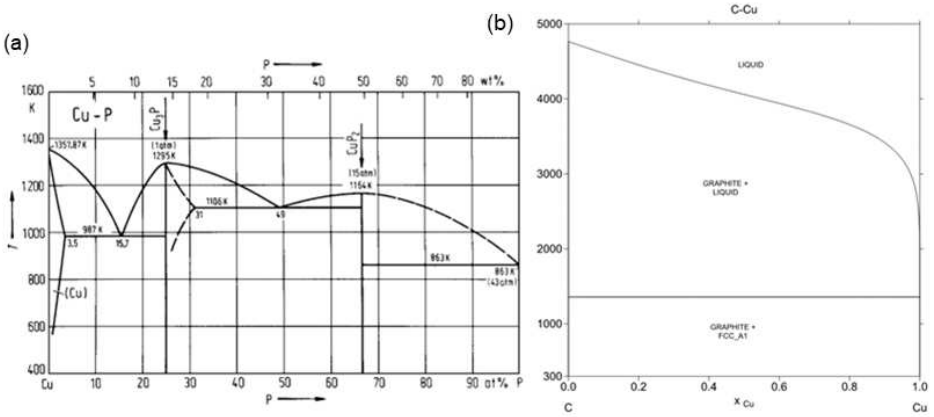

Figure 2.2: (a) Typical metal-P phase diagram, showing the formation of various phosphides. At intermediate P concentrations (i.e. not corresponding the phosphide stoichiometry), there is decomposition into Cu and Cu_3P, or between Cu_3P and CuP_2, but there is never segregation of P at the surface as encountered for example in the Cu-C phase diagram (b). Reproduced from [86] with permission from Springer, and from National Physical Laboratory (open access).

Hence there is a need to seek CVD growth paradigms for phosphorene, which should necessarily involve arresting the formation of phosphides. This can be achieved by prior growth of a monolayer of graphene or hexagonal boron nitride (hBN) on common metal

substrates. The phosphorus precursors, i.e., P_2, P_4, or PH_3, are large enough and inert enough that they cannot penetrate the monolayer graphene [87] or hBN (similar lattice constant) to reach the metal hence the phosphide formation is avoided. There still remains the issue of whether there is sufficient adsorption of these precursors on graphene- or hBN-covered metals. In this work, we use two common substrates, Ni(111) and Cu(111), based on their range of interaction with monolayer hBN or graphene: Ni is strongly interacting, while Cu is weakly interacting. Using density DFT calculations, we determine the adsorption energies of all three precursors and their radicals on the four model substrates (i.e., graphene- or hBN-covered Ni and Cu). Subsequently, we focus on one of these precursors, PH_3, and analyze the dehydrogenation reactions on the surface: the formation of these radicals on the surface will likely enable the formation of phosphorene by polymerization of P chains on the surface.

2.2 Details of the DFT calculations

To analyze the adsorption of precursor molecules and radicals on the hBN-covered Ni and Cu surfaces, we have used the plane-wave based DFT package Vienna Ab initio Simulation Package VASP [88, 89] to perform calculations (DFT) in the framework of the generalized gradient approximation (GGA) with the Perdew-Burke-Ernzerhof (PBE) functional [90]. The weak van der Waals (vdW) interactions between monolayer and the metal surface, and between the adsorbed molecules and the graphene- or hBN-covered metal substrates, were included using the DFT-D2 vdW functional of Grimme [91]. We have carried out spin-independent DFT calculations (geometry relaxations) calculations for P_2, P_4, and PH_3 (Figure 2.3)and their intermediates reaction intermediates P, PH, PH_2. The reactivity of surfaces is assessed through the adsorption of these reaction intermediates, and in the case of phosphine (PH_3) also by calculating the barriers for various steps of dehydrogenation. We have studied the adsorption of radicals on different sites on graphen/Cu, hBN/Cu, graphene/Ni, and hBN/Ni, using a three layer thick, 4×4 Ni(111) or Cu(111) slab with either graphene or hBN monolayer on it, with an 18 Åvacuum spacing. The hBN sheet in our computational

supercell has the registry with the substrate proposed by Bokdam et al., with the N atom above a top layer Cu or Ni atom, and the B atom above a hollow site [92]. Keeping fixed the bottom two layers of Cu and Ni, the geometries were relaxed via conjugate-gradient in the presence of dipole corrections using a plane-wave cutoff of 500 eV, a Monkhorst-Pack k-point grid of $3 \times 3 \times 1$, and a force tolerance criterion of 0.02 eV/Å.

For the phosphine precursor, PH_3, we have also analyzed the dehydrogenation processes by calculating the associated energy barriers using the nudged elastic band (NEB) method [93–95]. In this method, the initial (reactants) and final (products) are known and intermediate configurations between them are generated by a python script. For determining the barriers, we have used NEB with 9 intermediate configurations between the initial and final. During the NEB, these configurations are optimized so as to yield the minimum energy pathway between the initial and final configurations. From the final optimized configurations and their energies, we determine the reaction pathway and the corresponding energy barrier.

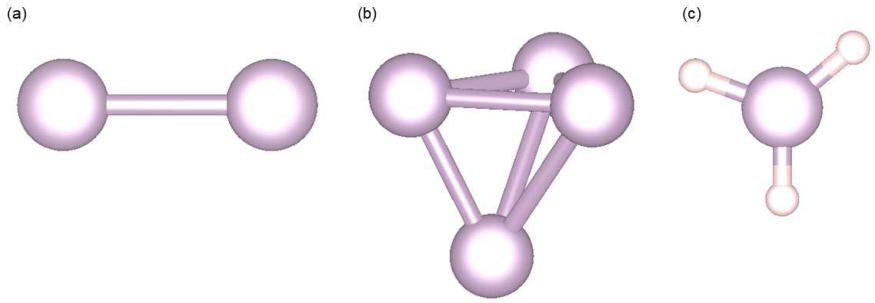

Figure 2.3: Molecules making up the gaseous precursors that can be used for the synthesis of phosphorene: (a) P_2, (b) P_4, and (c) PH_3.

2.3 Results on adsorption of precursors and their radicals

Figure 2.4, Figure 2.5, Figure 2.6, and Figure 2.7 show the adsorption sites considered for the precursors and (some of) their radicals. For PH_3, PH_2, PH, P and P_4, we considered four high symmetry sites above which they could be placed: N (or top, for graphene-covered

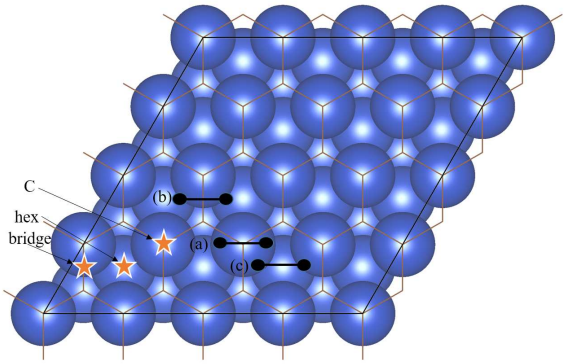

Figure 2.4: Adsorption locations for PH_x (x = 0,1,2,3), vertical P_2, vertical P_4 (C, hex, bridge), and the horizontal P_2 molecules (a-c).

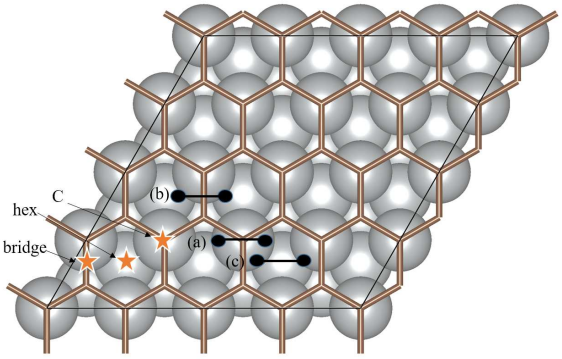

Figure 2.5: Adsorption locations for PH_x (x = 0,1,2,3), vertical P_2, vertical P_4 (C, hex, bridge), and the horizontal P_2 molecules (a-c).

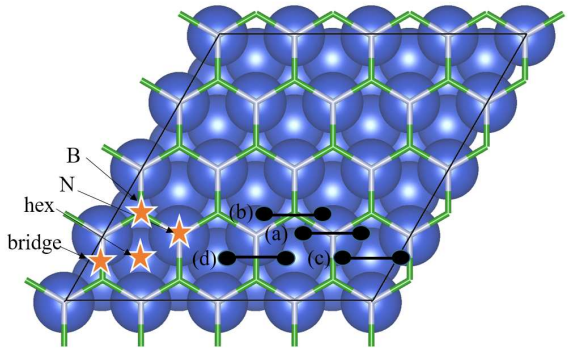

Figure 2.6: Adsorption locations for PH_x (x = 0,1,2,3), vertical P_2, vertical P_4 (N, B, hex, bridge), and the horizontal P_2 molecules (a-d).

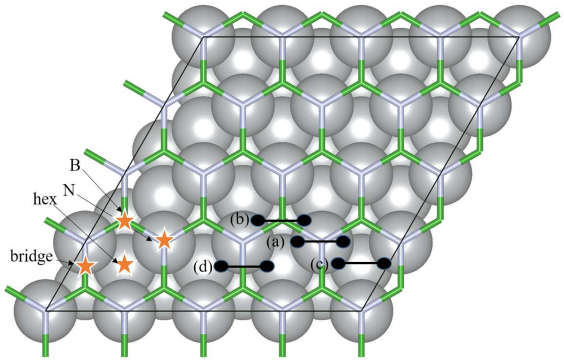

Figure 2.7: Adsorption locations for PH_x (x = 0,1,2,3), vertical P_2, vertical P_4 (N, B, hex, bridge), and the horizontal P_2 molecules (a-d).

metals), B (or hollow), bridge bond, and the center of the hexagon, hex (Figure 2.4 to Figure 2.7). PH_x are placed with the P atom above the site, while P_4 are placed with one corner of the tetrahedron above the site and the opposite plane away from the surface. For simplicity, this is the only orientation in which we placed the P_4 molecule, even though there are other high-symmetry orientations in which this molecule can face the substrate, e.g. with an edge down or with a facet down. The P_2 molecules are placed vertically (sites N (top), B (hollow), bridge and hex) or horizontally (locations (a) through (e) in Figure 2.4 to Figure 2.7. All the adsorption energies calculations are listed in Tables Table 2.2, Table 2.3, Table 2.4, and Table 2.5.

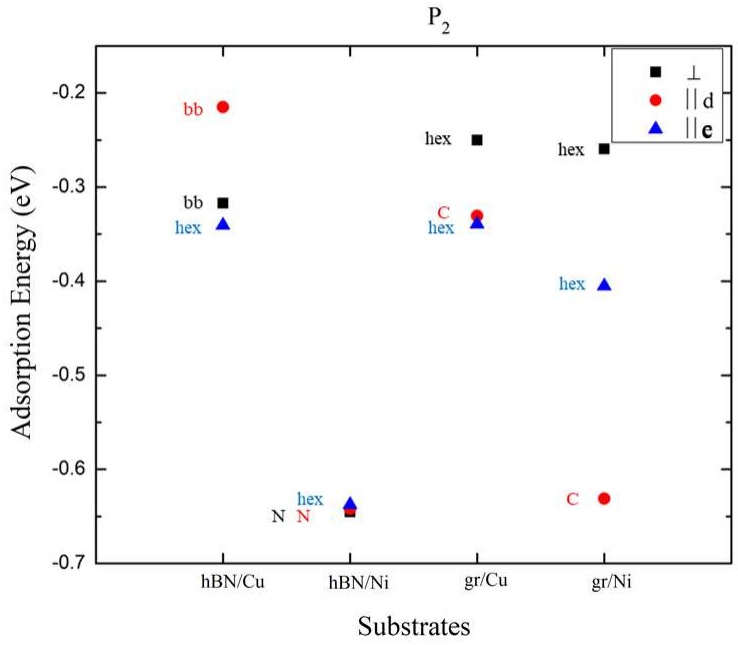

Figure 2.8: Adsorption energies for the P_2 molecule on graphene- or hBN-covered Ni and Cu substrates, for several selected positions. The symbols $\perp$ and $\parallel$ stand for the vertical and horizontal orientations of the molecule, respectively; C is a top site, bb bridge site, and the other symbols are shown in Figure 2.4 to Figure 2.7

First, we analyze the P_2 molecule on the four substrates. This precursor adsorbs somewhat strongly on the hBN- or graphene-covered Ni, and more weakly when the metal is Cu (Figure 2.8). This is expected, given the proximity of the Ni substrate to the graphene

or hBN (chemical binding [62]), as opposed to the Cu metal which is vdW bonded to the monolayer [63, 85]. This proximity is expected to have a catalyzing effect on the dissociation of the P_2 molecule or other precursors. By itself, the P_2 molecule has a bond energy of 9 eV, with an adsorption energy of the order 0.65 eV (Figure 2.8). For two P atoms adsorbed on separate sites, the adsorption energy is approximately 2×3.25 eV = 6.5 eV (Figure 2.8, adsorption of P on hBN/Ni). Therefore, we expect a barrier of at least $9.656.5 = 3.25$ eV. This barrier is rather high, and it could be overcome for large fluxes and/or exposure time, or, presumably, in the presence of other radicals on the surface. For example, atomic hydrogen and other radicals have been shown to influence the films structure and morphology in other cases [96–98]. The reason for this expectation is that in separate studies, there was significant evidence that hBN can grow from borazine on graphene-covered nickel [99–101]. The barriers are significant in this case also (a computed N-H bond energy of 6.5 eV), as they involve the dehydrogenation of borazine nevertheless, they were overcome by using a well-chosen interplay between flux, exposure time, and temperature, to the final result that a monolayer hBN grows on a very weakly catalytic substrate (graphene/Ni) [99]. Similar to these previous studies [99–101], it is reasonable to envision that flux, exposure time, and temperature can be tuned to lead to the nucleation and growth of a phosphorene layer from the P_2 precursor. The analysis of P_4 adsorption on the four selected substrates suggests that this molecule adsorbs somewhat more strongly on the hBN/Cu substrate as opposed to any other one. The dissociation of this molecule is more facile, since our calculations reveal that the energy per bond in P_4 is 1 eV smaller than that in P_2. The adsorption energy calculations suggest no particular impediment against growing from P_4. However, this molecule is larger than P_2 or PH_3 and non-planar, hence it diffusion could be slower: this means that a large flux is more conducive to the growth on amorphous structures, as P_4 can accumulate without significant dissociation or diffusion on the substrate: once such nucleation of amorphous P islands proceeds, there is no factor to drive the formation of 2-D phosphorene.

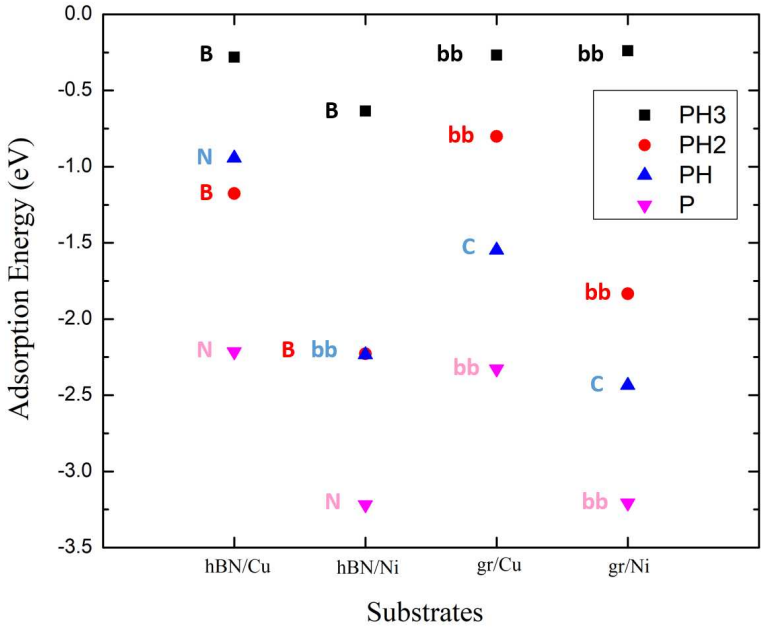

Figure 2.9: Adsorption energies for PH_x (x = 0,1,2,3) on graphene- or hBN-covered Ni and Cu substrates.

2.4 Results on energy barriers for dehydrogenation on the surface

We now discuss the adsorption and dehydrogenation of PH_3 on the substrates. The lowest adsorption energies across the adsorption locations considered are shown in Figure 2.9 . The first important conclusion is the PH_3 sticks to all substrates, for example more strongly than ammonia [85]. The barrier for the first dehydrogenation step ($PH_3 \rightarrow PH_2$) can be assessed comparatively by adsorption energy of PH_2, by virtue of the Evans-Polanyi principle [102–105]. The stronger the adsorption of PH_2, the lower the barrier for the first dehydrogenation step. In this respect, the dehydrogenation process should be the most facile on the hBN/Ni and graphene/Ni substrates. This may also have been inferred by virtue of the fact that the Ni substrate is closer (2.1 Å) to the monolayer (graphene or hBN) compared to Cu, which is van der Waals bonded (∼3 Å): this proximity facilitates a better transmission of the catalytic activity of the metal [106]. through the monolayer covering it. For a better assessment of the initial stages of phosphine deposition, we also compute the energy barriers and reaction pathways for the two dehydrogenation steps $PH_3 \rightarrow PH_2$ and $PH_2 \rightarrow PH$ where in radicals and atomic H remain on the substrate, i.e., prior to atomic H migration and its molecular desorption from the surface. In other words, we are computing the reaction barrier for the bottleneck part of the dehydrogenation reactions, in which an H atom splits from PH_3 or PH_2 by virtue of the catalytic activity of the substrate, or by interactions with other radicals. The reaction barriers are listed in Table Table 2.1 for each stage and each substrate.

Table 2.1: Calculated reaction barriers for the dehydrogenation steps on hBN or graphene covered Ni or Cu substrates.

Substrate	$PH_3 \rightarrow PH_2 + H$	$PH_2 \rightarrow$ PH+H
hBN/Ni	**1.937**	**2.487**
hBN/Cu	**3.339**	**2.928**
gr/Ni	**1.627**	**1.145**
gr/Cu	**2.320**	**1.623**

The NEB for the reaction pathways and the associated energy barriers are shown in Figure 2.10, Figure 2.11, Figure 2.12 and Figure 2.13.

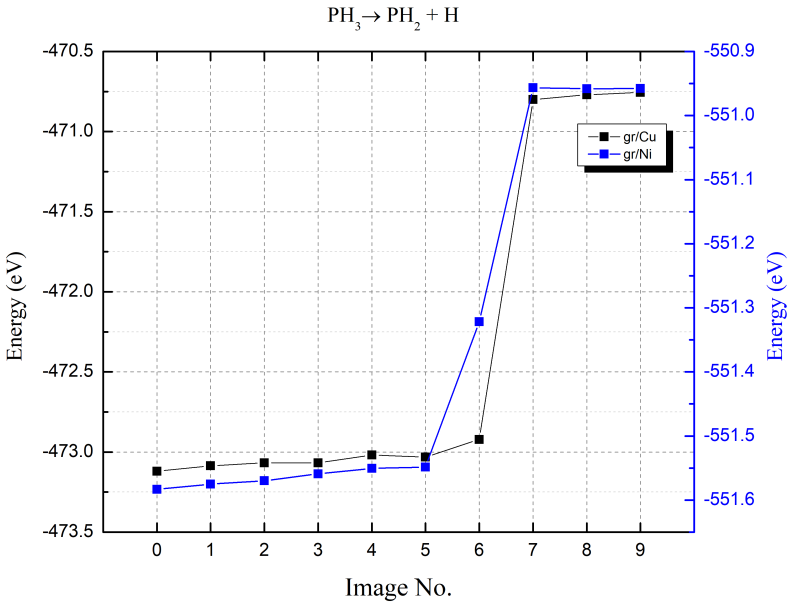

Figure 2.10: reaction pathway for the dehydrogenation step $PH_3 \rightarrow PH_2 + H$ on gr/Cu and gr/Ni surfaces

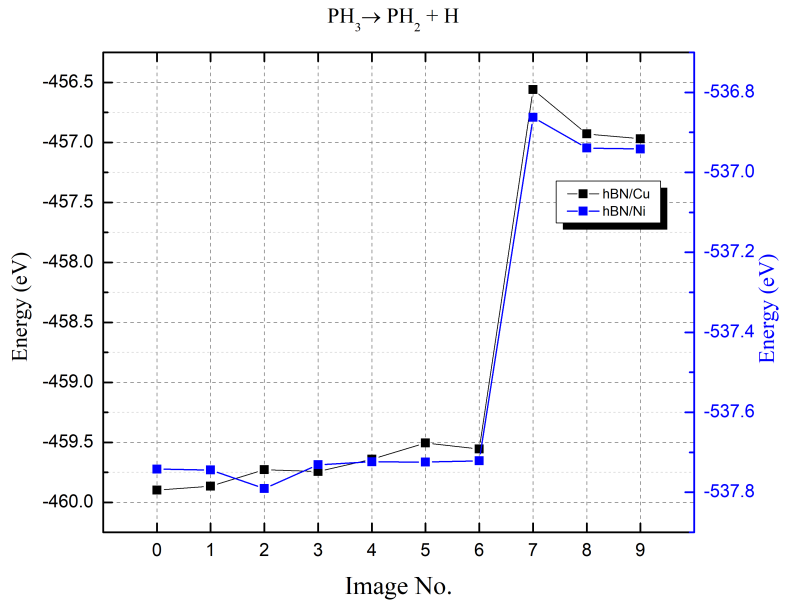

Figure 2.11: reaction pathway for the dehydrogenation step $PH_3 \rightarrow PH_2 + H$ on hBN/Cu and hBN/Ni surfaces

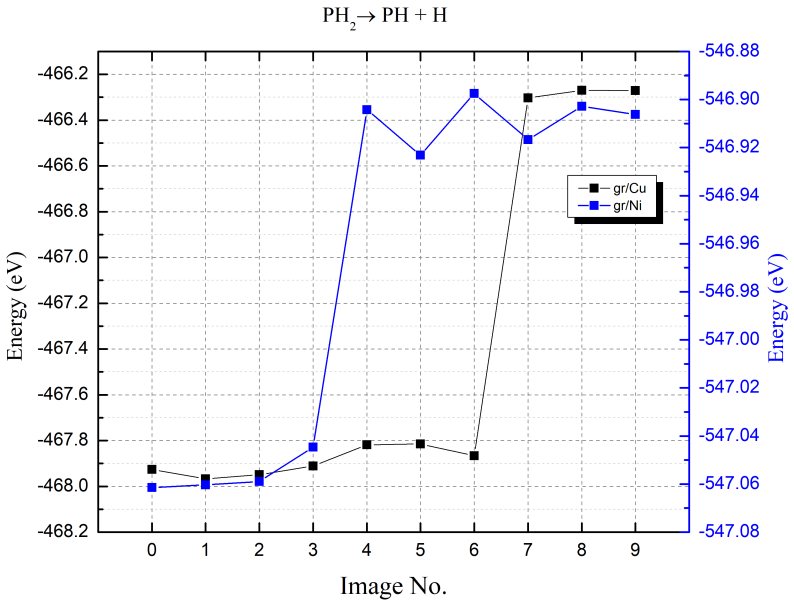

Figure 2.12: reaction pathway for the dehydrogenation step $PH_2 \rightarrow PH + H$ on gr/Cu and gr/Ni surfaces

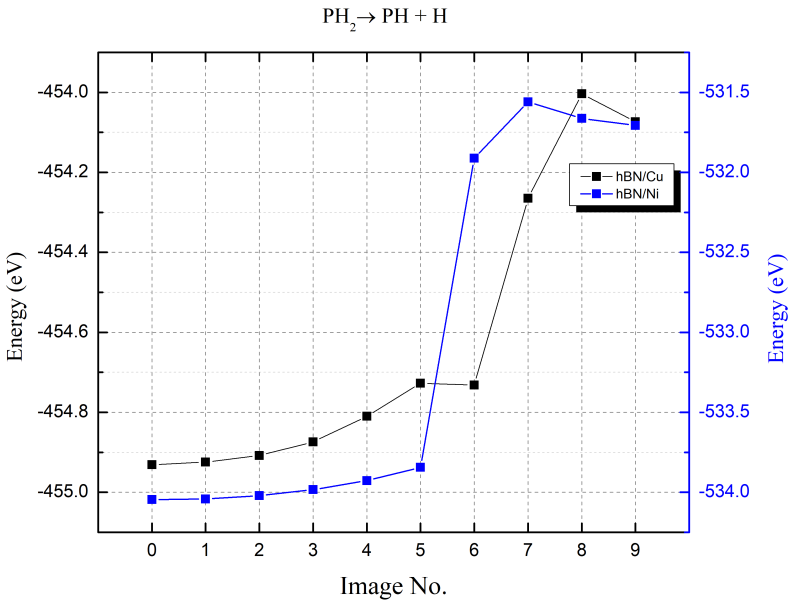

Figure 2.13: reaction pathway for the dehydrogenation step $PH_2 \rightarrow PH + H$ on hBN/Cu and hBN/Ni surfaces

In experimental conditions, the substrate by itself may not be sufficient to lead to dehydrogenation, but temperature, flux, and diffusion of atomic or molecular hydrogen or radicals on the surface can potentially make these reactions feasible. It is instructive to notice that some of the barriers listed in Table 2.1 are similar to those encountered in the dehydrogenation of ammonia directly on the catalytic substrate Cu(111), 1.84 eV and 1.59 eV ([85] and references therein). While this may come as a surprise, we note that phosphine is in general more reactive than ammonia, hence it can dehydrogenate reasonably easily when the metallic substrate is covered, e.g., with graphene.

Based on these adsorption calculations, the growth of very thin layers of phosphorus should proceed on either of these two substrates (i.e. hBN/Ni and gr/Ni) from the PH_3 precursor. Two necessary conditions for growth of phosphorus are met, namely avoiding the formation of a phosphide and catalyzing the dehydrogenation of the precursor. It is not a priori clear that the growth would yield a phosphorene layer, since these necessary conditions are not automatically sufficient, i.e., they do not address the later stages of growth during which different competing allotropes of phosphorus may compete to form on the substrate. We surmise, however, that a control of the temperature and flux of the precursors to the substrate can yield the desired low energy allotrope.

2.5 Conclusions

Therefore, we summarize the guidance for future experiments that is offered by these calculations as follows. In order to enable the growth of 2-D crystalline phosphorene, is is feasible to first grow graphene or boron nitride on them so as to prevent the formation of phosphides. Secondly, the best precursors are PH_3 and P_2, or a combination thereof. Thirdly, the best substrates are hBN- or graphene-covered Ni, since it these two substrate have the highest "activity" as assessed by the strength of adsorption of the precursors and their radicals. To expand on this results and narrow the search field for suitable substrates, we specify that the metal simply has to be Ni, rather than any other strongly interacting metal. The reason for this prescription is that other metals with strong interactions (e.g., Ru

[20, 107, 108]) do not have surface lattices that match that of graphene or hBN that cover the substrate. This lattice mismatch is accomodated by the formation of large, corrugated moire patterns in which there are regions strongly bonded to the substrate (which will contain adsorption sites for the precursors) and regions that are away from the substrate (an example shown in Chapter 4) and vdW bonded to it: for the vdW region, the adsorption is weak which is likely to prevent the formation of continuous 2-D phosphorene layers.

Table 2.2: Adsorption Energy of PH(0,1,2,3) , P_2 and P_4 Molecules on gr/Cu

Substrate	Molecules	Positions	Adsorption Energy (eV)
gr/Cu	PH_3	C	-0.2668
		bridge	**-0.2679**
		hex	-0.2592
	PH_2	C	-0.6105
		bridge	**-0.8014**
		hex	-0.4874
	PH	C	**-1.5468**
		bridge	-1.0191
		hex	-0.4580
	P	C	-2.3274
		bridge	**-2.3275**
		hex	-2.3231
	P_2 horizontal	C	**-0.3306**
		bridge	-0.3283
		hex	-0.2963
	P_2 vertical	C	-0.2232
		bridge	-0.2339
		hex	**-0.2501**
	P_4	C	**-0.4296**
		bridge	-0.4029
		hex	-0.3755

Table 2.3: Adsorption Energy of PH(0,1,2,3) , P_2 and P_4 Molecules on gr/Ni

Substrate	Molecules	Positions	Adsorption Energy (eV)
gr/Ni	PH_3	C	-0.2333
		bridge	**-0.2390**
		hex	-0.2306
	PH_2	C	-1.0452
		bridge	**-1.8332**
		hex	-0.6960
	PH	C	**-2.3586**
		bridge	-2.4344
		hex	-0.8898
	P	C	-3.1361
		bridge	**-3.2083**
		hex	-2.4020
	P_2 horizontal	C	**-0.6311**
		bridge	-0.3880
		hex	-0.6300
	P_2 vertical	C	-0.2203
		bridge	-0.2230
		hex	**-0.2594**
	P_4	C	**-0.4370**
		bridge	-0.4021
		hex	-0.3901

Table 2.4: Adsorption Energy of PH(0,1,2,3) , P_2 and P_4 Molecules on hBN/Cu

Substrate	Molecules	Positions	Adsorption Energy (eV)
hBN/Cu	PH_3	B	**-0.2808**
		bridge	-0.2770
		hex	-0.2695
		N	-0.2787
	PH_2	B	**-1.1754**
		bridge	-1.0324
		hex	-0.4825
		N	-0.6482
	PH	B	-0.5632
		bridge	-0.6994
		hex	-0.3706
		N	**-0.9428**
	P	B	-1.6459
		bridge	-2.2141
		hex	-1.5937
		N	**-2.5553**
	P_2 horizontal	B	-0.1926
		bridge	**-0.2150**
		hex	-0.1939
		N	-0.2137
	P_2 vertical	B	-0.1927
		bridge	**-0.3171**
		hex	-0.1901
		N	-0.2182
	P_4	B	-0.3790
		bridge	-0.3791
		hex	-0.3495
		N	**-0.3982**

Table 2.5: Adsorption Energy of PH(0,1,2,3) , P_2 and P_4 Molecules on hBN/Ni

Substrate	Molecules	Positions	Adsorption Energy (eV)
hBN/Ni	PH_3	B	**-0.6347**
		bridge	-0.6333
		hex	-0.2448
		N	-0.6335
	PH_2	B	**-2.2276**
		bridge	-1.0599
		hex	-1.0425
		N	-1.2626
	PH	B	-1.0771
		bridge	**-2.2336**
		hex	-1.1363
		N	-1.8947
	P	B	-2.8319
		bridge	-2.9839
		hex	-2.6645
		N	**-3.2193**
	P_2 horizontal	B	-0.6142
		bridge	-0.6385
		hex	-0.6185
		N	**-0.6421**
	P_2 vertical	B	-0.6154
		bridge	-0.6082
		hex	-0.6127
		N	**-0.6453**
	P_4	B	-0.4545
		bridge	-0.4462
		hex	-0.4184
		N	**-0.5166**

CHAPTER 3

GROWTH OF BILAYER HEXAGONAL BORON NITRIDE ON COPPER SUBSTRATES

Synopsis: Hexagonal boron nitride (hBN) is an important insulator with nearly the same lattice constant as graphene. With its insulating properties and similar lattice constant, hBN has become an important support for graphene, and in general as an ultrathin 2D dielectric material: hence, synthesizing hBN has become important in its own right. Recent CVD growth have shown that hBN can be synthesized on metallic surfaces, since the metal substrate acts as a catalyst on the precursor molecules and enables their reactions on the substrate and the formation of the first layer of hBN. However, after the growth of the first hBN layer, the catalytic effect of the metal ceases for the next precursors that come to the surface, because they only meet the (passive) hBN layer. It is therefore intriguing why additional layers of hBN can be grown [109]. Most often the growth of additional hBN layers is observed for the case when there are two precursors, i.e., one source of boron (borane, diborane, triethylborane (TEB), etc) and one source of nitrogen (e.g., ammonia). Since the catalytic activity of the substrate is virtually voided after the growth of the first hBN layer, recent work [85] suggested that in the case of growth from two precursors molecules one of the precursors decompose thermally at the surface (pyrolizes), and the surface bound radicals resulting from it activate the reaction with ammonia that ultimately leads to the formation of a new hBN layer. Since this recently proposed mechanism has focused mostly on the adsorption and dehydrogenation of ammonia on hBN-covered Cu, in this chapter we look at the other precursor as well, i.e. the source of boron. We study the adsorption of borane and TEB, as well as ammonia, on Cu, hBN/Cu and hBN –with the pure hBN layer meant to simulate the adsortion on multiple hBN layers covering the substrate and therefore fully passivating it. We find that, indeed the boron precursors, and the radicals resulted

from them adsorb on the hBN-passivated surfaces and could thereafter act as catalytic sites themselves for the adsorption and dehydrogenation of ammonia.

3.1 Motivation

Hexagonal boron nitride (h-BN) is a layered material similar to graphite. In its 2-D version, hBN is a promising dielectric substrate for growing graphene and other 2-D materials [32]. hBN shows many unique physical and electronic properties such as high thermal conductivity, low density, high melting point, high-temperature stability [110], and high mechanical strength [29, 30]; also, it is an isolator with band gap 5.7 eV [111]. hBN can be used for graphene-based nanoelectronic devices as a chemically inactive substrate [112, 113], and for atomically thin capacitors [114].

3.2 Current state of the art

hBN in atomic monolayers is largely grown from single precursors, either borazine or ammonia borane, via chemical vapor deposition (CVD) on various metallic substrates [110, 115, 116]. Flat hBN monolayers can be grown on metals with small lattice mismatch (Cu) [63, 117]. However, for various application control over the quality, uniformity, and the number of layers is necessary [29, 30, 32, 118, 119]. The mechanism of growing multiple hBN layers on metallic substrate has not been well understood; recently, it was proposed [85] that when using two precursor gases (one source of boron, and one source of nitrogen) then one of the precursors pyrolizes at the surface and helps activating the other one (ammonia, the source of nitrogen). Siegel et al. [85], however, focused mostly on the adsorption and dehydrogenation of ammonia; guided by their work, here we study the adsorption of the source of boron and their radicals as well.

3.3 Adsorption geometries and computational details

In order for any reaction to proceed at the surface, the precursor molecular have to be able to adsorb (bind) to the surface. We therefore focus in this study on adsorption of

precursors and their radicals. As substrates, we use bare Cu, hBN/Cu (one layer of hBN on Cu), and single layer hBN. The single layer hBN is used as an approximation of the limiting case in which many hBN layers already cover the copper substrate, and therefore none of its catalytic effect reaches the surface.

We have performed the DFT calculations using the Vienna Ab-initio Simulation Package (VASP) [88], with the generalized gradient approximation (GGA) with the Perdew-Burke-Ernzerhof functional [90]. The interactions between hBN layer and a Cu(111) substrate are modeled in the calculations using the DFT-D2 method of Grimme. We have studied the adsorption of molecules and their radicals on different sites on Cu(111) Figure 3.4, hBN Figure 3.6, hBN/Cu Figure 3.5, using a three layer of Cu, 4×4 Cu(111) slab , with an 18 $\mathring{A}$ vacuum spacing. Keeping fixed the bottom two layers of Cu, the geometries were relaxed via conjugate-gradient in the presence of dipole corrections using a plane-wave cutoff of 500 eV, a Monkhorst-Pack k-point grid of $3 \times 3 \times 1$, and a force tolerance criterion of 0.02 $eV/\mathring{A}$ for relaxations.

The molecules studied (along with their radicals) are TEB (Figure 3.1), borane (Figure 3.2), and ammonia (Figure 3.3). As such, these calculations in this chapter are relevant for two synthesis procedures, one based on TEB and ammonia, and the other based on borane and ammonia.

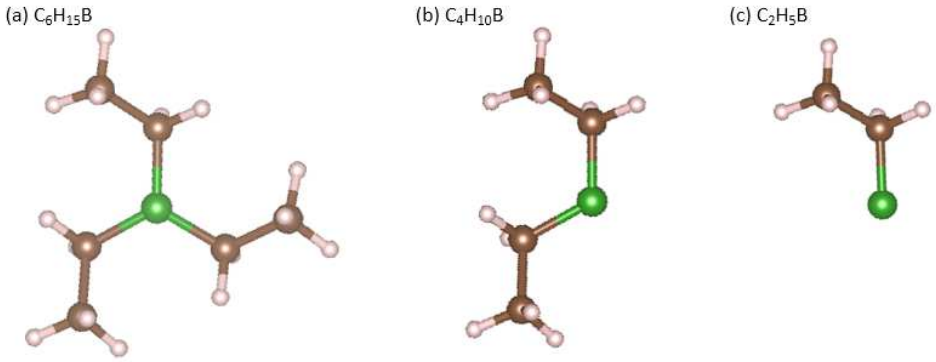

Figure 3.1: TEB ($C_6H_{15}B$) and its radicals $C_4H_{10}B$ and C_2H_5B.

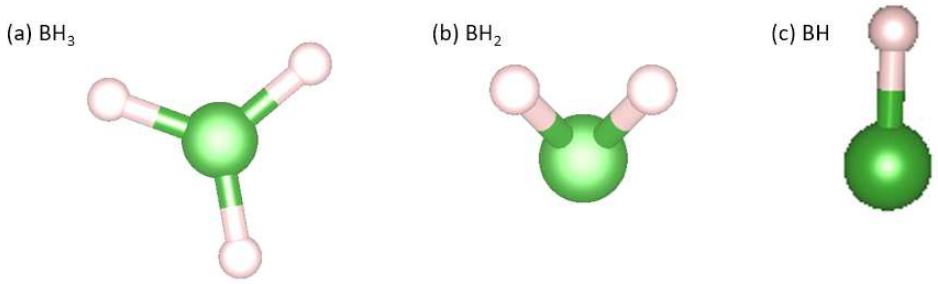

Figure 3.2: Borane and its radicals, BH_x (x = 1,2,3).

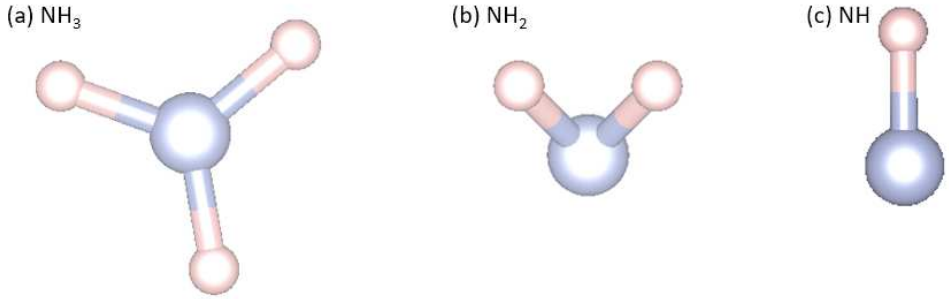

Figure 3.3: Ammonia and its radicals, NH_x (x = 1,2,3) molecule

The adsorption energy usually depends on specific adsorption sites, so he have considered several high-symmetry adsorption sites on each of the substrates (Cu, hBN/Cu, hBN). These sites are shown in Figure 3.4, Figure 3.5 andFigure 3.6.

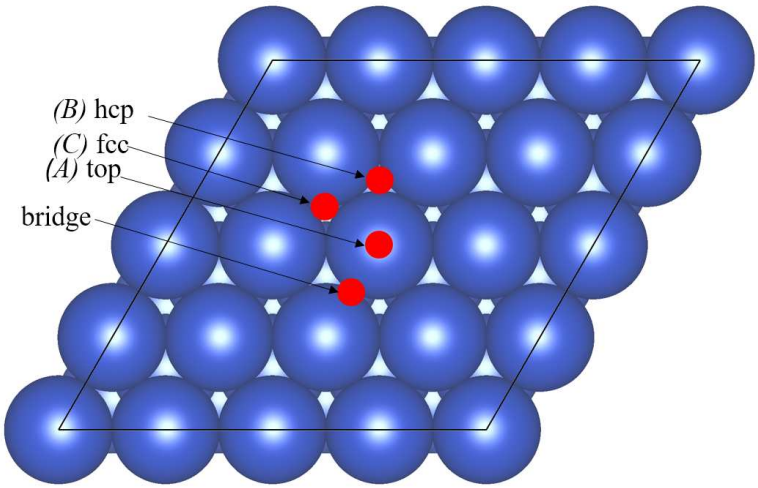

Figure 3.4: Adsorption locations for molecules on Cu(111) surface

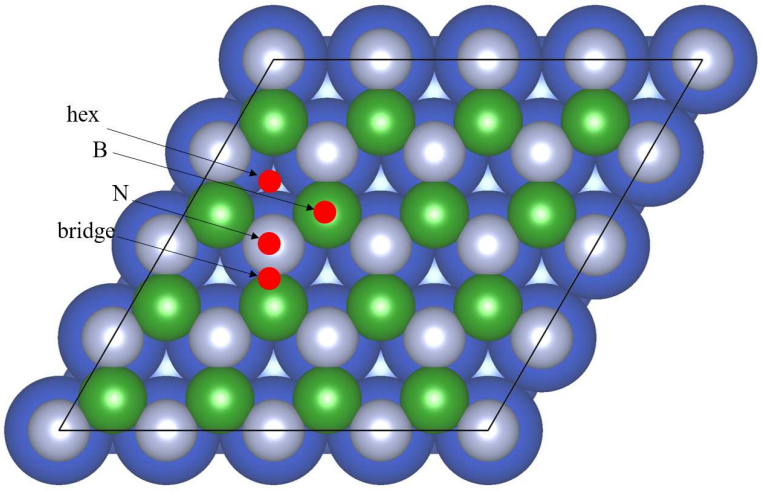

Figure 3.5: Adsorption locations for molecules on hBn/Cu surface

3.4 Results

The adsorption results are discussed below for each precursor molecule.

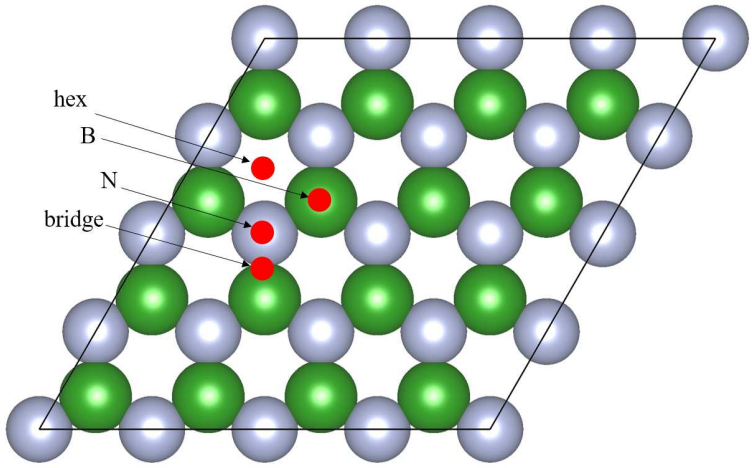

Figure 3.6: Adsorption locations for molecules on hBN surface

3.4.1 Adsorption of TEB and its radicals

First, we analyze the tri-ethyl borane and its radicals: referring to Figure 3.7 for tri-ethyl borane, we note that the adsorption energy values for all three substrates are close to one another. The two-ethyl borane has stronger adsorption energy than one-ethyl borane. The most strongly bound radical is two-ethyl borane, and the difference between first layer and second layers adsorption energy is $\approx$ 2 eV. The adsorption energies for TEB and its radicals on the high-symmetry sites on each substrate are shown in Table Table 3.1. For TEB, we note that adsorption depends mostly on the substrate, with the bare copper being the one interacting the strongest. Within any one given substrate, however, the adsorption of TEB depends only weakly on the exact sites. This observation, coupled with calculations of the molecule-substrate distances, indicates that TEB is weakly adorbed on the metal (physisorbed). Its radicals, however, bind strongly since for these radicals the central boron atom has one or two dangling bonds. For the radical with two ethyl arms, the adsorption is chemical and depends strongly both on the substrate and on the exact site on the substrate (Table Table 3.1 and Figure 3.7). The radical with one ethyl displays similar trends as that with two ethyls, but the adsorption is very weak and somewhat independent on site for the hBN-covered substrates (hBN/Cu and hBN) (Table Table 3.1 and Figure 3.7).

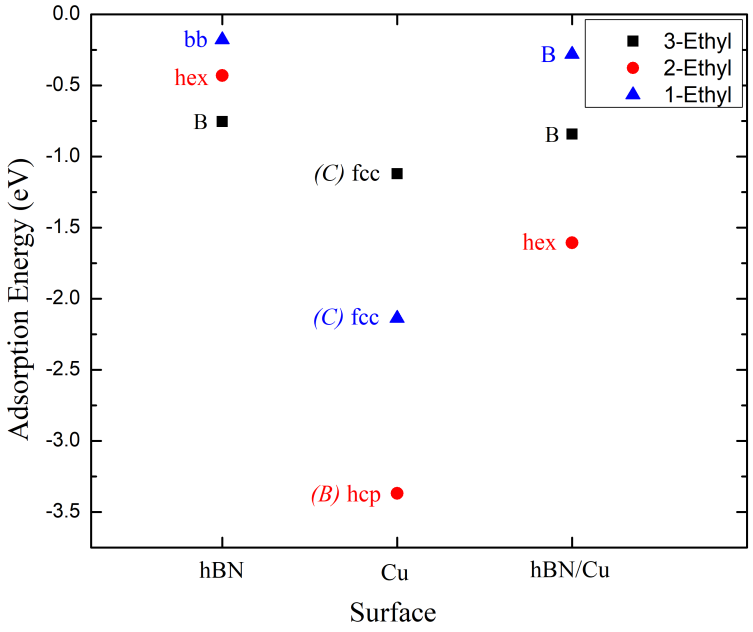

Figure 3.7: Adsorption energies at the strongest binding sites for $C_6H_{15}B$, $C_4H_{10}B$ and C_2H_5B on Cu(111), hBN/Cu, and hBN substrates.

3.4.2 Adsorption of borane and its radicals

Now we discuss the adsorption energy of borane and its radicals. According to the Figure 3.8 is clear that the values of adsorption energy for BH_3,BH_2,BH on hBN/Cu are almost the same values on hBN. Furthermore, the most adsorption precursor is BH,and the difference between first layer and second layers adsorption energy is $\approx$ 3 eV. The adsorption energy for three substrate is given in Table Table 3.2.

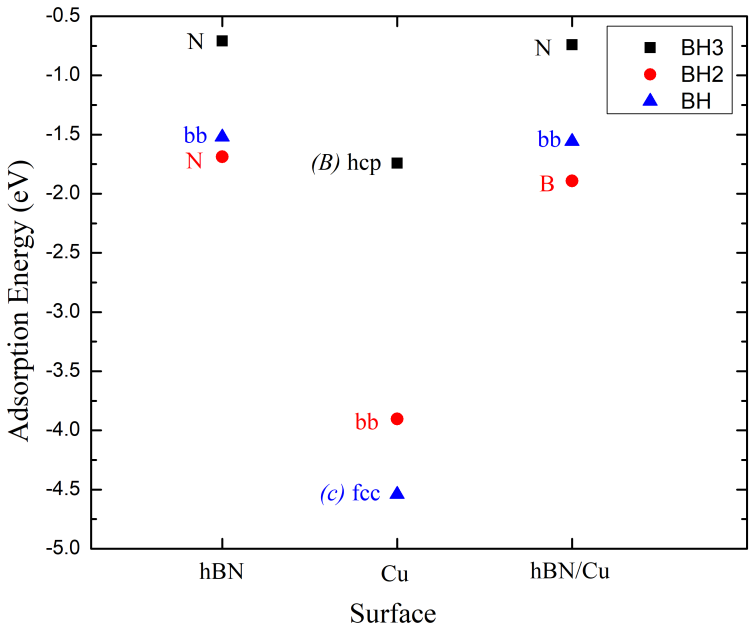

Figure 3.8: Adsorption energies for BH_x (x = 0,1,2,3) on hBN, Cu(111),and hBN/Cu substrates.

3.4.3 Adsorption of ammonia and its radicals

Finally, we discuss the adsorption energy of ammonia and its radicals. As shown in Figure 3.9, the ammonia molecule NH_3 has almost the same adsorption energy on all three substrates. NH is the most adsorption radical. The adsorption energy on Cu pure metallic substrate and hBN/Cu metallic covered with hBN for NH are $\approx$ 5.6 eV and 4.3 eV $\approx$

respectively, therefore the difference between first layer and second layers adsorption energy is ≈ 1.3 eV. Our results for a both ammonia and it's radical on Cu(111) and hBN/Cu substrates are consistent with [85, 120]. The adsorption energy values for each substrate are reported in Table Table 3.3.

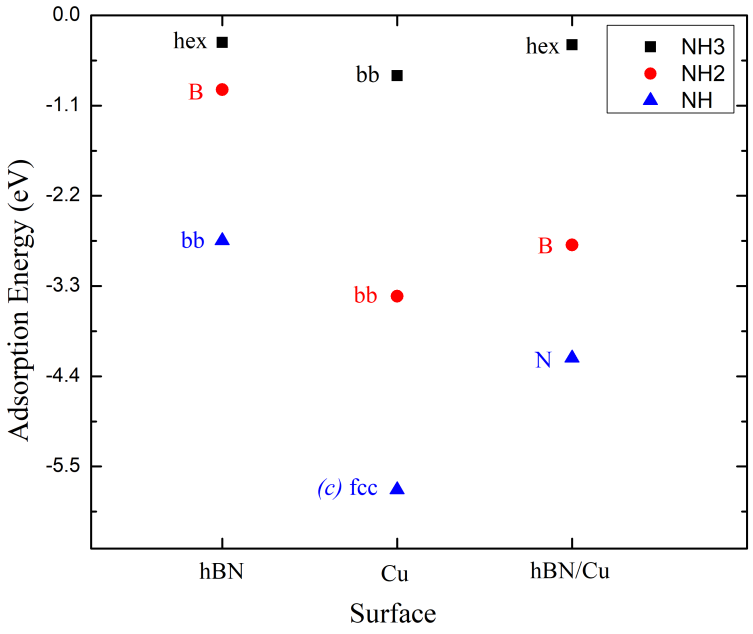

Figure 3.9: Adsorption energies for NH_x (x = 0,1,2,3) on hBN, Cu(111),and hBN/Cu substrates.

3.5 Summary

Growth procedures with possibility to control the layer number of one or a few layers of hBN has been recently reported [29, 109, 121–123]. There is a clear evidence of a mechanism which relies on catalyst to crack the precursor and adsorption into substrate then forming hBN layer during cooling [123, 124]. The heterogeneous pyrolysis mechanism [85] is different, in that one precursors thermally cracks and then activates the other. The adsorption of ammonia on the second layer was less effective than tri-ethyl borane and borane. In summary, the DFT calculations calculations show that the second layer growth requires significant

adsorption energies, and ghe growth always encounter high kinetic barriers. Yet, these barriers are comparable with other systems for which it had been shown that nucleation and growth are possible. For boron sources,the tri-ethyl borane are more efficient than borane based on adsorption energy.

Table 3.1: Adsorption energy for TEB (3-Ethyl) and its radicals with 2- and 1-Ethyl grops.

Molecule	Substrates	Position	Adsorption Energy (eV)
3- Ethyl	Cu(111)	*(A)* top	-1.0560
		(B) hcp	-1.0955
		(C) fcc	**-1.1199**
		bridge	-1.0782
	hBN	B	**-0.7544**
		bridge	-0.7392
		hex	-0.7465
		N	-0.7366
	hBN/Cu	B	**-0.8414**
		bridge	-0.7633
		hex	-0.8215
		N	-0.7637
2- Ethyl	Cu(111)	*(A)* top	-3.1304
		(B) hcp	-3.2121
		(C) fcc	**-3.3694**
		bridge	-3.2585
	hBN	B	-0.2653
		bridge	**-0.4313**
		hex	-0.2653
		N	-0.3528
	hBN/Cu	B	**-1.6071**
		bridge	-1.1234
		hex	-0.5757
		N	-1.3507
1- Ethyl	Cu(111)	*(A)* top	-2.0972
		(B) hcp	**-2.1379**
		(C) fcc	-2.1215
		bridge	-2.1362
	hBN	B	-0.1518
		bridge	-0.1619
		hex	**-0.1786**
		N	-0.1535
	hBN/Cu	B	-0.2643
		bridge	-0.2601
		hex	**-0.2799**
		N	-0.2369

Table 3.2: Adsorption energy of boron-containing molecules and radicals

Molecules	Substrates	Position	Adsorption Energy (eV)
BH3	Cu(111)	*(A)* top	-0.8313
		(B) hcp	**-1.7418**
		(C) fcc	-1.7347
		bridge	-1.4400
	hBN	B	-0.1648
		bridge	-0.6784
		hex	-0.2461
		N	**-0.7096**
	hBN/Cu	B	-0.3067
		bridge	-0.5553
		hex	-0.2761
		N	**-0.7398**
BH2	Cu(111)	*(A)* top	-3.2790
		(B) hcp	-3.8757
		(C) fcc	-3.8918
		bridge	**-3.9041**
	hBN	B	-1.6778
		bridge	-1.3434
		hex	-0.2495
		N	**-1.6871**
	hBN/Cu	B	**-1.8919**
		bridge	-1.2000
		hex	-1.3033
		N	-1.8496
BH	Cu(111)	*(A)* top	-3.6308
		(B) hcp	-4.4984
		(C) fcc	**-4.5396**
		bridge	-4.4397
	hBN	B	-0.4417
		bridge	**-1.5199**
		hex	-0.0971
		N	-1.5004
	hBN/Cu	B	-0.8376
		bridge	**-1.5584**
		hex	-0.6218
		N	-0.0625

Table 3.3: Adsorption energy of nitrogen-containing molecules and radicals.

Molecules	Substrates	Position	Adsorption Energy (eV)
NH3	Cu(111)	*(A)* top	-0.5729
		(B) hcp	-0.6468
		(C) fcc	-0.6384
		bridge	**-0.7346**
	hBN	B	-0.3258
		bridge	-0.3249
		hex	**-0.3291**
		N	-0.2861
	hBN/Cu	B	-0.1809
		bridge	-0.3516
		hex	**-0.3589**
		N	-0.3312
NH2	Cu(111)	*(A)* top	-2.8459
		(B) hcp	-3.1944
		(C) fcc	-3.2094
		bridge	**-3.4224**
	hBN	B	**-0.9064**
		bridge	-0.9020
		hex	-0.2336
		N	-0.3064
	hBN/Cu	B	**-2.7976**
		bridge	-2.5619
		hex	-2.1405
		N	-0.8893
NH	Cu(111)	*(A)* top	-3.8892
		(B) hcp	-5.7061
		(C) fcc	**-5.7826**
		bridge	-5.5376
	hBN	B	-0.6374
		bridge	**-2.7474**
		hex	-0.2818
		N	-2.3349
	hBN/Cu	B	-2.7671
		bridge	-2.3531
		hex	-3.4431
		N	**-4.1773**

CHAPTER 4

CORRUGATION OF HEXAGONAL BORON NITRIDE ON PALLADIUM

Part of ϕ Orientation-Dependent Corrugation of Two-Dimensional Hexagonal Boron Nitride Domains on Pd(111) submitted to The Journal of *Nano Letters*

Pedro Arias[1], Abdulfattah Abdulslam [2], Abbas Ebnonnasir[1], Cristian V. Ciobanu[2], and Suneel Kodambaka [1]

Synopsis: This work is part of a manuscript in preparation, recently submitted to Nano Letters. The work in the manuscript is joint experimental (performed at University of California Los Angeles) and computational: the latter was performed by the candidate at Colorado School of Mines, and is described in the sections below, with only a small section on experimental motivation. There is a recurring problem in the analysis of STM images obtained with a metallic tip when scanning geometrically corrugated surfaces. These corrugations occur at the atomic scale, but in addition to geometric corrugation there are electronic effects that change the (apparent) height measured by STM. Therefore, the STM data cannot directly be used to infer actual geometrical height variations (corrugations) on the surface, and has to be analyzed via, e.g., atomic scale computations and modeling wherein geometric corrugation are explicit. In this work, the corrugations measured for hBN on palladium have been analyzed using DFT calculations and interface energy modeling. The STM measurements suggest a bifurcation behaviour of the hBN monolayer on Pd in which both flat monolayers and "blistered" (having a morphology akin to that of bubble wrap) could exist together on the same hBN sheet. The phenomenological model presented here rationalize this behavior in terms of an energetic competition between chemical bonding (lower regions), vdW bonding (upper regions of the blisters), and bending energy of the sheet. At the same time, our DFT show that the hBN/Pd system can have domains with multiple

[1] Department of Materials Science and Engineering, University of California Los Angeles , CA 90095 USA
[2]Department of Mechanical Engineering & Materials Science Program Colorado School of Mines, Golden, CO 80401 USA

orientations, some of which having the blistered morphology. These results are applicable for interactions between hBN sheet and other substrates in the intermediate range.

4.1 Introduction

As described in the previous chapter, hBN is an important substrate for nanoelectronics since it is insulating (at least in its free-standing state) and can serve as passivating agent for metal substrates. hBN can grow on a variety of transition metal surfaces such as such as Ni(111) [125], Pd(111) [125, 126] and Pd(110) [127] , Pt(111) [125], Rh(111) [128], Ru(0001) [129], Ir(111) [130], and Cu(111) [131]. Graphene or other 2-D materials can be synthesized onto hBN-covered substrates. In addition, hBN is often investigated as a material for ultra-thin capacitors. As such, the morphology of hBN on different substrates becomes important, as the subsequent 2-D layers that could be grown on it would be bonded by weak vdW forces, and hence would be conformal to the hBN layer. Depending on the lattice mismatch with the substrate (defined as the difference in lattice constants between hBN and the substrate, divided by the lattice constant of the substrate), and on the strength of the interaction, hBN can acquire a variety of morphologies on the metallic substrate: (a) it is commensurate on Ni(111) due to the very low lattice mismatch, with the N atoms atop Ni atoms and the B atoms in the hollow site between them, (b) incommensurate and forming moire patterns on domains at vdW distance ($\sim$ 3Å) from the substrate (e.g., on Cu(111)[63] or Ir(111) [130], and (c) incommensurate and strongly bonded to the substrate such as on Ru(0001)[129]. Previous studies [42, 62, 80, 117, 131–135] indicated that the properties of hBN can depend on the underlying substrate, in particular on the surface orientation and the interaction strength for the binding with hBN. For example, hBN/Ni(111) shows metallic or insulating behavior depending on the registry of B and N atoms on the nickel top layer [62]. hBN on weakly interacting Cu(111) [63, 131] and Pt(111) [125] surface, the properties of hBN are insulating, and multiple domains (regions with different orientation with regard to the substrate) have been observed. Certainly, the substrates referred to above fall into two clear categories [92]: strongly interacting (Co, Ni, Ti) and weakly interacting (Cu, Ir, Pt, Au etc).

There is an additional category, however, with a few metallic representatives (perhaps only one, Pd [92]) but potentially many metal oxides: qualitatively speaking, this is the category of intermediate interactions –neither too strong to be considered strictly chemical bonds, nor too weak so as to be considered pure vdW interactions. In this category, we expect lower bandgap for hBN (likely becoming semiconductor, or close to it), and fewer orientational domains on the substrate, than, for example of the vdW interacting Cu(111) substrate. Given that the intermediate value of the interactions and the fact that the lattice mismatch is large on Pd(111), it is not a priori clear if the hBN monolayer is always flat or can support actual geometric corrugations. These corrugations, as mentioned, can be important as they can serve as templates for the self-organizations of the large organic molecules or metallic clusters. In what follows, we described briefly experimental evidence (unpublished as of the date of the thesis defense) from collaborators at University of California Los Angeles that the Pd substrate can sustain several orientational domains of hBN and that some have geometric corrugations, while most are actually flat despite displaying apparent hill and valley patterns in STM.

4.2 Moiré Patterns on Metallic Substrates

Regardless of the interaction strength, the atomic layers of hBN on nominally flat metal substrates often form so called moiré patterns. These patterns are periodic or quasi-periodic structures that form because the lattice constants of hBN (a_{hBN}) and the substrate (a_{Pd}) are different and the crystalline vectors of the layer and substrates are not aligned. Depending on the alignment on the periodic vectors of hBN and the substrate, there can be multiple spatial periodicities. To briefly explain the concept of moiré periodicity, in a theoretical one-dimensional situation in which the layer has the lattice constant of 2Å and the substrate a lattice constant of 5Å then the moiré periodicity would be the smallest common multiple of the lattice constants of the substrate and the layer, i.e. 10Å. This situation remains true in principle when turning to two dimensions; however, there are several complexities that arise:

(a) the lattice constants do not have a small common multiple, and both are rational numbers rather than integers

(b) the spatial periodicity is not only a function of the lattice constants of the hBN and the substrate, but also of the in-plane rotation of the hBN layer on top of the substrate, and

(c) the substrate and the lattice interact with each other, which often results in modifications of the ideal spatial periodicity of the moiré structures (by ideal periodicity we mean the periodicity that is obtained mathematically from overlapping the hBN and the metal top layer lattices) [136].

The spatial (quasi-)periodicity λ of the moiré patterns of hBN on the Pd(111) surface is a function of the angle θ between two given crystalline directions, one on the hBN sheet (the so called zigzag direction, [1-120]) and the other on the top Pd(111) layer (the [1-10]direction), described by [136]:

$$\lambda = \frac{a_{\mathrm{Pd}} a_{\mathrm{hBN}}}{\sqrt{a_{\mathrm{Pd}}^2 + a_{\mathrm{hBN}}^2 - 2a_{\mathrm{Pd}} a_{\mathrm{hBN}} \cos\theta}}. \tag{4.1}$$

This dependence is important as it constitutes a direct way to assess the crystalline orientation of the hBN layer on the substrate simply by measuring its spatial periodicity in STM images.

The function $\lambda(\theta)$, Equation (4.1), is plotted in Figure 4.1, which shows that the maximum spatial periodicity is achieved for $\theta = 0°$, while the lowest periodicity is achieved for $\theta = 30°$. As an illustrative example, atomic structure models corresponding to the moiré structures of hBN on Pd(111) observed in experiments are shown in Figure 4.2.

While the (horizontal) spatial periodicity λ measured from STM scan has no intrinsic ambiguity other than usual uncertainties associated with the measurements, this is not the case for the height information obtained from STM. The way STM operates [137–141] is based on the tunneling of electrons between a sharp conductive tip and the "sample" (Figure 4.3), which in this case is the hBN-covered palladium. There is a potential difference maintained between tip and sample, and usually the STM is operated in a constant-current mode [138].

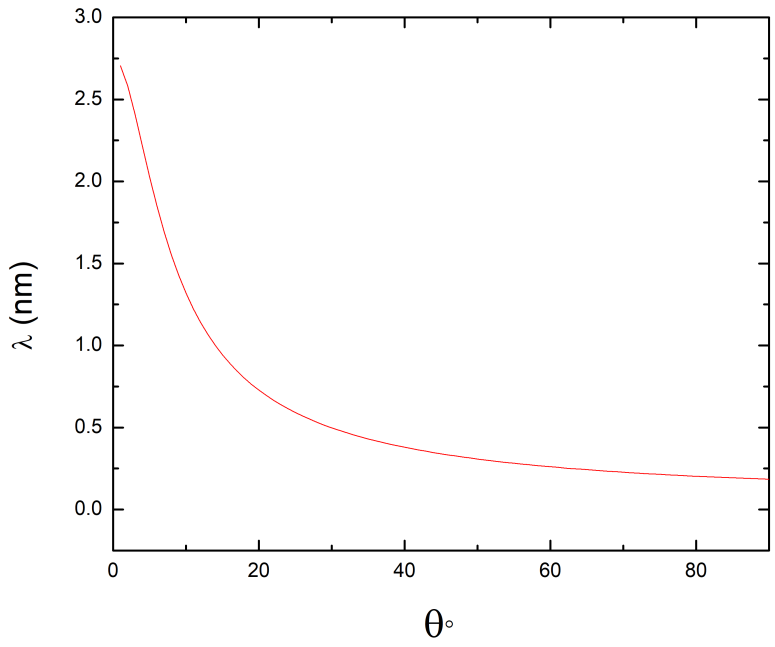

Figure 4.1: The dependence of spatial periodicity λ of orientation θ, Equation (4.1).

In this mode, the current between the tip and the sample is kept constant during the raster scanning of the sample by automatically (feedback loop) changing the distance between the tip and the substrate. If the tip encounters a geometric protuberance, then effectively the tip would be approaching the sample thus increasing the tunneling current: through the feedback look, the tip is subsequently moved upward/away in order to maintain the current at the constant prescribed value. However, another reason why a tip height changes is that there could be regions on the substrate where there exists a larger density of states, and that tends to increase the tunneling current (Figure 4.3): to balance the increase in the current stemming from variable density of states across the sample, the tip height again has to change. Therefore the height profile $z = z(x, y)$ traced by the tip is not always reflecting actual height variations, but very often encumbers both geometric and electronic effects. For this reason, STM height profiles are called apparent height profiles. In the case of 2-D monolayers on metallic substrates, it is already known that there are situations in which the

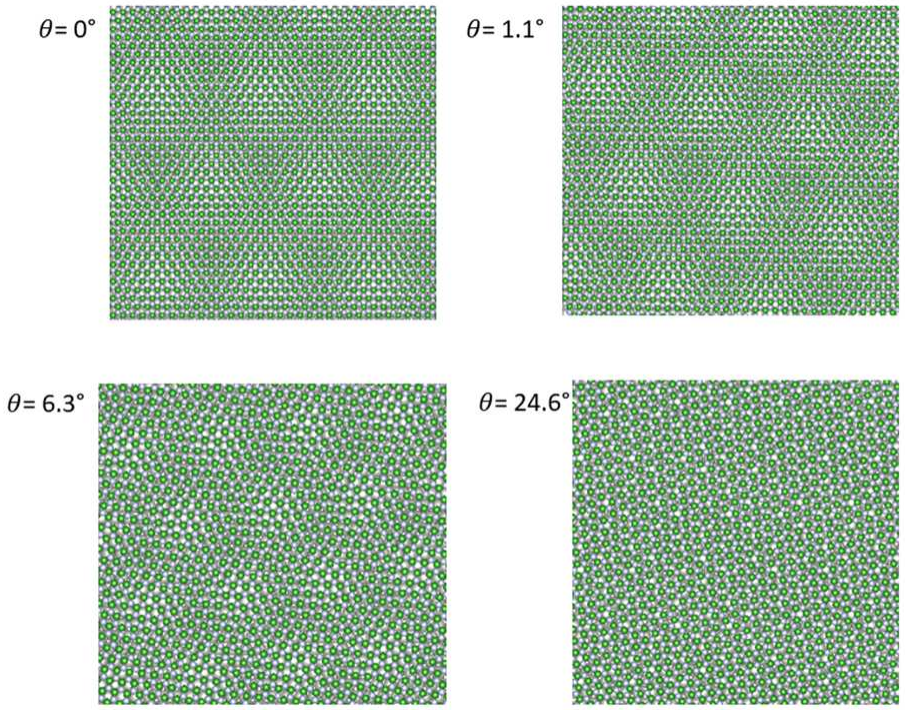

Figure 4.2: Atomic structures for the moiré patterns associated with the experimentally observed periodicities $\lambda = 0.6$, 1.8, 2.7 and 2.8 nm: these periodicities correspond to θ values of 24.6, 6.3, 1.1, and 0.0 °, respectively.

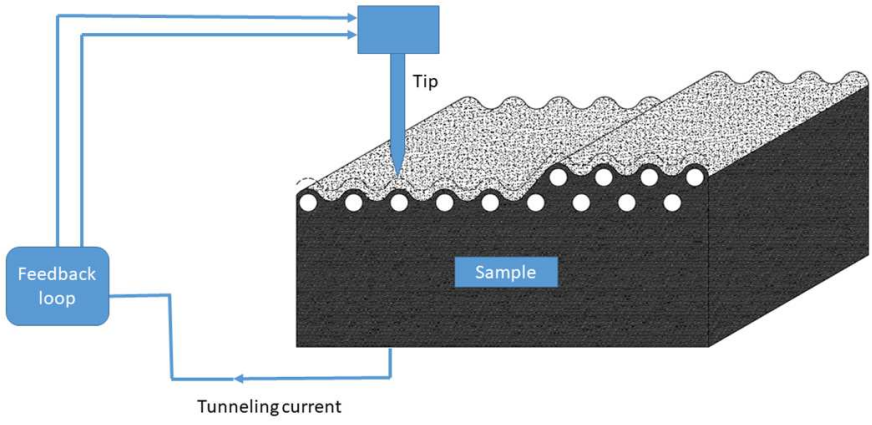

Figure 4.3: Schematic diagram showing the operation of STM. The tunneling current depends on the distance between the tip and the sample, as well as on the density of states of the tip and the sample

apparent height variations or corrugations are mainly electronic in nature (case of graphene or hBN on Cu(111) [142, 143] or mainly geometric in nature (for example, graphene or hBN on Ru(0001) [108, 135, 143]. As we shall see below, in the case of hBN on Pd we can encounter both of these situation, which makes this system unique among other epitaxial monolayers on metallic substrates.

4.3 Experimental Motivation

Figure 4.4 shows the variation of the apparent corrugation (i.e., hill-to-valley height difference) as given by the STM measurements.

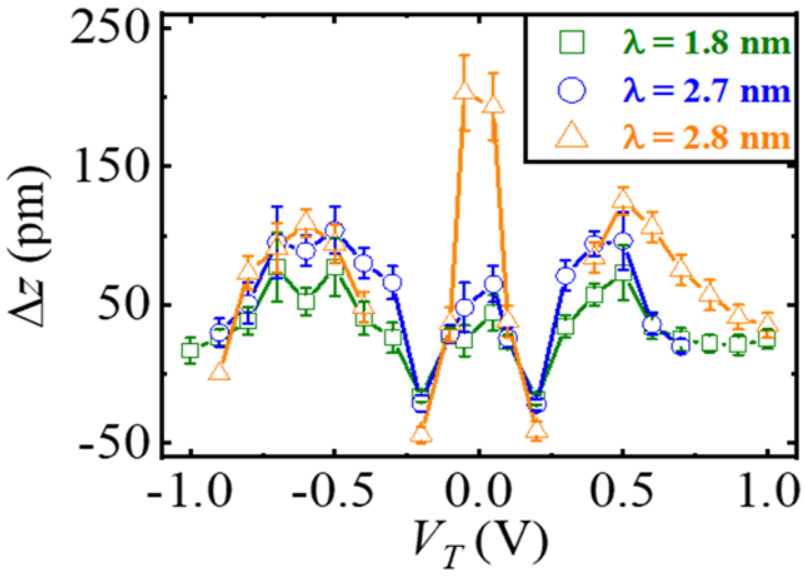

Figure 4.4: Plots of the apparent corrugation Δz as a function of the bias voltage V for a tunelling current I=7.0 nA, for multiple domains: λ=1.8 nm (green squares), 2.7 nm (blue circles), and 2.8 nm (orange triangles). Courtesy of Pedro Arias and Prof. Suneel Kodambaka.

In Figure 4.4, several trends suggests insights into the nature of the apparent corrugation Δz measured in STM. First, there is a significant dependence on the bias voltage for all the curves, which means that the electronic effects are an important part of the apparent height

profiles measured in STM. However, for the spatial periodicities of 0.6, 1.8, and 2.7 nm the values of corrugation at each bias voltage are very similar to each other, practically exhibiting no significant dependence on the periodicity λ. This suggests that the nature of the corrugation is merely electronic in nature, at least for moiré patterns with that have less than maximal periodicity. For the structure with the largest periodicity (corresponding the orientation angle $\theta = 0$) there is a clear jump in the corrugation value Δz in the vicinity of zero bias: since this occurs at very low bias, it is likely that the largest corrugation observed (for λ =2.8 nm) is geometric in nature, with a hill-to-valley distance of approximately 150 pm. This geometric corrugation value is assessed as the difference between the $\Delta z \approx 200$ pm maximum (at $V = \pm$ 50 mV for the 2.8 nm moiré pattern) and the $\approx$ 50 pm value of the corrugation for all the other moiré patterns at $V = \pm$ 50 mV. This estimate effectively amounts to subtracting the mainly electronic corrugation, which we ascribed to all the domains with non-zero orientation angle θ, from the total apparent corrugation observed for the domain with maximal periodicity ($\theta = 0$). In order to rationalize the physical origin of the trends in the STM observations in Figure 4.4, we turn to atomic scale calculations at the level of DFT, and to modeling the interfacial energy of hBN on Pd.

4.4 Details of the DFT calculations.

We have performed the DFT calculations using the Vienna Ab-initio Simulation Package (VASP) [88], with the generalized gradient approximation (GGA) with the Perdew-Burke-Ernzerhof functional [90]. The interactions between hBN monolayer and a Pd(111) substrate are weak [63, 131, 144], and we have incorporated them using the DFT-D2 method of Grimme [112]. There are two types of calculations carried out:

(i) relaxation and electronic structure of the complete hBN monolayer with periodic boundary conditions corresponding to the smallest and largest spatial periodicities observed in experiments;

(ii) hBN flakes ($B_7N_6H_9$, $B_6N_7H_9$, and $B_{12}N_{12}H_{12}$) adsorbed on Pd(111) with different registries and angular orientations, in order to assess the physisorption or chemisorption for

these flakes in the absence of the continuous monolayer.

Figure 4.5 shows the small flakes that we use as molecular probes to investigate the strength of the interactions at the local level, in the absence of possible artifacts that can be induced by using periodic boundary conditions in our computations. In each case, the center of the molecule is placed at one of the four adsorption locations shown in Figure 4.6, namely the top, face-centered cubic (fcc), hexagonal close-packed (hcp), and bridge configurations.

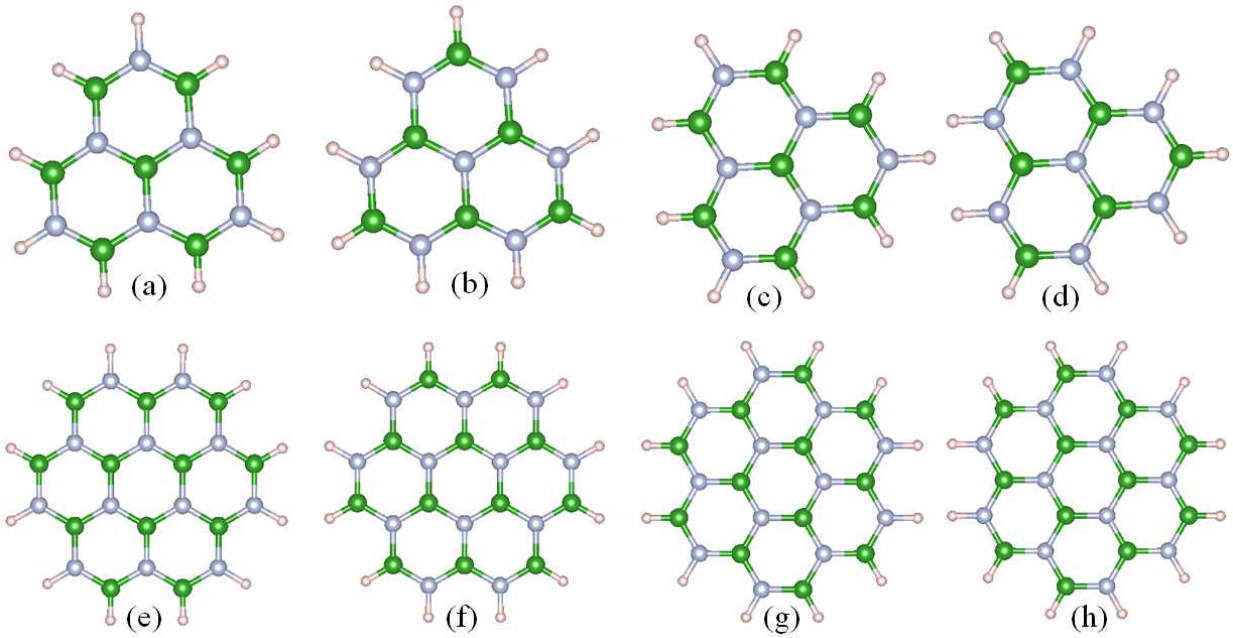

Figure 4.5: Molecular probes used for assessing the local interaction strength via density functional theory (DFT) calculations. The molecules are in two orientations, zigzag (a, b, e, f) and armchair (c, d, g, h). The larger molecule, $B_{12}N_{12}H_{12}$, has two configurations α and β, depending on the succession of the B and N atoms in the central six-atom ring. The center of the molecule is placed above the Pd surface, in a top site, fcc site, hcp site, and bridge bond. These configurations are relaxed, and adsorption energies and the minimum and maximum distance from any atom of the probe molecule to the top Pd layer are reported Tables Table 4.1 and Table 4.2.

For these adsorption calculations, we have employed 5×5 surface unit cells of Pd (four layers, fixed) so as to ensure that the flakes do not overlap with themselves through the use of periodic boundary conditions. The computational cell included an 18 $\AA$ vacuum spacing. The flake structures were relaxed via conjugate-gradient in the presence of dipole corrections

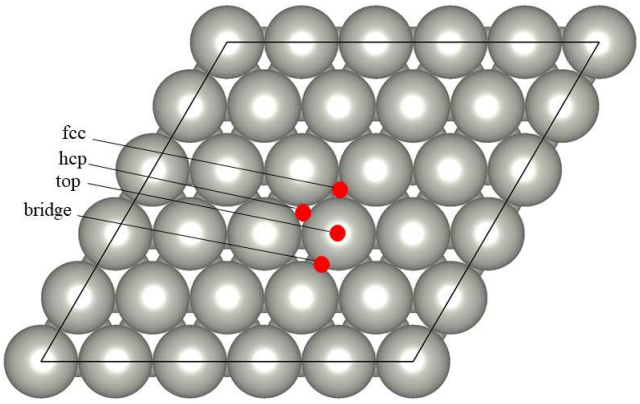

Figure 4.6: Adsorption locations for center of BN-molecules on Pd(111) surface, top, face-centered cubic (fcc), hexagonal close-packed (hcp), and bridge.

using a plane-wave cutoff of 500 eV, a Monkhorst-Pack k-point grid of $3 \times 3 \times 1$, and a force tolerance criterion of 0.02 eV/$\mathring{A}$.

4.5 Results from complete hBN monolayers on Pd

There are several possibilities for the interplay between the electronic and geometric corrugation:

(i) the corrugation is mainly electronic in nature and the hBN monolayer is (nearly) flat, similar to hBN/Cu(111) [145];

(ii) the corrugation is short-ranged, and no moiré patterns arise, akin to that of commensurate 1×1 hBN/Ni(111) [146];

(iii) the corrugation is mainly geometric, similar to the moiré patterns formed by hBN or graphene on Ru(0001) [143, 147];and, finally,

(iv) one in which there is a moiré pattern with meaningful contributions from both electronic and geometric effects.

Based on binding energy assessments previously published [92], we rule out the commensurate 1×1 structures, (ii). As mentioned, Figure 4.4 shows significant dependence of Δz on the bias V, which rules out case (iii) for the structures with $\lambda = 1.8$ nm and 2.7 nm, which

exhibit similar variations of the corrugation with bias voltage despite the fact that they have very different orientations. The structure with $\lambda = 0.6$ nm periodicity also does not have any significant geometric corrugation ($\approx$ 3pm, from our DFT calculations) because its periodicity is too short to accommodate vertical oscillations. For this structure (Figure 4.7), we have also performed calculations of the electronic structure and density of states at the surface. The results of these calculations are shown in Figure 4.8. Due to the presence of the metallic substrate, the bandap of hBN [shown for free-standing sheets in Figure 4.8(a)] decreases to about 3.2 eV [Figure 4.8(b)]. This is consistent with our calculations of local density of states at the surface [Figure 4.8(c)] , which shows the same bandgap.

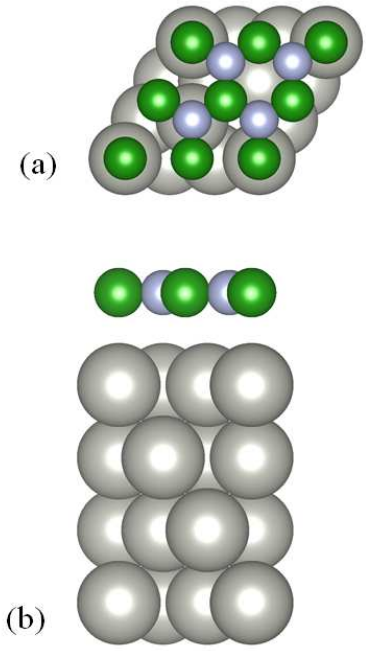

Figure 4.7: Small hBN/Pd unit cell for calculations of electronic properties, (a) top view, (b) side view.

Returning to the discussion of corrugation, the structures with $\lambda = 0.6$, 1.8, and 2.7 nm display a corrugation which is mainly electronic in nature, although we cannot fully rule out a small geometric component. For $\lambda = 2.8$ nm, we notice a sharp increase in the corrugation close to zero bias, which is not present for any of the other cases at any bias voltage.

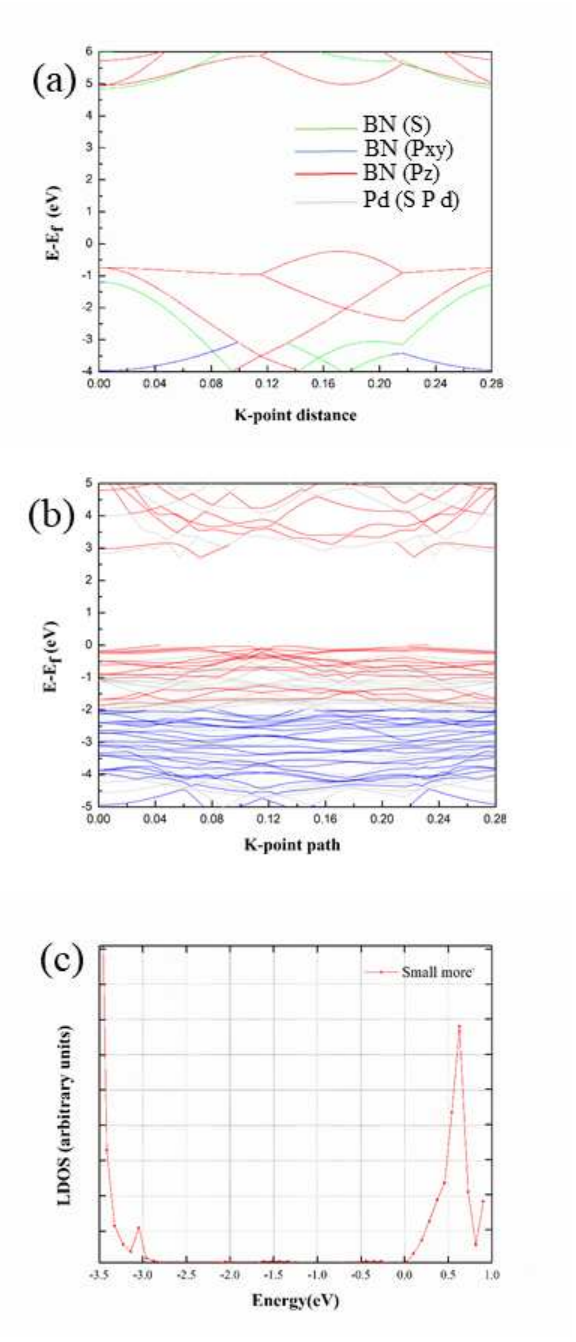

Figure 4.8: (a) Band structure of free-standing hBN. (b) Bandstructure of hBN/Pd for the surface unit cell shown in Figure 4.7. (c) Local density of states at the surface.

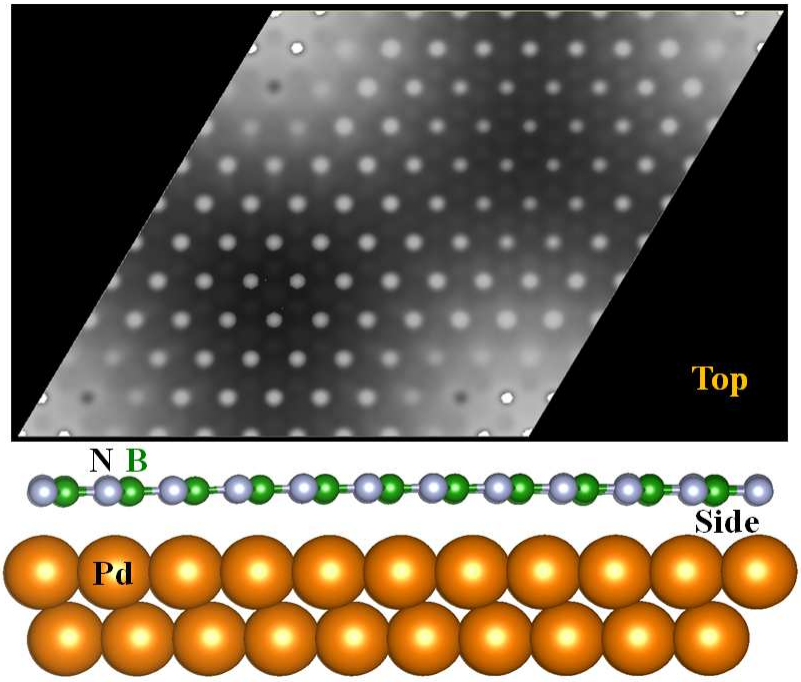

Figure 4.9: Simulated STM image for a supercell with 11×11 hBN on 10×10 Pd substrate. The top view shows the simulated STM image (sharp white dots are the N atoms beneath) with obvious large scale moiré pattern (color gradient) and the side image shows the relaxed atomic structure without any noticeable geometric corrugation of the hBN monolayer.

We performed further DFT in order to understand the different contributions (geometric vs. electronic) to the measured STM corrugation. The 2.7 ± 0.20 nm and 2.8 ± 0.14 nm moiré structures have significantly different corrugations (Figure 4.4), despite the fact that their periodicities are the same within the experimental uncertainties: this prompted us to investigate more closely the possibility that the both geometrically flat and geometrically corrugated structures could be encountered in domains with very similar orientations around $\theta = 0$. We note that an atomically flat layer can occur under conditions of commensurability: for example, at $\theta = 0$, a 10×10 Pd substrate with the lattice constant of $a_{\mathrm{Pd}} = 0.275$ nm is perfectly commensurate with an 11×11 hBN monolayer with $a_{\mathrm{hBN}} = 0.250$ nm. This is a very likely configuration for the structure with the largest spatial periodicity. Due to commensurability, a geometrically corrugated structure with this precise in-plane unit cell would involve straining the B-N bonds to create hills and valleys, which would in turn require high energetic penalties and hence does not occur. We have tested this assertion using DFT calculations for this orientation and periodicity (11×11 hBN on 10×10 Pd): the perfectly commensurate hBN layer with $\theta = 0$ and $\lambda = 2.75$ nm remains flat and settles a distance of 280 pm from the substrate. The bonding character with the substrate is necessarily mixed: it cannot be purely vdW, since that would require about 320 pm separation from the substrate. The DFT calculations for the 2.75 nm structure shows that the layer remains nearly flat, with no noticeable geometric corrugation (6). However, the STM simulated image for the 2.75 nm moié structure displays a large scale corrugation pattern (Figure 4.9). This is consistent with the STM measurements that show similar corrugations for structures with periodicities of 0.6, 1.8, 2.7 nm, and support the earlier assertion that the corrugation for these structures is mainly electronic in nature.

4.6 Results from adsorption of molecular probes

We have also tested the possibility that a significant geometric corrugation may develop for the maximal moiré periodicity $\lambda = 2.8$ nm, which is strongly suggested by the measurements in Figure 4.4 showing an additional 150 pm corrugation difference between the moiré

pattern at $\theta = 0$ and the other hBN domains. In order to do this and avoid computational artifacts stemming from the use of fixed periodic boundary condition in the surface plane, we have decided to locally test the hBN/Pd bonding by using small 2-D molecular flakes ($B_7N_6H_9$, $B_6N_7H_9$, and $B_{12}N_{12}H_{12}$) placed at different locations around the Pd substrate and studying the distance at which they settle with respect to the substrate. At certain orientations (0 and 30°) and registries above the substrate, these molecular flakes simulate various portions of a complete hBN/Pd layer (Figure 4.10).

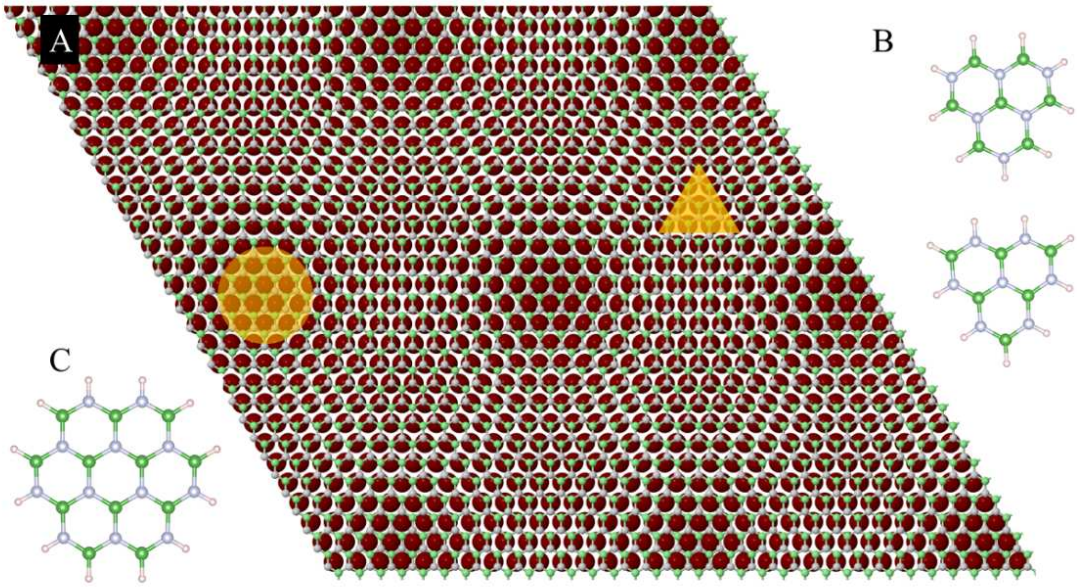

Figure 4.10: (a) Structure of the hBN/Pd(111) with maximal periodicity, obtained from flat layers with lattice constants ahBN = 0.250 nm and aPd(111) = 0.275 nm. Small flakes (b) $B_7N_6H_9$ (top) and $B_6N_7H_9$ (bottom) and (c) $B_{12}N_{12}H_{12}$ employed to determine the adsorption tendencies for different portions (highlighted) of the moir structure. The circular region is van der Waals (vdW) bonded to the substrate, while the triangular region represents the strongest bonded core of the remaining chemically-bonded area in the unit cell.

We have used the flakes to effectively probe the strength of the interaction and the height of the flake with respect to the substrate. Depending on the location on the substrate, the $B_7N_6H_9$ and $B_6N_7H_9$ flakes experience mostly localized geometric corrugations ranging from 8 pm to 56 pm and can settle such that the minimum distance to the substrate ranges from

214 pm to 257 pm (Table 4.1). There is no doubt that the distance of 214 pm is indicative of strong chemical bonding similar to that one encountered for hBN on Ni [125, 125, 131]. On the other hand, the larger flakes ($B_{12}N_{12}H_{12}$) experience bowing even though they are only about 1 nm wide (Table 4.2). The bowing corresponds to a geometric corrugation of 90 pm achieved between its center (295 pm away from the substrate) and periphery (205 pm away): this value can be viewed as a crude estimate of the actual geometric corrugation of the $\lambda = 2.8$ nm structure, in which most of the local interfacial configurations probed using our small flakes are present. An inspection of Figure 4.10 suggests that better estimate of the geometric corrugation can be glean from the molecular probe results as the height difference between the z_{max} value from the large bowed molecule $B_{12}N_{12}H_{12}$ from the substrate, and the z_{min} value corresponding to a small strongly bounded flake, i.e. $\approx$ 83 pm (Table 4.1, Table 4.2). This is still only about 55% of the value estimated from STM (Figure 4.4: this is likely to occur because of our method of using unconnected flakes to probe the interaction, so the order of magnitude agreement suffices.

Table 4.1: Adsorption energy (E_{ads}) and the minimum (z_{min}) and maximum (z_{max}) distance between atoms in the small molecular probs $B_7N_6H_9$ and $B_6N_7H_9$ on Pd(111).

Edge shape	Molecules	Positions	E_{ads}(eV)	z_{min}(nm)	z_{max}(nm)
Zigzag	$B_7N_6H_9$	top	-3.5344	0.234	0.246
		fcc	-2.9517	0.257	0.280
		hcp	-3.5160	0.220	0.250
		bridge	**-3.5669**	0.214	0.256
	$B_6N_7H_9$	top	**-3.0471**	0.254	0.262
		fcc	-2.7690	0.254	0.291
		hcp	-3.0223	0.242	0.265
		bridge	-3.0210	0.219	0.265
Armchair	$B_7N_6H_9$	top	**-3.6227**	0.234	0.246
		fcc	-3.3029	0.234	0.260
		hcp	3.5172	0.218‘	0.258
		bridge	-3.2502‘	0.215	0.271
	$B_6N_7H_9$	top	-2.9631	0.241	0.273
		fcc	**-2.9971**	0.248	0.264
		hcp	-2.9568	0.252	0. 270
		bridge	-2.9801	0.244	0.275

Table 4.2: Adsorption energy (E_{ads}) and the minimum (z_{min}) and maximum (z_{max}) distance between atoms in the large molecular probs $B_{12}N_{12}H_{12}$ on Pd(111).

Edge shape	Molecules	Positions	E_{ads}(eV)	z_{min}(nm)	z_{max}(nm)
Zigzag	$B_{12}N_{12}H_{12}$-α	top	-4.948	0.248	0.297
		fcc	-5.6716	0.227	0.268
		hcp	-5.1902	0.257	0.276
		bridge	**-5.6580**	0.210	0.262
	$B_{12}N_{12}H_{12}$-β	top	-5.0444	0.246	0.294
		fcc	-5.1994	0.259	0.273
		hcp	-5.4870	0.219	0.276
		bridge	**-5.5431**	0.209	0.266
Armchair	$B_{12}N_{12}H_{12}$-α	top	-5.1724	0.239	0.270
		fcc	-5.2846	0.211	0.290
		hcp	**-5.2988**	0.208	0.290
		bridge	-5.1856	0.226	0.282
	$B_{12}N_{12}H_{12}$-β	top	-5.1715	0.240	0.270
		fcc	-5.2855	0.210	0.283
		hcp	**-5.2996**	0.205	0.294
		bridge	-5.1850	0.225	0.282

4.7 Model for the energetic competition between blistered and flat structures

The strength of the chemical bond between hBN and Pd may be influenced by the orientation θ between BN clusters and the Pd surface similar to the case of graphene/Pd(111) [132]. Given the above DFT results from the molecular probes, we hypothesize that axial strain in the bonds can be avoided for (incommensurate) hBN layers that have in excess of 11×11 hBN unit cells within the (average) maximal moiré structure of 2.8 nm. In this case, axial strain is traded for bending strains, which are significantly lower and can lead to the formation of "blisters", i.e. geometric corrugations. These blisters can be supported (or pinned to the substrate at their periphery) if the binding energy for the regions closest to the substrate is sufficiently strong. We now describe a simple model of the energetic competition between the flat and blistered configurations of the hBN monolayer on the substrate, with the goal of assessing the possibility of blister formation on a moiré pattern with (average) maximal periodicity. Within a moiré period, we calculate the interface energy per area starting from

three (positive) binding energies:

(i) E_{ch} , an average (per area) corresponding to regions of the moiré structure that are chemically bonded to the substrate (interlayer distance 230 pm) [148],

(ii) E_{vdW}, corresponding to regions that are vdW bonded (interlayer distance $\sim$ 320 pm), and

(iii) E_f, corresponding to an atomically flat monolayer situated at an intermediate distance, e.g., 280 pm.

While E_{ch} and E_{vdW} are local averages for their corresponding regions (close or far from the substrate, respectively), E_f is a function of θ whose value is averaged over the *entire* (periodic) area, which is an increasing function of the misorientation angle θ, based on graphene on Pd results [149].

We first derive the interfacial energy of the monolayer with periodic geometric corrugation in the form of blisters, and subsequently compare it to that of a flat monolayer. The blistered monolayer has the schematic profile in Figure 4.11, wherein the lower regions are approximated as flat and strongly bonded to the substrate (binding energy per area E_{ch}), and the upper regions are approximated as spherical segments that are vdW bonded to the substrate (E_{vdW}). The model is qualitative and meant to capture the main features of the interface energy of the blistered layer; as such, it neglects in the first approximation the transition region between the flat portions and the spherical segments. The geometric parameters are the height of the spherical calotte, h, the radius of the sphere, ρ, and the radius of the circular projection of the blister R.

The total interfacial energy γ_{b} per unit area of the blistered periodic structure can be written as:

$$\gamma_b(R,\lambda) = \frac{2}{\lambda^2\sqrt{3}}[-E_{ch}(\frac{\lambda^2\sqrt{3}}{2} - \pi R^2) - E_{vdw}\pi R^2 + Mk^2\pi R^2] \tag{4.2}$$

where $\lambda^2\sqrt{3}/2$ is the area of the moiré surface cell with the periodicity λ, M is the bending modulus of the hBN monolayer and κ is the curvature of the spherical segment. Equation

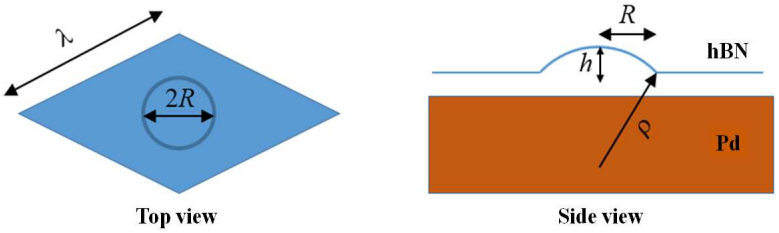

Figure 4.11: Schematic of a surface unit cell of hBN/Pd with a blistered configuration. The blister is approximated as a spherical calotte of height h and base radius R.

(4.2) combines the energies of the two regions shown in Figure 4.11 (both negative because of the positive binding), with the elastic energy of the (bent) spherical portion (positive), and to obtain the interface energy (per area) γ_b, which is a function of the radius R and the periodicity λ. The curvature κ of the blister can be estimated as:

$$\kappa = \frac{1}{\rho} = \frac{2h}{R^2 + h^2} \approx \frac{2h}{R^2} \tag{4.3}$$

where the height h is neglected in comparison to R in the denominator. Substituting (4.3) in (4.2), we obtain the interface energy as a function of R and λ:

$$\gamma_b(R, \lambda) = \frac{2}{\lambda^2\sqrt{3}}[-E_{ch}(\frac{\lambda^2\sqrt{3}}{2} - \pi R^2) - E_{vdw}\pi R^2 + \frac{M4\pi h^2}{R^2}] \tag{4.4}$$

At a fixed periodicity λ, the radius R should be optimal, i.e., it should assume the value R^* that minimizes the interface energy Eq. (4.4). Setting to zero the derivative $\mathrm{d}\gamma_b/\mathrm{d}R$, we obtain:

$$R^* = \left(\frac{4Mh^2}{E_{ch} - E_{vdw}}\right)^{1/4} \tag{4.5}$$

The minimum energy is then obtained by substituting (4.5) into (4.4), so that the minimum interface energy of the blistered configuration becomes a function only of λ:

$$\gamma_b = -E_{ch} + \frac{8\pi h\sqrt{M(E_{ch} - E_{vdw})}}{\lambda^2\sqrt{3}} \tag{4.6}$$

Given than the periodicity is related to the misorientation angle [136] via:

$$\lambda(\theta) = \frac{a_{pd}a_{hBN}}{\sqrt{a_{pd}^2 + a_{hBN}^2 - 2a_{pd}a_{hBN}\cos\theta)}} \tag{4.7}$$

the interface energy γ_b can be expressed as a function of the misorientation θ as:

$$\gamma_b = -E_{ch} + \frac{8\pi h\sqrt{M(E_{ch} - E_{vdw})}}{\sqrt{3}}\left(\frac{1}{a_{pd}^2} + \frac{1}{a_{hBN}^2} - \frac{2\cos\theta}{a_{pd}a_{hBN}}\right) \tag{4.8}$$

This energy is to be compared with the interfacial energy γ_f of a flat hBN monolayer (no significant geometric corrugation), which is a monotonically decreasing function of θ based on results derived for graphene on Pd(111) [149]. The comparison of interfacial energies for the flat and blistered configurations is illustrated in Figure 4.12. The relationship between the binding energies is necessarily $E_{ch} > E_f(\theta = 0) > E_{vdW}$, based on the corresponding distances with respect to the substrate. This inequality is not changed by the addition of the constant terms proportional to $\sqrt{M}$ in Eq. (4.8), and thus leads to the interface energy curves " γ_b and γ_f with the relative positions shown in Figure 4.12. At $\theta = 0$, $E_{ch} > E_f$ requires that $\gamma_b < \gamma_f$, which shows that the blistered configuration is favorable at least at $\theta = 0$. However, given that γ_b decreases with θ while γ_f increases, the two curves necessarily intersect (Figure 4.12), and the flat configuration becomes more stable at a nonzero angle θ_c. Based on experiments which show both blistered and flat configurations at similar periodicities (2.7-2.8 nm), the intersection must occur at a small angle $\theta_c \sim 1°$. The fact that the critical angle is small amounts to a bifurcation behaviour in which for angles that are slightly below θ_c it is energetically favorable for the surface to develop blisters, and for angles above θ_c a flat monolayer settling at a distance closer to the vdW separation (rather than to the interlayer spacing corresponding to strong bonding) is preferred.

4.8 Conclusions

In conclusion, we used DFT to understand the geometric and electronic contributions to the apparent surface corrugation measured by STM on multiple hBN domains on Pd(111). We have found that for most hBN domains on Pd, the apparent corrugation is mostly

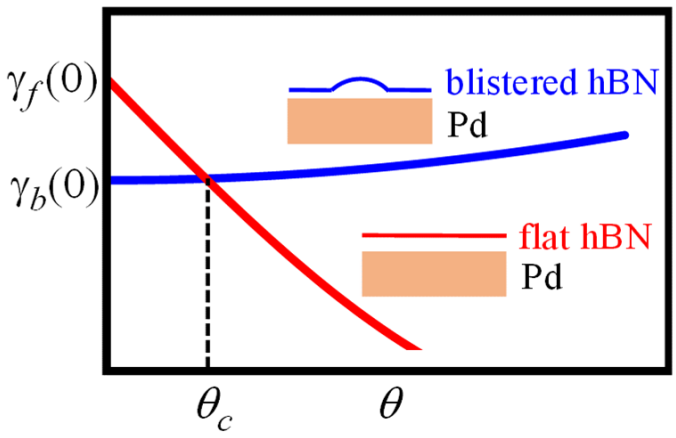

Figure 4.12: Schematic of a surface unit cell of hBN/Pd with a blistered configuration. The blister is approximated as a spherical calotte of height h and base radius R.

electronic in nature. For domains of maximal or near maximal periodicity, we found that geometric blisters could form on hBN via the interplay of chemical binding, vdW binding, and bending within the moiré period: this was inferred by a general (yet qualitative) model for this behavior and for the associated interface energy of the blistered configuration. The existence of both flat and blistered domains on supported 2-D hBN is atypical, and in the case of hBN/Pd it is enabled by the intermediate binding energy per unit area, i.e. between strong (akin to Ni [131] or Ru [150]) and weak (akin to Cu [131] or Pt [117]). We expect similar bifurcation behavior to occur on hBN when supported by other substrates with intermediate interactions, not necessarily metallic ones (for example, metal oxides). This behavior can potentially be used to control of the templated self-organization of molecules or nanocrystals on hBN/Pd(111), as they could form either sparse patterns or compact agglomerations on the same hBN monolayer depending on whether its structure is blistered or flat.

CHAPTER 5

MECHANICAL AND ELECTRONIC PROPERTIES OF 2-D SILICA

Synopsis: With the quest for newer and more inexpensive 2-D materials well underway, there have recently been proposals for layers phases of silica, SiO_2. The material itself is certainly inexpensive, but at the present is not well understood what the best conditions to grow it are or what is the range of structure and properties that can be attained from this 2-D material. In order to gain insight into the properties that can be derived from 2-D phases of silica, in this chapter we propose several 2-D silica configurations and calculate their electronic and mechanical properties. Using DFT calculations, a wide variety of properties are predicted. These properties could serve to guide future growth efforts, as well as serve as a starting point for future simulation efforts aimed at understanding how the presence of substrates (metallic or semiconducting) may alter the properties of 2-D silica grown on them.

5.1 Introduction

Three dimensional silica (SiO_2, sometimes with deviations from this composition, SiO_x) has a very rich phase diagram [151], with a large number of phases present. At ambient pressures, the local environment of the Si atoms is a tetrahedron with oxygen corners, while at high pressure the Si atom is the center of octahedra [152]. Silica is a ceramic with large bandgap for both crystalline and amorphous phases. These structures are all made of tetrahedra centered on Si atoms and having O atoms as corners. The tetrahedra usually share the O-atom corners and thus they make up the structure in three dimensions: $\alpha-$quartz, $\beta-$quartz, cristobalite, other crystalline phases Figure 5.1), or amorphous (Figure 5.2). Interestingly, in the amorphous structure the tetrahedra are sharing corners in the same way as in the crystals, only they do not have long range order. Silicon wafers spontaneously "cover" themselves with amorphous layer(s) of silica when they are in contact with ambient

atmosphere, and this insulating layer contributes to their passivation. This passivating layer is usually hundreds of nanometers thick (amounts to what is called a thin film), and has found uses in electronics industry as dielectric layer [153], as well as in catalysis [154]. In light of these technological applications, it would be interesting to attempt to create periodic arrays or crystalline 2-D silica layers instead of the naturally occurring amorphous ones, since the properties of crystalline layers are more reproducible and display less variation –which could be important at least for catalytic applications that require a large number of active catalytic sites per unit area.

In general, lowering dimensionality of a material may or may not lead to new structural configurations being formed. For example, in the case of graphene there is no difference between the layers in graphite and those in graphene. However, other materials may adopt new structures with lowering the dimensionality. In general, there are fully developed global optimization methods for surface reconstructions and supported 2-D materials [155–162], as well as for 1-D nanostructures [162–166]. In recent years, a number of 2-D silica structures were proposed using DFT calculations [167–172]. Some of these structures are shown in Figure 5.3, and they can be single layers or bilayers. Experimentally, these 2-D structures (Figure 5.3) have not yet been realized, but recent efforts have been successful at growing 2-D phases of silica and germania on metals [173–177]. The metallic substrate stabilizes these 2-D phases, offering them both support and stability against decay or wrinkling: the layers are made of Si-centered tetrahedra in which an O plane made of three corners is exposed at the surface, while the fourth oxygen is strongly bonded to the metallic substrate (Figure 5.4).

In this chapter, we describe DFT calculations that show how much the properties of 2D silica layers vary with the specific configuration. These efforts are important in that they show very wide electronic behaviour, from metallic, to semiconductor, to insulator. The results could serve as guide for future experiments aimed at producing inexpensive 2D materials with a specifically desired electronic bandgap.

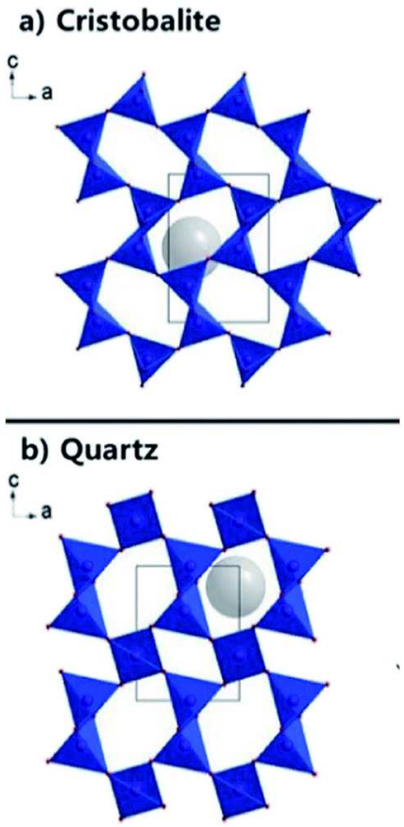

Figure 5.1: Common 3D crystalline phases of silica. From [178], with permission of Royal Society of Chemistry.

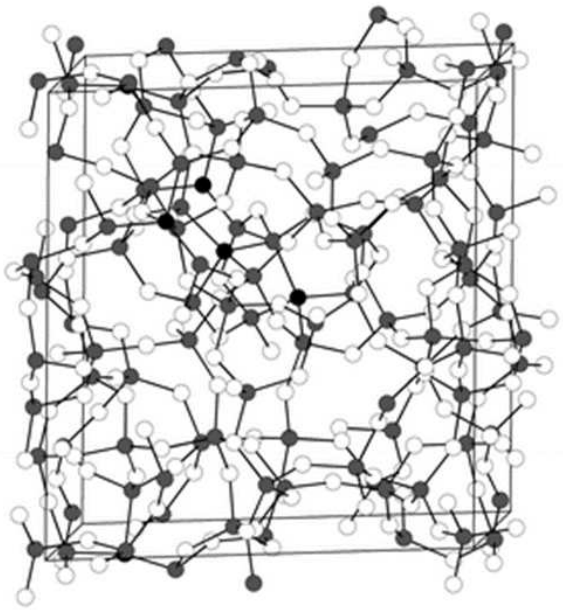

Figure 5.2: 3D amorphous phase of silica. From [179], with permission of Royal Society of Chemistry.

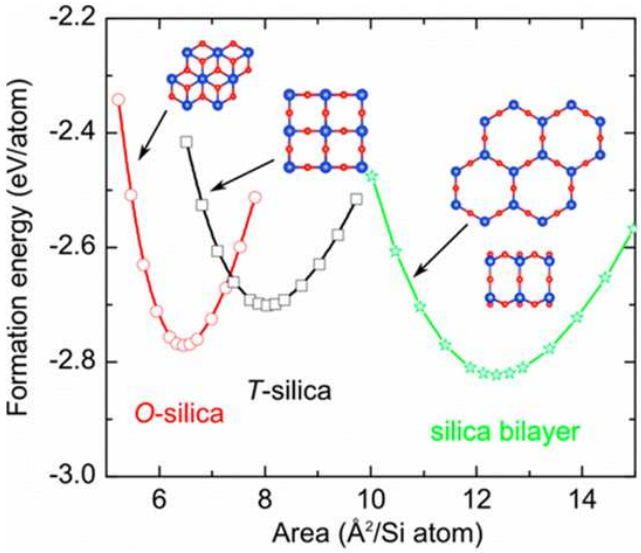

Figure 5.3: Theoretical 2D phases of silica proposed in the literature [172] and their formation energy. Reproduced with permission from American Chemical Society.

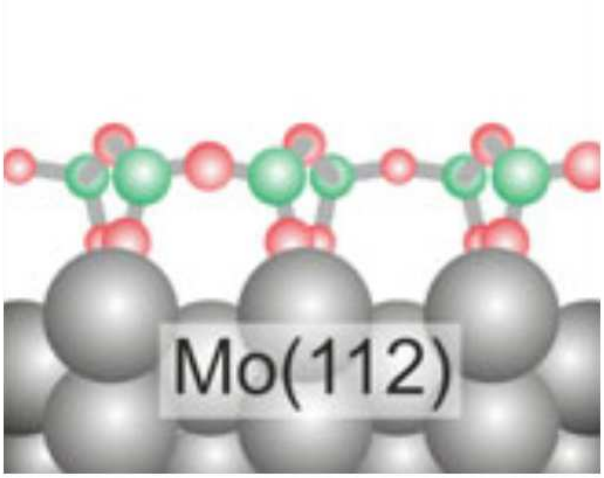

Figure 5.4: Silica 2D layer epitaxially grown on Molybdenum from Ref. [180]. Reproduced with permission from the Institute of Physics.

5.2 Description of the simulation protocol

One of the methods to control the properties of materials is to change their atomic structure and their chemical composition. We have examined six different structures of 2D Silica. We performed DFT calculations within the framework of the generalized gradient approximation (GGA) [90], using the projector-augmented wave (PAW) potentials [181]. Each 2D SiO_x structure is subjected to the same simulation protocol, described below.

- Obtaining relaxed structure

  While the atomic structure (stored in the POSCAR file, which is the geometry input to the DFT package called VASP) are easy to construct using Matlab programming, they do not necessarily have the precise lattice parameter and interatomic bond lengths. Because of that, the first step in the protocol is to carry out atomic relaxations. In these relaxations, atoms are moved slightly in the direction of force gradients until the total energy has come to a local minimum. In this process, not only the atoms are

allowed to relax, but the lattice parameters of the 2D crystal as well.

- Calculating mechanical properties

  Mechanical properties, in particular the stiffness matrix C_{ijkl}, can be computed after relaxation by setting appropriate commands in the VASP command file called INCAR. These stiffness's are calculated by taking the numerical derivatives of the total energy with respect to strain components in different directions [182]:

$$C_{ijkl} = \frac{\partial^2(E/V)}{\partial\epsilon_{ij}\partial\epsilon_{kl}}, \tag{5.1}$$

  where E is the elastic energy stored in the domain of volume V of the crystal subjected to the appropriate deformations.

- Density of state (DOS) calculation

  The density of states (DOS) is essentially the number of states (per unit volume) that fall within an interval $(E, E+\Delta E)$ of energies. As such, DOS is a function of the energy E, and can give us information on the electronic nature of the material. Moreover, various partitions of the DOS (e.g., per atom, per type of angular momentum, spin etc) give even more detailed information about bonding and about the available states for, e.g. , interactions with the environment.

  The calculations of DOS is triggerred by specific commands in the input files, commands that results also in the storage of electron density at every point in space (CHGCAR file) and the complex wavefunctions of occupied and unoccupied states of the electrons (stored in the binary WAVECAR file) . These files are used for the calculations of band structures, which are dispersion relations of the type $E_n(\mathbf{k})$, where n is the band index and $\mathbf{k}$ is the wave vector of the electrons in the material; the wave vector is the momentum of electron up to the multiplicative Plank's constant.

- Band structure calculation

  Calculations of the band gap of materials are important in order to classify the materials as semiconductors, insulators, or metals. For band structure calculations, we need to use two output files, WAVECAR and CHGCAR from density of state DOS calculation as input files for the computation of the dispersion relationship $E_n(\mathbf{k})$. The band structure and DOS is extracted from the VASP output file called vasprun.xml.

5.3 Proposed structures of 2D silica

Six different geometrical configurations have been examined. These configurations differ in terms of:

(i) how the tetrahedra are connected in 2D (sharing corners or sharing edges),

(ii) what type of interstices are developing in the 2D lattice (triangular holes or hexagonal holes), and

(iii) whether all tetrahedra are on the same side of the base plane or not.

The six structures, labelled 1 through 6, fall into two categories: structures with corner-sharing tetrahedra (1 through 4), and those with edge-sharing tetrahedra (5,6).

Structure 1

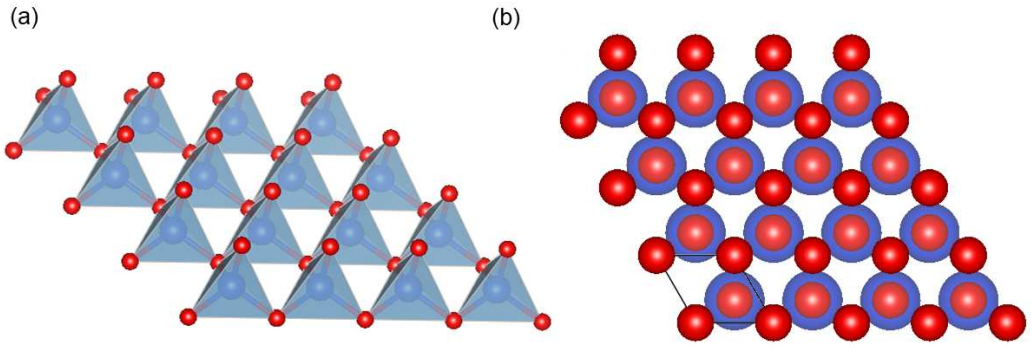

Figure 5.5: Atomic structure of 2D silica where the tetrahedra share corners, forming triangular holes, with all tetrahedra on one side of the surface: (a) perspective view showing the Si-centered tetrahedra, and (b) top view, with atoms shows as red (O) or blue (Si) spheres.

Figure 5.5 shows the suggested atomic structure of 2D silica where the tetrahedra share corners forming triangular holes with all tetrahedra on one side of the surface. The lattice vectors of the primitive cell and their unit in angstrom (Å) are:

$$\mathbf{a} = a\,\hat{\mathbf{i}} \tag{5.2}$$

$$\mathbf{b} = -\frac{1}{2}b\,\hat{\mathbf{i}} + \frac{\sqrt{3}}{2}b\,\hat{\mathbf{j}} \tag{5.3}$$

$$\mathbf{c} = c\,\hat{\mathbf{k}} \tag{5.4}$$

where: $a = b = 2.678$ Å , and $c = 20$ Å ,

Structure 2

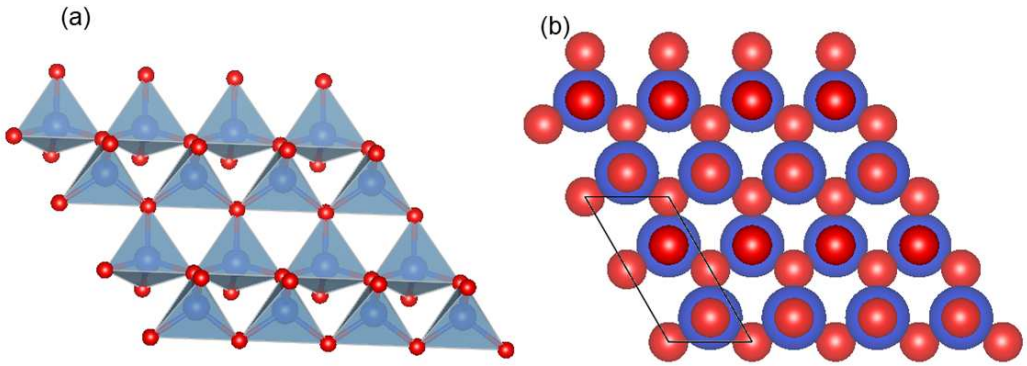

Figure 5.6: Atomic structure of 2D silica where tetrahedra share corners, forming triangular holes with half of tetrahedra on each side of the surface:(a) perspective view showing the Si-centered tetrahedra, and (b) top view, with atoms shows as red (O) or blue (Si) spheres.

Figure 5.6 demonstrates the way to distribute the tetrahedra equally in two existing sides of the surface. The lattice vectors of the primitive cell and their unit in angstrom (Å) are:

$$\mathbf{a} = 2a\,\hat{\mathbf{i}} \tag{5.5}$$

$$\mathbf{b} = -\frac{1}{2}b\,\hat{\mathbf{i}} + \frac{\sqrt{3}}{2}b\,\hat{\mathbf{j}} \tag{5.6}$$

$$\mathbf{c} = c\,\hat{\mathbf{k}} \tag{5.7}$$

where: $a = 2.678$Å , $b = 5.356$ Å and c= 20 Å

Structure 3

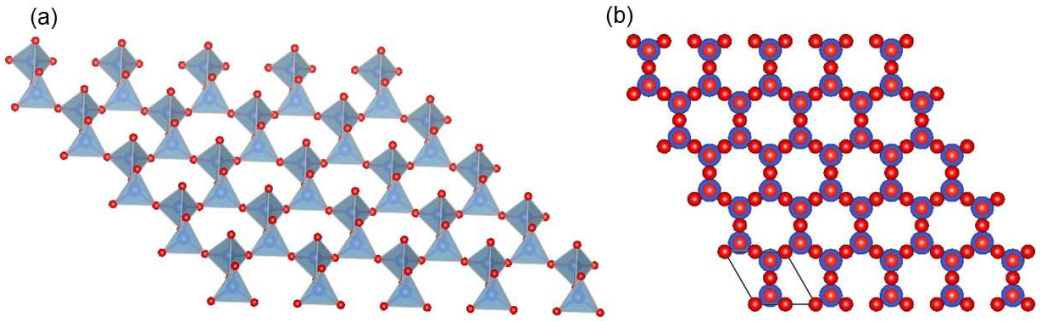

Figure 5.7: Atomic structure of 2D silica where the tetrahedra share corners, forming hexagonal holes with all tetrahedra on one side of the surface:(a) perspective view showing the Si-centered tetrahedra, and (b) top view, with atoms shows as red (O) or blue (Si) spheres.

The Figure 5.7 shows the atomic structure of 2D silica where the tetrahedra share corners, forming hexagonal holes with all tetrahedra on one side of the surface. Lattice vectors in angstrom (Å) are:

$$\mathbf{a} = a\,\hat{\mathbf{i}} - \frac{1}{2}b\,\hat{\mathbf{i}} \tag{5.8}$$

$$\mathbf{b} = -\frac{1}{2}b\,\hat{\mathbf{i}} + \frac{\sqrt{3}}{2}b\,\hat{\mathbf{j}} \tag{5.9}$$

$$\mathbf{c} = c\,\hat{\mathbf{k}} \tag{5.10}$$

where: $a = b = 5.356$ Å and c= 20 Å

Structure 4

From the Figure 5.8 the atomic structure of 2D silica where the tetrahedra share corners, forming hexagonal holes with half of tetrahedrons on each side of the surface. The lattice vectors in angstrom (Å) are:

$$\mathbf{a} = a\,\hat{\mathbf{i}} - \frac{1}{2}b\,\hat{\mathbf{i}} \tag{5.11}$$

$$\mathbf{b} = -\frac{1}{2}b\,\hat{\mathbf{i}} + \frac{\sqrt{3}}{2}b\,\hat{\mathbf{j}} \tag{5.12}$$

$$\mathbf{c} = c\,\hat{\mathbf{k}} \tag{5.13}$$

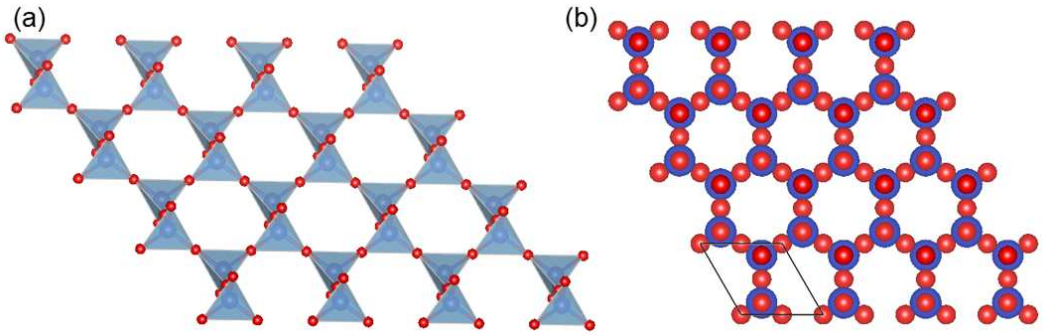

Figure 5.8: Atomic structure of 2D silica where the tetrahedra share corners, forming hexagonal holes with half of tetrahedra on each side of the surface:(a) perspective view showing the Si-centered tetrahedra, and (b) top view, with atoms shows as red (O) or blue (Si) spheres.

where: $a = b = 5.356$ Å and c= 20 Å

Structure 5

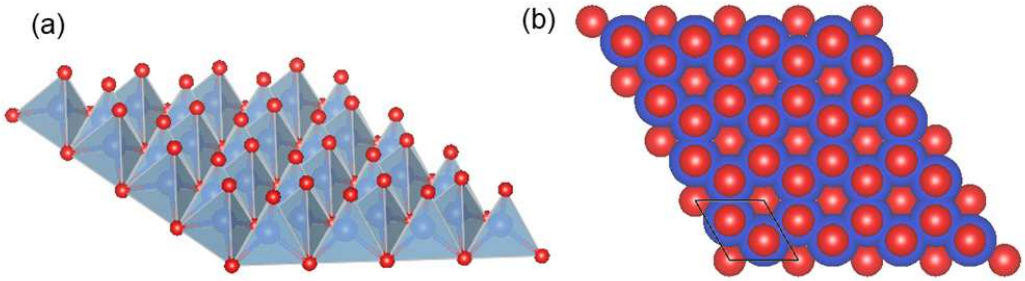

Figure 5.9: Atomic structure of 2D silica where the tetrahedra share edges, all the tetrahedra on one side of the surface:(a) perspective view showing the Si-centered tetrahedra, and (b) top view, with atoms shows as red (O) or blue (Si) spheres.

From the Figure 5.9, the atomic structure of 2D silica where the tetrahedra share edges, all the tetrahedra on one side of the surface. The lattice vectors in angstrom (Å) are:

$$\mathbf{a} = a\,\hat{\mathbf{i}} \tag{5.14}$$

$$\mathbf{b} = -\frac{1}{2}b\,\hat{\mathbf{i}} + \frac{\sqrt{3}}{2}b\,\hat{\mathbf{j}} \tag{5.15}$$

$$\mathbf{c} = c\,\hat{\mathbf{k}} \tag{5.16}$$

where: $a = b = 3.593$ Å and $c = 20$ Å

Structure 6

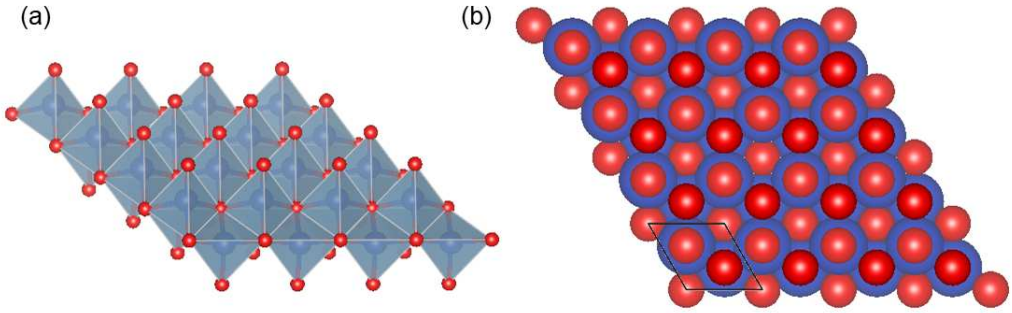

Figure 5.10: Atomic structure of 2D silica where the tetrahedra share edges, half the tetrahedra on each side:(a) perspective view showing the Si-centered tetrahedra, and (b) top view, with atoms shows as red (O) or blue (Si) spheres.

From the Figure 5.10, the atomic structure of 2D silica where the tetrahedra share edges, half of the tetrahedra on each side of the surface. The lattice vectors in angstrom (Å) are:

$$\mathbf{a} = a\ \hat{\mathbf{i}} \tag{5.17}$$

$$\mathbf{b} = -\frac{1}{2}b\ \hat{\mathbf{i}} + \frac{\sqrt{3}}{2}b\ \hat{\mathbf{j}} \tag{5.18}$$

$$\mathbf{c} = c\ \hat{\mathbf{k}} \tag{5.19}$$

where: $a = b = 2.678$ Å and $c = 20$ Å

Table 5.1 shows the summary of lattice vectors of all six structures, five of them have been relaxed. The relaxed structures have a low formation energy which indicate they are would be quite easy to synthesize. Only one structure has not been relaxed / converged : this is structure 5, with shared edges and no holes in the structures. In this structures, the oxygen ions too close to each other which leads to large electrostatic repulsion and failure to converge.

Table 5.1: Lattice parameters of the proposed 2D silica structures

Sharing type	Structure No.	Lattice parameters					
		a (Å)	b (Å)	c (Å)	$\alpha(^\circ)$	$\beta(^\circ)$	$\gamma(^\circ)$
Corners	1	2.678	2.678	20	90	90	120
	2	2.678	5.356				
	3	5.356	5.356				
	4						
Edges	5	3.593	3.593				
	6	2.678	2.678				

5.4 Mechanical properties of the 2D silica structures

The generalized form of Hooke's Law expresses the stress components in terms of the strain components via [183]:

$$\sigma_{ij} = c_{ijkl}\epsilon_{kl}, \tag{5.20}$$

where c_{ijkl} are the 81 components of the stiffness tensor. For convenience, a matrix notation based on Voigt's convention will be used. This can be done after extracting all the components of the four rank tensor c_{ijkl}, and converting them to Voigt's notation as shown in Table 5.2.

Table 5.2: Converting the stiffness tensor to Voigt notation

Regular indices	11	22	33	23,32	31,13	12,21
Voigt notation	1	2	3	4	5	6

In this notation, the stiffness matrix becomes:

$$\mathbf{c} = \begin{bmatrix} c_{11} & c_{12} & c_{13} & c_{14} & c_{15} & c_{16} \\ c_{21} & c_{22} & c_{23} & c_{24} & c_{25} & c_{26} \\ c_{31} & c_{32} & c_{33} & c_{34} & c_{35} & c_{36} \\ c_{41} & c_{42} & c_{43} & c_{44} & c_{45} & c_{46} \\ c_{51} & c_{52} & c_{53} & c_{54} & c_{55} & c_{56} \\ c_{61} & c_{62} & c_{63} & c_{64} & c_{65} & c_{66} \end{bmatrix}$$

where: $c_{12} = c_{21}, c_{13} = c_{31}, c_{14} = c_{41}, c_{15} = c_{51}, c_{16} = c_{61}, c_{23} = c_{32}, c_{24} = c_{42}, c_{25} = c_{52}, c_{26} = c_{62}, c_{34} = c_{43}, c_{35} = c_{53}, c_{36} = c_{63}, c_{45} = c_{54}, c_{46} = c_{64}$, and $c_{56} = c_{65}$

So the general stiffness matrix has 21 independent stiffness constants. Furthermore, the crystals symmetry will reduce the number of these stiffness components. For bulk materials with hexagonal geometry, the stiffness matrix has only five independent stiffness constants:

$$\mathbf{c} = \begin{bmatrix} c_{11} & c_{12} & c_{13} & 0 & 0 & 0 \\ c_{21} & c_{22} & c_{23} & 0 & 0 & 0 \\ c_{31} & c_{32} & c_{33} & 0 & 0 & 0 \\ 0 & 0 & 0 & c_{44} & 0 & 0 \\ 0 & 0 & 0 & 0 & c_{55} & 0 \\ 0 & 0 & 0 & 0 & 0 & c_{66} \end{bmatrix}$$

where $c_{11} = c_{22}, c_{13} = c_{23}, c_{44} = c_{55}, c_{12} = c_{21}, c_{13} = c_{31}$ and $c_{66} = \frac{1}{2}(c_{11} - c_{12})$.

To convert the 3D system to 2D, we assume ($\epsilon_{ij} = 0$, $\sigma_{ij} = 0$ for $i = 3$ or $j = 3$), which leads to an elastic tensor with only two independent constants. The elastic tensor for 2D materials thus becomes:

$$\mathbf{c} = \begin{bmatrix} c_{11}^{2D} & c_{12}^{2D} & 0 \\ c_{21}^{2D} & c_{22}^{2D} & 0 \\ 0 & 0 & c_{66}^{2D} \end{bmatrix}$$

where $c_{11}^{2D} = c_{22}^{2D}, c_{12}^{2D} = c_{21}^{2D}$, and $c_{66}^{2D} = \frac{1}{2}(c_{11}^{2D} - c_{12}^{2D})$.

The VASP package software always calculates these coefficients using periodic boundary conditions in three dimensions; because of this, the 2D coefficients c_{ij}^{2D} must be normalized by the c lattice parameter [171, 184].

We validate our results by computing the stiffness matrix for a well known 2D material (graphene) and comparing the results to other published work as shown in Table 5.3.

Table 5.3: The stiffness constant $c_{11}^{2D}$of graphene.

stiffness constant c_{11} in TPa			
present work	Ref. [185]	Ref. [186]	Ref. [187]
1.057	0.992	1.029	1.025

After ensuring that the computed stiffness components are indeed close to those reported in the literature [185–187] (with the differences coming from the details of the specific methodologies used in various articles), we turn to calculating the stiffness constants for our 2D silica structures described above. These elastic constants are summarized in Table Table 5.4.

Table 5.4: Stiffness constants

Stiffness constants for 2D Silica in GPa			
Chemical formula	Structure No.	c_{11}	c_{12}
SiO_2	1	356	362
SiO_2	2	449	242
Si_2O_5	3	281	116
Si_2O_5	4	160	73
Si_2O_3	6	90	423

Structure 5 has one of the computed stiffness constants negative, which indicates that it is mechanically unstable. For this reason, it has been dropped from Table Table 5.4 and from the electronic structure calculations.

5.5 Band structures and Density of states (DOS)

The band structure plot represents the available energies for electrons in the materials. When represented as functions of the wave number, these energies form bands, which fill up with electrons starting at the lowest energy and continuing towards the higher energies. The last filled band is called the valence band, and the first unoccupied band is called the conduction band. If there is a gap between valence and conduction bands, this means that electrons in the valence would have to be supplied a minimum energy in order for them to cross the gap and become conduction electrons. This is called bandgap, and its exact value determines the electronic behavior of the materials (metal, semiconductor, or insulator.) It is often useful to plot DOS next to the band structure, which we do in the next figures

- Band structure and DOS of Structure 1

  From the DOS and band structure graphs, Figure 5.11 it is shown that the valence and conduction band are contact at Γ point only, meaning that Structure 1 is metallic. The precise nomenclature is "semimetallic" to indicate that the valence and conduction bands cross only at one point: this is an electronic behavior similar to graphene, which is also a semimetal.

- Band structure and DOS of Structure 2

  The atomic structure of 2D silica with share corners forming triangular holes with half of tetrahedra on each side of the plane show the DOS and band structure graph Figure 5.12, a band gap of 1.8 eV, that allow the structure as a candidate of semiconductor material. The precise value of 1.8 eV can make this material suitable for photovoltaic application; this is a proposal which can be tested experimentally in the future.

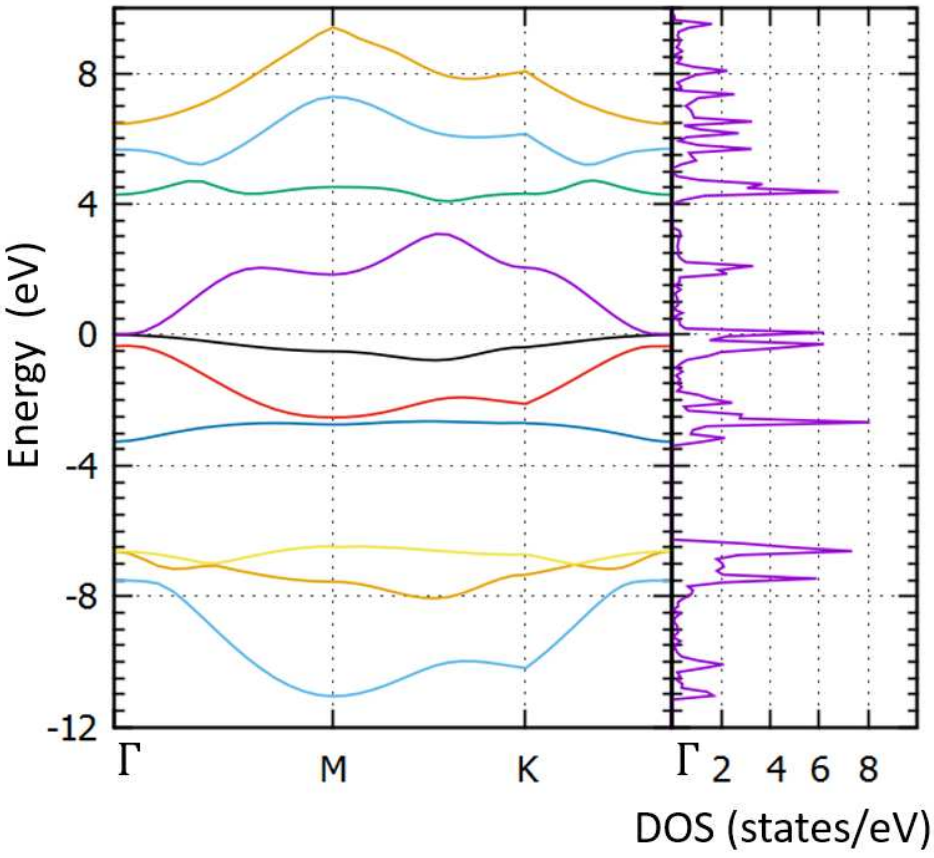

Figure 5.11: Band structure and DOS for structure 1

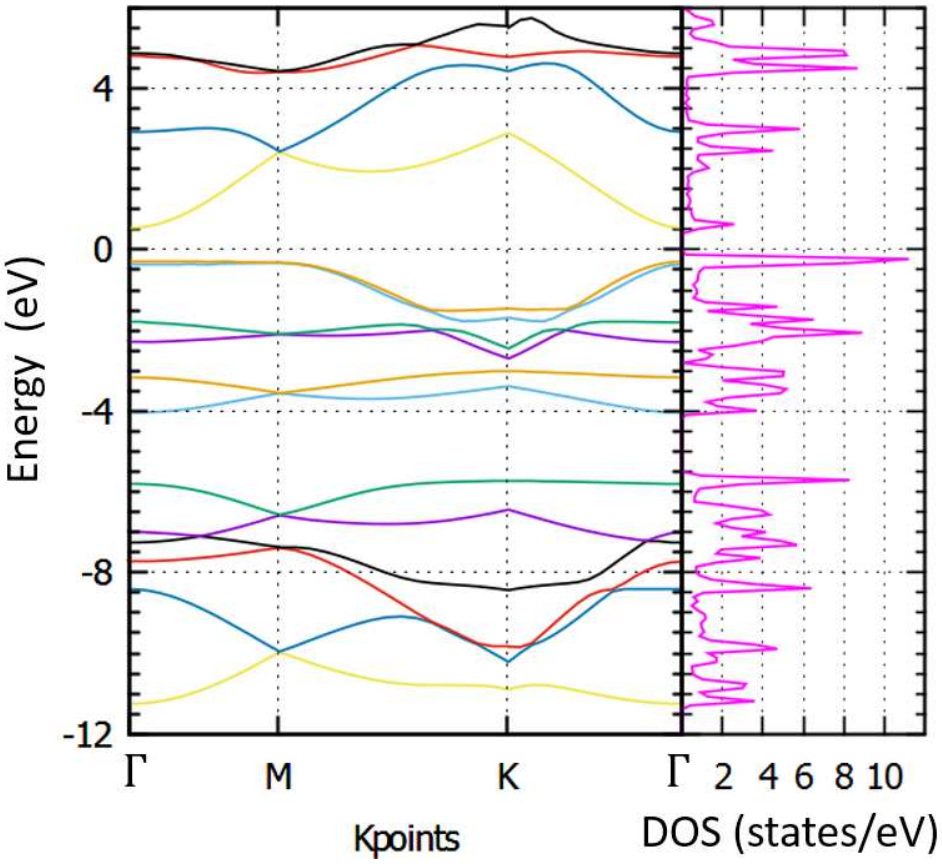

Figure 5.12: Band structure and DOS for structure 2

- Band structure and DOS of Structure 3

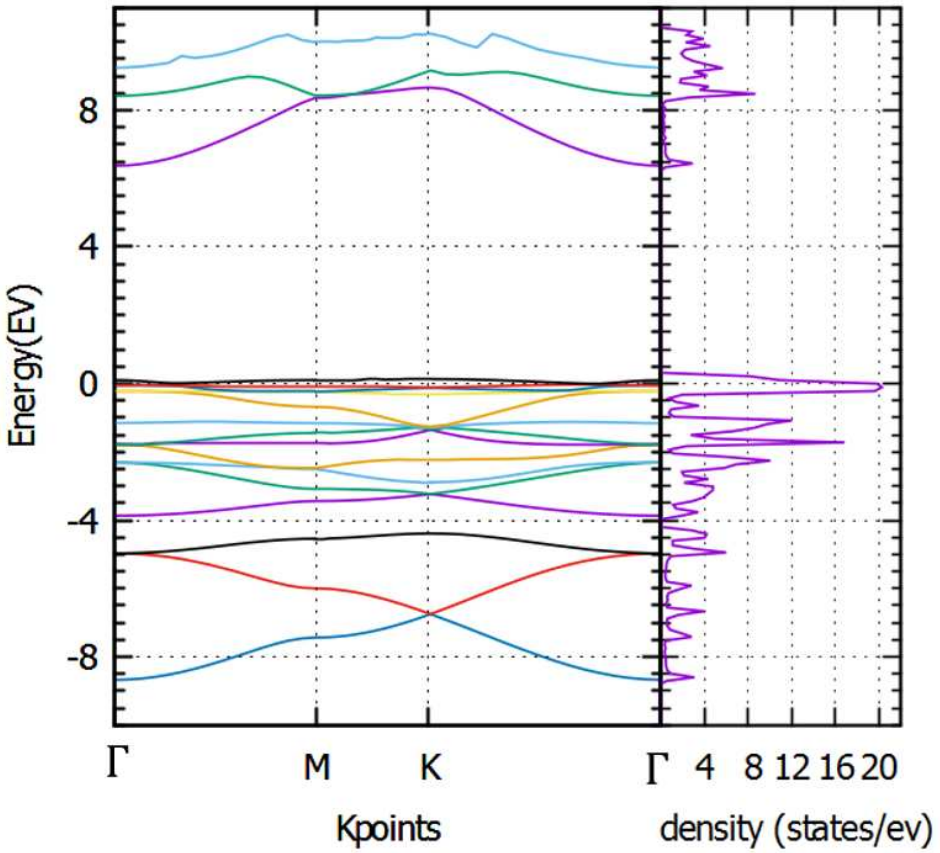

Figure 5.13: Band structure and DOS for Structure 3

From the Figure 5.13, it is clear that the atomic structure with share corners forming hexagonal holes with sll tetrahedrons on one side of the surface has the band gap of 6.5 eV, which makes this structure an insulator.

- Band structure and DOS of Structure 4

Referring to the Figure 5.14, the atomic structure of 2D silica with shared corners forming hexagonal holes with half of the tetrahedra on each side of the surface has a large band gap, 6 eV. This structure is therefore an insulator.

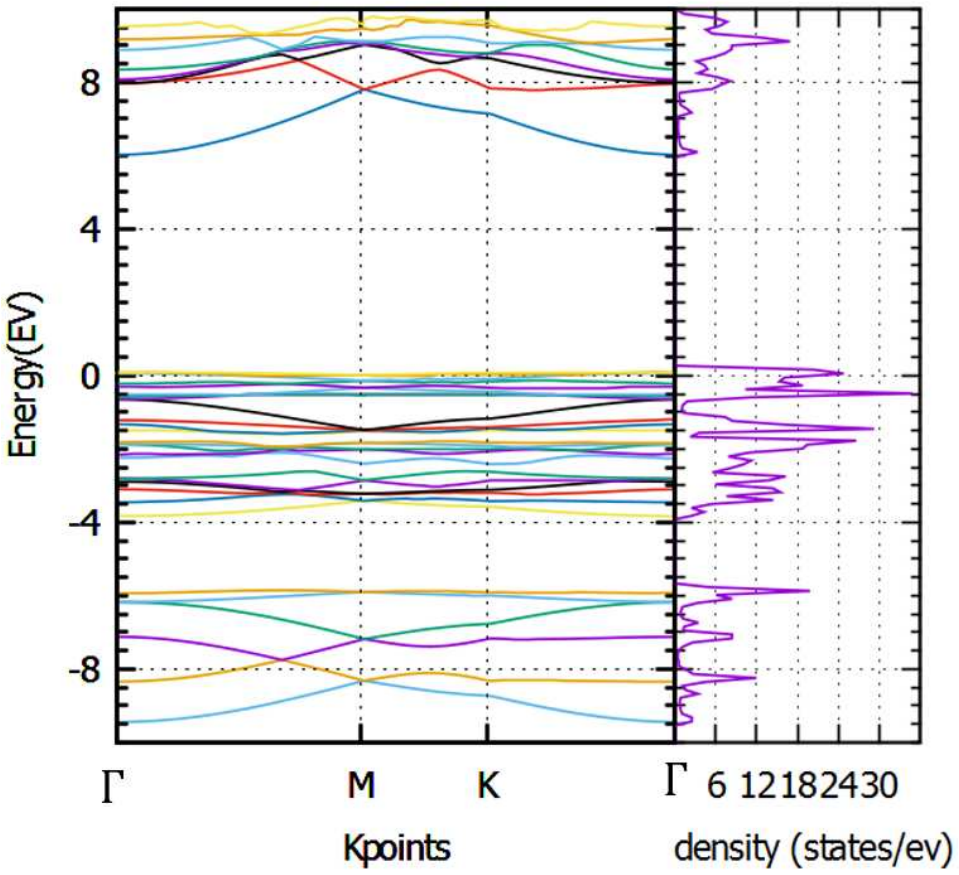

Figure 5.14: Band structure and DOS for Structure 4

- Band structure and DOS of Structure 6

  From Figure 5.15, the 2D silica sharing edges half the tetrahedrons on each side of the surface behaves as a semiconductor with band gap of 1 eV at M point.

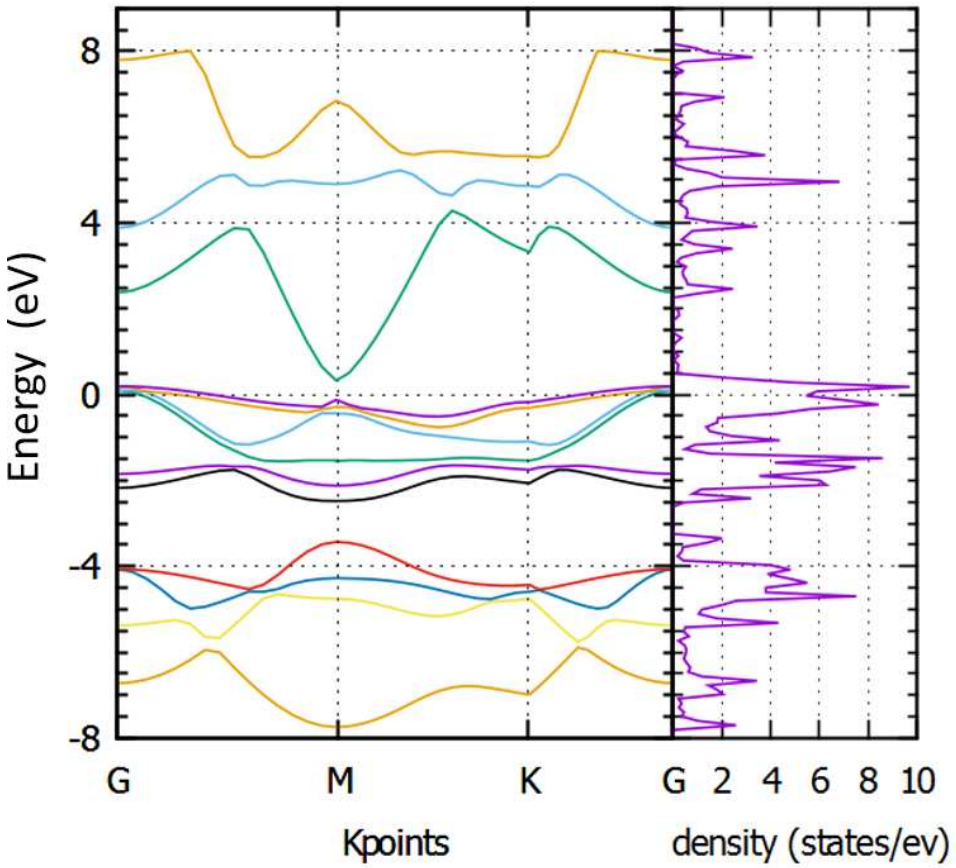

Figure 5.15: Band structure and DOS for 2D silica, Structure 6

Table Table 5.5 summarizes the calculated band gaps for the stable structures.

Electronic behaviors similar to those in Table Table 5.5 have been reported for graphene (semimetal), MoS_2 (semiconductor with bandgap of 1.8 eV), and hBN (insulator with bandgap of 5 eV). 2D silica is able to realize all electronic behaviors, with the precise structure determining the electronic properties.

Table 5.5: Summary of Band gap

Structure number	Band gap (eV)
1	0, contact only at Γ point
2	1.8
3	6.5
4	6.0
6	1.0

5.6 Summary

With the noted exception of Structure 5 (which is mechanically unstable), it is very likely that all the remaining structures can be snthesized in the future as they are mechanically stable. The 2D silica display as wide range of possible electronic behaviours, depending on the exact structure. Future efforts should be aimed at understanding what parameters during growth can be tuned to determined one particular structure or another. These efforts are not particularly facile, given that currently the silica structure are formed on metallic substrates, and they are strongly bonded to these substrate. The strong bonding with the substrates alters the electronic properties of 2D silica, practically "short-circuiting" them from an electronic point of view. Thus, in the future growth efforts should also proceed using insulating substrate which will only provide support (against wrinkling) and not alter the electronic properties.

APPENDIX

PERMISSIONS FOR CONTENT REUSED

Several figures in this thesis are reused with permission from different journal articles, as follows:

- Figure 2.1, with permission from American Physical Society.
- Figure 2.2(b), with permission from Springer Nature.
- Figure 5.1, with permission from Royal Society of Chemistry.
- Figure 5.2, with permission from Royal Society of Chemistry.
- Figure 5.3, with permission from American Chemical Society.
- Figure 5.4, with permission from Institute of Physics.

In addition, certain content from a manuscript (written with coauthors from University of California Los Angeles and Colorado School of Mines, and submitted to Nano Letters) currently constitutes a large part of Chapter 4: this content is reused with the explicit permission of all the coauthors.

American Physical Society
Reuse and Permissions License

27-Mar-2018

This license agreement between the American Physical Society ("APS") and Abdulfattah Abdulslam ("You") consists of your license details and the terms and conditions provided by the American Physical Society and SciPris.

Licensed Content Information

License Number:	**RNP/18/MAR/002713**
License date:	27-Mar-2018
DOI:	10.1103/PhysRevB.89.235319
Title:	Layer-controlled band gap and anisotropic excitons in few-layer black phosphorus
Author:	Vy Tran et al.
Publication:	Physical Review B
Publisher:	American Physical Society
Cost:	USD $ 0.00

Request Details

Does your reuse require significant modifications: No

Specify intended distribution locations:	United States
Reuse Category:	Reuse in a thesis/dissertation
Requestor Type:	Student
Items for Reuse:	Figures/Tables
Number of Figure/Tables:	2
Figure/Tables Details:	Han Liu, Adam T. Neal, Zhen Zhu, Zhe Luo, Xianfan Xu, David Tomanek, and Peide D. Ye, ´ ACS Nano 8, 4033 (2014)
Format for Reuse:	Electronic

Information about New Publication:

University/Publisher:	Colorado School Of Mines
Title of dissertation/thesis:	GROWTH, STRUCTURE, AND PROPERTIES OF SELECTED TWO-DIMENSIONAL MATERIALS FROM DENSITY FUNCTIONAL THEORY INVESTIGATIONS
Author(s):	Abdulfattah Abdulslam
Expected completion date:	May. 2018

License Requestor Information

Name:	Abdulfattah Abdulslam
Affiliation:	Individual
Email Id:	aabdulsl@mines.edu
Country:	United States

American Physical Society
Reuse and Permissions License

TERMS AND CONDITIONS

The American Physical Society (APS) is pleased to grant the Requestor of this license a non-exclusive, non-transferable permission, limited to Electronic format, provided all criteria outlined below are followed.

1. You must also obtain permission from at least one of the lead authors for each separate work, if you haven't done so already. The author's name and affiliation can be found on the first page of the published Article.
2. For electronic format permissions, Requestor agrees to provide a hyperlink from the reprinted APS material using the source material's DOI on the web page where the work appears. The hyperlink should use the standard DOI resolution URL, http://dx.doi.org/{DOI}. The hyperlink may be embedded in the copyright credit line.
3. For print format permissions, Requestor agrees to print the required copyright credit line on the first page where the material appears: "Reprinted (abstract/excerpt/figure) with permission from [(FULL REFERENCE CITATION) as follows: Author's Names, APS Journal Title, Volume Number, Page Number and Year of Publication.] Copyright (YEAR) by the American Physical Society."
4. Permission granted in this license is for a one-time use and does not include permission for any future editions, updates, databases, formats or other matters. Permission must be sought for any additional use.
5. Use of the material does not and must not imply any endorsement by APS.
6. APS does not imply, purport or intend to grant permission to reuse materials to which it does not hold copyright. It is the requestor's sole responsibility to ensure the licensed material is original to APS and does not contain the copyright of another entity, and that the copyright notice of the figure, photograph, cover or table does not indicate it was reprinted by APS with permission from another source.
7. The permission granted herein is personal to the Requestor for the use specified and is not transferable or assignable without express written permission of APS. This license may not be amended except in writing by APS.
8. You may not alter, edit or modify the material in any manner.
9. You may translate the materials only when translation rights have been granted.
10. APS is not responsible for any errors or omissions due to translation.
11. You may not use the material for promotional, sales, advertising or marketing purposes.
12. The foregoing license shall not take effect unless and until APS or its agent, Aptara, receives payment in full in accordance with Aptara Billing and Payment Terms and Conditions, which are incorporated herein by reference.
13. Should the terms of this license be violated at any time, APS or Aptara may revoke the license with no refund to you and seek relief to the fullest extent of the laws of the USA. Official written notice will be made using the contact information provided with the permission request. Failure to receive such notice will not nullify revocation of the permission.
14. APS reserves all rights not specifically granted herein.
15. This document, including the Aptara Billing and Payment Terms and Conditions, shall be the entire agreement between the parties relating to the subject matter hereof.

SPRINGER NATURE LICENSE TERMS AND CONDITIONS

Mar 28, 2018

This Agreement between Abdulfattah Abdulslam ("You") and Springer Nature ("Springer Nature") consists of your license details and the terms and conditions provided by Springer Nature and Copyright Clearance Center.

License Number	4317490443456
License date	Mar 28, 2018
Licensed Content Publisher	Springer Nature
Licensed Content Publication	Springer eBook
Licensed Content Title	Cu-P (Copper-Phosphorus)
Licensed Content Author	B. Predel
Licensed Content Date	Dec 31, 1969
Type of Use	Thesis/Dissertation
Requestor type	non-commercial (non-profit)
Format	electronic
Portion	figures/tables/illustrations
Number of figures/tables/illustrations	1
Will you be translating?	no
Circulation/distribution	<501
Author of this Springer Nature content	no
Title	GROWTH, STRUCTURE, AND PROPERTIES OF SELECTED TWO-DIMENSIONAL MATERIALS FROM DENSITY FUNCTIONAL THEORY INVESTIGATIONS
Instructor name	Cristian V. Ciobanu
Institution name	Colorado School Of Mines
Expected presentation date	Apr 2018
Order reference number	1
Portions	Cu-P (Copper-Phosphorus) Phase diagram
Requestor Location	Abdulfattah Abdulslam 1302 S Parker RD apt 217 DENVER, CO 80231 United States Attn: Abdulfattah Abdulslam
Billing Type	Invoice
Billing Address	Abdulfattah Abdulslam 1302 S Parker RD apt 217 DENVER, CO 80231

United States
Attn: Abdulfattah Abdulslam

Total 0.00 USD

Terms and Conditions

Springer Nature Terms and Conditions for RightsLink Permissions

Springer Customer Service Centre GmbH (the Licensor) hereby grants you a non-exclusive, world-wide licence to reproduce the material and for the purpose and requirements specified in the attached copy of your order form, and for no other use, subject to the conditions below:

1. The Licensor warrants that it has, to the best of its knowledge, the rights to license reuse of this material. However, you should ensure that the material you are requesting is original to the Licensor and does not carry the copyright of another entity (as credited in the published version).

   If the credit line on any part of the material you have requested indicates that it was reprinted or adapted with permission from another source, then you should also seek permission from that source to reuse the material.

2. Where **print only** permission has been granted for a fee, separate permission must be obtained for any additional electronic re-use.

3. Permission granted **free of charge** for material in print is also usually granted for any electronic version of that work, provided that the material is incidental to your work as a whole and that the electronic version is essentially equivalent to, or substitutes for, the print version.

4. A licence for 'post on a website' is valid for 12 months from the licence date. This licence does not cover use of full text articles on websites.

5. Where **'reuse in a dissertation/thesis'** has been selected the following terms apply: Print rights for up to 100 copies, electronic rights for use only on a personal website or institutional repository as defined by the Sherpa guideline (www.sherpa.ac.uk/romeo/).

6. Permission granted for books and journals is granted for the lifetime of the first edition and does not apply to second and subsequent editions (except where the first edition permission was granted free of charge or for signatories to the STM Permissions Guidelines http://www.stm-assoc.org/copyright-legal-affairs/permissions/permissions-guidelines/), and does not apply for editions in other languages unless additional translation rights have been granted separately in the licence.

7. Rights for additional components such as custom editions and derivatives require additional permission and may be subject to an additional fee. Please apply to Journalpermissions@springernature.com/bookpermissions@springernature.com for these rights.

8. The Licensor's permission must be acknowledged next to the licensed material in print. In electronic form, this acknowledgement must be visible at the same time as the figures/tables/illustrations or abstract, and must be hyperlinked to the journal/book's homepage. Our required acknowledgement format is in the Appendix below.

9. Use of the material for incidental promotional use, minor editing privileges (this does not include cropping, adapting, omitting material or any other changes that affect the meaning, intention or moral rights of the author) and copies for the disabled are permitted under this licence.

10. Minor adaptations of single figures (changes of format, colour and style) do not require the Licensor's approval. However, the adaptation should be credited as shown in Appendix below.

Appendix — Acknowledgements:

For Journal Content:
Reprinted by permission from [**the Licensor**]: [**Journal Publisher** (e.g. Nature/Springer/Palgrave)] [**JOURNAL NAME**] [**REFERENCE CITATION** (Article name, Author(s) Name), [**COPYRIGHT**] (year of publication)

For **Advance Online Publication papers:**
Reprinted by permission from [**the Licensor**]: [**Journal Publisher** (e.g. Nature/Springer/Palgrave)] [**JOURNAL NAME**] [**REFERENCE CITATION** (Article name, Author(s) Name), [**COPYRIGHT**] (year of publication), advance online publication, day month year (doi: 10.1038/sj.[JOURNAL ACRONYM].)

For Adaptations/Translations:
Adapted/Translated by permission from [**the Licensor**]: [**Journal Publisher** (e.g. Nature/Springer/Palgrave)] [**JOURNAL NAME**] [**REFERENCE CITATION** (Article name, Author(s) Name), [**COPYRIGHT**] (year of publication)

Note: For any republication from the British Journal of Cancer, the following credit line style applies:

Reprinted/adapted/translated by permission from [**the Licensor**]: on behalf of Cancer Research UK: : [**Journal Publisher** (e.g. Nature/Springer/Palgrave)] [**JOURNAL NAME**] [**REFERENCE CITATION** (Article name, Author(s) Name), [**COPYRIGHT]** (year of publication)

For **Advance Online Publication** papers:
Reprinted by permission from The [**the Licensor**]: on behalf of Cancer Research UK: [**Journal Publisher** (e.g. Nature/Springer/Palgrave)] [**JOURNAL NAME**] [**REFERENCE CITATION** (Article name, Author(s) Name), [**COPYRIGHT**] (year of publication), advance online publication, day month year (doi: 10.1038/sj.[JOURNAL ACRONYM])

For Book content:
Reprinted/adapted by permission from [**the Licensor**]: [**Book Publisher** (e.g. Palgrave Macmillan, Springer etc) [**Book Title**] by [**Book author**(s)] [**COPYRIGHT**] (year of publication)

Other Conditions:

Version 1.0

ROYAL SOCIETY OF CHEMISTRY LICENSE TERMS AND CONDITIONS

Apr 02, 2018

This Agreement between Abdulfattah Abdulslam ("You") and Royal Society of Chemistry ("Royal Society of Chemistry") consists of your license details and the terms and conditions provided by Royal Society of Chemistry and Copyright Clearance Center.

License Number	4320820476515
License date	Apr 02, 2018
Licensed Content Publisher	Royal Society of Chemistry
Licensed Content Publication	RSC Advances
Licensed Content Title	Blue-silica by Eu2+-activator occupied in interstitial sites
Licensed Content Author	Donghyeon Kim,Yoeng-Hun Jin,Ki-Wan Jeon,Sungyun Kim,Seung-Joo Kim,Oc Hee Han,Dong-Kyun Seo,Jung-Chul Park
Licensed Content Date	Aug 12, 2015
Licensed Content Volume	5
Licensed Content Issue	91
Type of Use	Thesis/Dissertation
Requestor type	non-commercial (non-profit)
Portion	figures/tables/images
Number of figures/tables/images	1
Format	electronic
Distribution quantity	20
Will you be translating?	no
Order reference number	
Title of the thesis/dissertation	GROWTH, STRUCTURE, AND PROPERTIES OF SELECTED TWO-DIMENSIONAL MATERIALS FROM DENSITY FUNCTIONAL THEORY INVESTIGATIONS
Expected completion date	Apr 2018
Estimated size	1
Requestor Location	Abdulfattah Abdulslam 1302 S Parker RD apt 217 DENVER, CO 80231 United States Attn: Abdulfattah Abdulslam
Billing Type	Invoice
Billing Address	Abdulfattah Abdulslam 1302 S Parker RD apt 217 DENVER, CO 80231 United States Attn: Abdulfattah Abdulslam

Total 0.00 USD

Terms and Conditions

This License Agreement is between {Requestor Name} ("You") and The Royal Society of Chemistry ("RSC") provided by the Copyright Clearance Center ("CCC"). The license consists of your order details, the terms and conditions provided by the Royal Society of Chemistry, and the payment terms and conditions.

RSC / TERMS AND CONDITIONS

INTRODUCTION

The publisher for this copyrighted material is The Royal Society of Chemistry. By clicking "accept" in connection with completing this licensing transaction, you agree that the following terms and conditions apply to this transaction (along with the Billing and Payment terms and conditions established by CCC, at the time that you opened your RightsLink account and that are available at any time at .

LICENSE GRANTED

The RSC hereby grants you a non-exclusive license to use the aforementioned material anywhere in the world subject to the terms and conditions indicated herein. Reproduction of the material is confined to the purpose and/or media for which permission is hereby given.

RESERVATION OF RIGHTS

The RSC reserves all rights not specifically granted in the combination of (i) the license details provided by your and accepted in the course of this licensing transaction; (ii) these terms and conditions; and (iii) CCC's Billing and Payment terms and conditions.

REVOCATION

The RSC reserves the right to revoke this license for any reason, including, but not limited to, advertising and promotional uses of RSC content, third party usage, and incorrect source figure attribution.

THIRD-PARTY MATERIAL DISCLAIMER

If part of the material to be used (for example, a figure) has appeared in the RSC publication with credit to another source, permission must also be sought from that source. If the other source is another RSC publication these details should be included in your RightsLink request. If the other source is a third party, permission must be obtained from the third party. The RSC disclaims any responsibility for the reproduction you make of items owned by a third party.

PAYMENT OF FEE

If the permission fee for the requested material is waived in this instance, please be advised that any future requests for the reproduction of RSC materials may attract a fee.

ACKNOWLEDGEMENT

The reproduction of the licensed material must be accompanied by the following acknowledgement:

Reproduced ("Adapted" or "in part") from {Reference Citation} (or Ref XX) with permission of The Royal Society of Chemistry.

If the licensed material is being reproduced from New Journal of Chemistry (NJC), Photochemical & Photobiological Sciences (PPS) or Physical Chemistry Chemical Physics (PCCP) you must include one of the following acknowledgements:

For figures originally published in NJC:

Reproduced ("Adapted" or "in part") from {Reference Citation} (or Ref XX) with permission of The Royal Society of Chemistry (RSC) on behalf of the European Society for Photobiology, the European Photochemistry Association and the RSC.

For figures originally published in PPS:

Reproduced ("Adapted" or "in part") from {Reference Citation} (or Ref XX) with permission of The Royal Society of Chemistry (RSC) on behalf of the Centre National de la Recherche Scientifique (CNRS) and the RSC.

For figures originally published in PCCP:

Reproduced ("Adapted" or "in part") from {Reference Citation} (or Ref XX) with permission of the PCCP Owner Societies.

HYPERTEXT LINKS

With any material which is being reproduced in electronic form, you must include a hypertext link to the original RSC article on the RSC's website. The recommended form for the hyperlink is http://dx.doi.org/10.1039/DOI suffix, for example in the link http://dx.doi.org/10.1039/b110420a the DOI suffix is 'b110420a'. To find the relevant DOI suffix for the RSC article in question, go to the Journals section of the website and locate the article in the list of papers for the volume and issue of your specific journal. You will find the DOI suffix quoted there.

LICENSE CONTINGENT ON PAYMENT

While you may exercise the rights licensed immediately upon issuance of the license at the end of the licensing process for the transaction, provided that you have disclosed complete and accurate details of your proposed use, no license is finally effective unless and until full payment is received from you (by CCC) as provided in CCC's Billing and Payment terms and conditions. If full payment is not received on a timely basis, then any license preliminarily granted shall be deemed automatically revoked and shall be void as if never granted. Further, in the event that you breach any of these terms and conditions or any of CCC's Billing and Payment terms and conditions, the license is automatically revoked and shall be void as if never granted. Use of materials as described in a revoked license, as well as any use of the materials beyond the scope of an unrevoked license, may constitute copyright infringement and the RSC reserves the right to take any and all action to protect its copyright in the materials.

WARRANTIES

The RSC makes no representations or warranties with respect to the licensed material.

INDEMNITY

You hereby indemnify and agree to hold harmless the RSC and the CCC, and their respective officers, directors, trustees, employees and agents, from and against any and all claims arising out of your use of the licensed material other than as specifically authorized pursuant to this licence.

NO TRANSFER OF LICENSE

This license is personal to you or your publisher and may not be sublicensed, assigned, or transferred by you to any other person without the RSC's written permission.

NO AMENDMENT EXCEPT IN WRITING

This license may not be amended except in a writing signed by both parties (or, in the case of "Other Conditions, v1.2", by CCC on the RSC's behalf).

OBJECTION TO CONTRARY TERMS

You hereby acknowledge and agree that these terms and conditions, together with CCC's Billing and Payment terms and conditions (which are incorporated herein), comprise the entire agreement between you and the RSC (and CCC) concerning this licensing transaction, to the exclusion of all other terms and conditions, written or verbal, express or implied (including any terms contained in any purchase order, acknowledgment, check endorsement or other writing prepared by you). In the event of any conflict between your obligations established by these terms and conditions and those established by CCC's Billing and Payment terms and conditions, these terms and conditions shall control.

JURISDICTION

This license transaction shall be governed by and construed in accordance with the laws of the District of Columbia. You hereby agree to submit to the jurisdiction of the courts located in the District of Columbia for purposes of resolving any disputes that may arise in connection with this licensing transaction.

LIMITED LICENSE

The following terms and conditions apply to specific license types:

Translation

This permission is granted for non-exclusive world English rights only unless your license was granted for translation rights. If you licensed translation rights you may only translate

this content into the languages you requested. A professional translator must perform all translations and reproduce the content word for word preserving the integrity of the article.

Intranet

If the licensed material is being posted on an Intranet, the Intranet is to be password-protected and made available only to bona fide students or employees only. All content posted to the Intranet must maintain the copyright information line on the bottom of each image. You must also fully reference the material and include a hypertext link as specified above.

Copies of Whole Articles

All copies of whole articles must maintain, if available, the copyright information line on the bottom of each page.

Other Conditions

v1.2

Gratis licenses (referencing $0 in the Total field) are free. Please retain this printable license for your reference. No payment is required.

If you would like to pay for this license now, please remit this license along with yourpayment made payable to "COPYRIGHT CLEARANCE CENTER" otherwise you will be invoiced within 48 hours of the license date. Payment should be in the form of a check or money order referencing your account number and this invoice number {Invoice Number}. Once you receive your invoice for this order, you may pay your invoice by credit card. Please follow instructions provided at that time.

Make Payment To:
Copyright Clearance Center
29118 Network Place
Chicago, IL 60673-1291

For suggestions or comments regarding this order, contact Rightslink Customer Support: customercare@copyright.com or +1-855-239-3415 (toll free in the US) or +1-978-646-2777.

Questions? customercare@copyright.com or +1-855-239-3415 (toll free in the US) or +1-978-646-2777.

ROYAL SOCIETY OF CHEMISTRY LICENSE TERMS AND CONDITIONS

Mar 30, 2018

This Agreement between Abdulfattah Abdulslam ("You") and Royal Society of Chemistry ("Royal Society of Chemistry") consists of your license details and the terms and conditions provided by Royal Society of Chemistry and Copyright Clearance Center.

License Number	4318630994382
License date	Mar 30, 2018
Licensed Content Publisher	Royal Society of Chemistry
Licensed Content Publication	Journal of Materials Chemistry
Licensed Content Title	Modelling and simulation of amorphous silicon oxycarbide
Licensed Content Author	Peter Kroll
Licensed Content Date	May 14, 2003
Licensed Content Volume	13
Licensed Content Issue	7
Type of Use	Thesis/Dissertation
Requestor type	non-commercial (non-profit)
Portion	figures/tables/images
Number of figures/tables/images	1
Format	electronic
Distribution quantity	10
Will you be translating?	no
Order reference number	
Title of the thesis/dissertation	GROWTH, STRUCTURE, AND PROPERTIES OF SELECTED TWO-DIMENSIONAL MATERIALS FROM DENSITY FUNCTIONAL THEORY INVESTIGATIONS
Expected completion date	Apr 2018
Estimated size	1
Requestor Location	Abdulfattah Abdulslam 1302 S Parker RD apt 217 DENVER, CO 80231 United States Attn: Abdulfattah Abdulslam
Billing Type	Invoice
Billing Address	Abdulfattah Abdulslam 1302 S Parker RD apt 217 DENVER, CO 80231 United States Attn: Abdulfattah Abdulslam
Total	0.00 USD

Terms and Conditions

This License Agreement is between {Requestor Name} ("You") and The Royal Society of Chemistry ("RSC") provided by the Copyright Clearance Center ("CCC"). The license consists of your order details, the terms and conditions provided by the Royal Society of Chemistry, and the payment terms and conditions.

RSC / TERMS AND CONDITIONS

INTRODUCTION

The publisher for this copyrighted material is The Royal Society of Chemistry. By clicking "accept" in connection with completing this licensing transaction, you agree that the following terms and conditions apply to this transaction (along with the Billing and Payment terms and conditions established by CCC, at the time that you opened your RightsLink account and that are available at any time at .

LICENSE GRANTED

The RSC hereby grants you a non-exclusive license to use the aforementioned material anywhere in the world subject to the terms and conditions indicated herein. Reproduction of the material is confined to the purpose and/or media for which permission is hereby given.

RESERVATION OF RIGHTS

The RSC reserves all rights not specifically granted in the combination of (i) the license details provided by your and accepted in the course of this licensing transaction; (ii) these terms and conditions; and (iii) CCC's Billing and Payment terms and conditions.

REVOCATION

The RSC reserves the right to revoke this license for any reason, including, but not limited to, advertising and promotional uses of RSC content, third party usage, and incorrect source figure attribution.

THIRD-PARTY MATERIAL DISCLAIMER

If part of the material to be used (for example, a figure) has appeared in the RSC publication with credit to another source, permission must also be sought from that source. If the other source is another RSC publication these details should be included in your RightsLink request. If the other source is a third party, permission must be obtained from the third party. The RSC disclaims any responsibility for the reproduction you make of items owned by a third party.

PAYMENT OF FEE

If the permission fee for the requested material is waived in this instance, please be advised that any future requests for the reproduction of RSC materials may attract a fee.

ACKNOWLEDGEMENT

The reproduction of the licensed material must be accompanied by the following acknowledgement:

Reproduced ("Adapted" or "in part") from {Reference Citation} (or Ref XX) with permission of The Royal Society of Chemistry.

If the licensed material is being reproduced from New Journal of Chemistry (NJC), Photochemical & Photobiological Sciences (PPS) or Physical Chemistry Chemical Physics (PCCP) you must include one of the following acknowledgements:

For figures originally published in NJC:

Reproduced ("Adapted" or "in part") from {Reference Citation} (or Ref XX) with permission of The Royal Society of Chemistry (RSC) on behalf of the European Society for Photobiology, the European Photochemistry Association and the RSC.

For figures originally published in PPS:

Reproduced ("Adapted" or "in part") from {Reference Citation} (or Ref XX) with permission of The Royal Society of Chemistry (RSC) on behalf of the Centre National de la Recherche Scientifique (CNRS) and the RSC.

For figures originally published in PCCP:

Reproduced ("Adapted" or "in part") from {Reference Citation} (or Ref XX) with permission of the PCCP Owner Societies.

HYPERTEXT LINKS

With any material which is being reproduced in electronic form, you must include a hypertext link to the original RSC article on the RSC's website. The recommended form for the hyperlink is http://dx.doi.org/10.1039/DOI suffix, for example in the link http://dx.doi.org/10.1039/b110420a the DOI suffix is 'b110420a'. To find the relevant DOI suffix for the RSC article in question, go to the Journals section of the website and locate the article in the list of papers for the volume and issue of your specific journal. You will find the DOI suffix quoted there.

LICENSE CONTINGENT ON PAYMENT

While you may exercise the rights licensed immediately upon issuance of the license at the end of the licensing process for the transaction, provided that you have disclosed complete and accurate details of your proposed use, no license is finally effective unless and until full payment is received from you (by CCC) as provided in CCC's Billing and Payment terms and conditions. If full payment is not received on a timely basis, then any license preliminarily granted shall be deemed automatically revoked and shall be void as if never granted. Further, in the event that you breach any of these terms and conditions or any of CCC's Billing and Payment terms and conditions, the license is automatically revoked and shall be void as if never granted. Use of materials as described in a revoked license, as well as any use of the materials beyond the scope of an unrevoked license, may constitute copyright infringement and the RSC reserves the right to take any and all action to protect its copyright in the materials.

WARRANTIES

The RSC makes no representations or warranties with respect to the licensed material.

INDEMNITY

You hereby indemnify and agree to hold harmless the RSC and the CCC, and their respective officers, directors, trustees, employees and agents, from and against any and all claims arising out of your use of the licensed material other than as specifically authorized pursuant to this licence.

NO TRANSFER OF LICENSE

This license is personal to you or your publisher and may not be sublicensed, assigned, or transferred by you to any other person without the RSC's written permission.

NO AMENDMENT EXCEPT IN WRITING

This license may not be amended except in a writing signed by both parties (or, in the case of "Other Conditions, v1.2", by CCC on the RSC's behalf).

OBJECTION TO CONTRARY TERMS

You hereby acknowledge and agree that these terms and conditions, together with CCC's Billing and Payment terms and conditions (which are incorporated herein), comprise the entire agreement between you and the RSC (and CCC) concerning this licensing transaction, to the exclusion of all other terms and conditions, written or verbal, express or implied (including any terms contained in any purchase order, acknowledgment, check endorsement or other writing prepared by you). In the event of any conflict between your obligations established by these terms and conditions and those established by CCC's Billing and Payment terms and conditions, these terms and conditions shall control.

JURISDICTION

This license transaction shall be governed by and construed in accordance with the laws of the District of Columbia. You hereby agree to submit to the jurisdiction of the courts located in the District of Columbia for purposes of resolving any disputes that may arise in connection with this licensing transaction.

LIMITED LICENSE

The following terms and conditions apply to specific license types:

Translation

This permission is granted for non-exclusive world English rights only unless your license was granted for translation rights. If you licensed translation rights you may only translate

this content into the languages you requested. A professional translator must perform all translations and reproduce the content word for word preserving the integrity of the article.
Intranet
If the licensed material is being posted on an Intranet, the Intranet is to be password-protected and made available only to bona fide students or employees only. All content posted to the Intranet must maintain the copyright information line on the bottom of each image. You must also fully reference the material and include a hypertext link as specified above.
Copies of Whole Articles
All copies of whole articles must maintain, if available, the copyright information line on the bottom of each page.
Other Conditions
v1.2
Gratis licenses (referencing $0 in the Total field) are free. Please retain this printable license for your reference. No payment is required.
If you would like to pay for this license now, please remit this license along with yourpayment made payable to "COPYRIGHT CLEARANCE CENTER" otherwise you will be invoiced within 48 hours of the license date. Payment should be in the form of a check or money order referencing your account number and this invoice number {Invoice Number}.
Once you receive your invoice for this order, you may pay your invoice by credit card. Please follow instructions provided at that time.
Make Payment To:
Copyright Clearance Center
29118 Network Place
Chicago, IL 60673-1291
For suggestions or comments regarding this order, contact Rightslink Customer Support: customercare@copyright.com or +1-855-239-3415 (toll free in the US) or +1-978-646-2777.

Questions? customercare@copyright.com or +1-855-239-3415 (toll free in the US) or +1-978-646-2777.

Title: Novel Two-Dimensional Silica Monolayers with Tetrahedral and Octahedral Configurations

Author: Gaoxue Wang, G. C. Loh, Ravindra Pandey, et al

Publication: The Journal of Physical Chemistry C

Publisher: American Chemical Society

Date: Jul 1, 2015

PERMISSION/LICENSE IS GRANTED FOR YOUR ORDER AT NO CHARGE

This type of permission/license, instead of the standard Terms & Conditions, is sent to you because no fee is being charged for your order. Please note the following:

- Permission is granted for your request in both print and electronic formats, and translations.
- If figures and/or tables were requested, they may be adapted or used in part.
- Please print this page for your records and send a copy of it to your publisher/graduate school.
- Appropriate credit for the requested material should be given as follows: "Reprinted (adapted) with permission from (COMPLETE REFERENCE CITATION). Copyright (YEAR) American Chemical Society." Insert appropriate information in place of the capitalized words.
- One-time permission is granted only for the use specified in your request. No additional uses are granted (such as derivative works or other editions). For any other uses, please submit a new request.

If credit is given to another source for the material you requested, permission must be obtained from that source.

Copyright Clearance Center

Note: Copyright.com supplies permissions but not the copyrighted content itself.

1 PAYMENT 2 REVIEW 3 CONFIRMATION

Step 3: Order Confirmation

Thank you for your order! A confirmation for your order will be sent to your account email address. If you have questions about your order, you can call us 24 hrs/day, M-F at +1.855.239.3415 Toll Free, or write to us at info@copyright.com. This is not an invoice.

Confirmation Number: 11707694
Order Date: 03/28/2018

If you paid by credit card, your order will be finalized and your card will be charged within 24 hours. If you choose to be invoiced, you can change or cancel your order until the invoice is generated.

Payment Information

Abdulfattah Abdulslam
aabdulsl@mines.edu
+1 (720) 325-9001
Payment Method: n/a

Order Details

Journal of Physics : Condensed Matter

Order detail ID:	71090019
Order License Id:	4317710612606
ISSN:	0953-8984
Publication Type:	Journal
Volume:	
Issue:	
Start page:	
Publisher:	IOP Publishing
Author/Editor:	American Institute of Physics ; Institute of Physics (Great Britain)

Permission Status: Granted

Permission type: Republish or display content
Type of use: Thesis/Dissertation

Requestor type	Not-for-profit entity
Format	Electronic
Portion	image/photo
Number of images/photos requested	1
The requesting person/organization	Abdulfattah Abdulslam
Title or numeric reference of the portion(s)	Figure 1
Title of the article or chapter the portion is from	Probing the properties of metal–oxide interfaces: silica films on Mo and Ru supports

Editor of portion(s)	N/A
Author of portion(s)	N/A
Volume of serial or monograph	24
Page range of portion	1
Publication date of portion	16 August 2012
Rights for	Main product
Duration of use	Life of current edition
Creation of copies for the disabled	no
With minor editing privileges	no
For distribution to	United States
In the following language(s)	Original language of publication
With incidental promotional use	no
Lifetime unit quantity of new product	Up to 499
Title	GROWTH, STRUCTURE, AND PROPERTIES OF SELECTED TWO-DIMENSIONAL MATERIALS FROM DENSITY FUNCTIONAL THEORY INVESTIGATIONS
Instructor name	Cristian V. Ciobanu
Institution name	Colorado School Of Mines
Expected presentation date	Apr 2018
Attachment	

Note: This item will be invoiced or charged separately through CCC's **RightsLink** service. More info **$ 0.00**

This is not an invoice.

Total order items: 1

Order Total: 0.00 USD

Confirmation Number: 11707694

Special Rightsholder Terms & Conditions

The following terms & conditions apply to the specific publication under which they are listed

Journal of Physics : Condensed Matter
Permission type: Republish or display content
Type of use: Thesis/Dissertation

TERMS AND CONDITIONS

The following terms are individual to this publisher:

These special terms and conditions are in addition to the standard terms and conditions for CCC's Republication Service and, together with those standard terms and conditions, govern the use of the Works.

As the "User" you will make all reasonable efforts to contact the author(s) of the article which the Work is to be reused from, to seek consent for your intended use. Contacting one author who is acting expressly as authorised agent for their co-author(s) is acceptable.

User will reproduce the following wording prominently alongside the Work:

- the source of the Work, including author, article title, title of journal, volume number, issue number (if relevant), page range (or first page if this is the only information available) and date of first publication. This information can be contained in a footnote or reference note; and
- a link back to the article (via DOI); and
- if practicable, and IN ALL CASES for new works published under any of the Creative Commons licences, the words "© IOP Publishing. Reproduced with permission. All rights reserved"

Without the express permission of the author(s) and the Rightsholder of the article from which the Work is to be reused, User shall not use it in any way which, in the opinion of the Rightsholder, could: (i) distort or alter the author(s)' original intention(s) and meaning; (ii) be prejudicial to the honour or reputation of the author(s); and/or (iii) imply endorsement by the author(s) and/or the Rightsholder.

This licence does not apply to any article which is credited to another source and which does not have the copyright line '© IOP Publishing Ltd'. User must check the copyright line of the article from which the Work is to be reused to check that IOP Publishing Ltd has all the necessary rights to be able to grant permission. User is solely responsible for identifying and obtaining separate licences and permissions from the copyright owner for reuse of any such third party material/figures which the Rightsholder is not the copyright owner of. The Rightsholder shall not reimburse any fees which User pays for a republication license for such third party content.

This licence does not apply to any material/figure which is credited to another source in the Rightsholder's publication or has been obtained from a third party. User must check the Version of Record of the article from which the Work is to be reused, to check whether any of the material in the Work is third party material. Third party citations and/or copyright notices and/or permissions statements may not be included in any other version of the article from which the Work is to be reused and so cannot be relied upon by the User. User is solely responsible for identifying and obtaining separate licences and permissions from the copyright owner for reuse of any such third party material/figures where the Rightsholder is not the copyright owner. The Rightsholder shall not reimburse any fees which User pays for a republication license for such third party content.

User and CCC acknowledge that the Rightsholder may, from time to time, make changes or additions to these special terms and conditions without express notification, provided that these shall not apply to permissions already secured and paid for by User prior to such change or addition.

User acknowledges that the Rightsholder (which includes companies within its group and third parties for whom it publishes its titles) may make use of personal data collected through the service in the course of their business.

If User is the author of the Work, User may automatically have the right to reuse it under the rights granted back when User transferred the copyright in the article to the Rightsholder. User should check the copyright form and the relevant author rights policy to check whether permission is required. If User is the author of the Work and does require permission for proposed reuse of the Work, User should select 'Author of requested content' as the Requestor Type. The Rightsholder shall not reimburse any fees which User pays for a republication license.

If User is the author of the article which User wishes to reuse in User's thesis or dissertation, the republication licence covers the right to include the Accepted Manuscript version (not the Version of Record) of the article. User must include citation details and, for online use, a link to the Version of Record of the article on the Rightsholder's website. User may need to obtain separate permission for any third party content included within the article. User must check this with the copyright owner of such third party content. User may not include the article in a thesis or dissertation which is published by ProQuest. Any other commercial use of User's thesis or dissertation containing the article would also need to be expressly notified in writing to the Rightsholder at the time of request and would require separate written permission from the Rightsholder.

Abdulfattah Abdulslam <aabdulsl@mymail.mines.edu>

Help please

Suneel Kodambaka <kodambaka@ucla.edu> Sat, Mar 17, 2018 at 12:33 PM
To: Abdulfattah Abdulslam <aabdulsl@mymail.mines.edu>
Cc: Pedro Arias <pedro.arias89@gmail.com>, Abbas Ebnonnasir <aebnonna@ucla.edu>, Cristian Ciobanu <cciobanu@mines.edu>

To Whom It May Concern:

I, Suneel Kodambaka, hereby give permission to Adbdulfattah Abdulslam to use the theory and modelling sections of the main text and supplementary information of the manuscript nl-2018-00966x entitled "Bifurcation and Orientation-Dependence of Corrugation of 2-D Hexagonal Boron Nitride on Palladium" submitted to Nano Letters on 3/12/2018. In addition, I also give permission to use the experimental figure 4c as motivation for the computational modelling.

Sincerely,
Suneel

--
Suneel Kodambaka
Associate Professor and Vice Chair, Undergraduate studies
Dept. Materials Science and Engineering, UCLA
E-V 3121J, 410 Westwood Plaza, Los Angeles, CA 90095

[Quoted text hidden]

Abdulfattah Abdulslam <aabdulsl@mymail.mines.edu>

Help please

Pedro Arias <pedro.arias89@gmail.com> Sat, Mar 17, 2018 at 12:40 PM
To: Suneel Kodambaka <kodambaka@ucla.edu>
Cc: Abbas Ebnonnasir <aebnonna@ucla.edu>, Abdulfattah Abdulslam <aabdulsl@mymail.mines.edu>, Cristian Ciobanu <cciobanu@mines.edu>

I, Pedro Arias, hereby give permission to Adbdulfattah Abdulslam to use the theory and modelling sections of the main text and supplementary information of the manuscript nl-2018-00966x entitled "Bifurcation and Orientation-Dependence of Corrugation of 2-D Hexagonal Boron Nitride on Palladium" submitted to Nano Letters on 3/12/2018. In addition, I also give permission to use the experimental figure 4c as motivation for the computational modelling.
[Quoted text hidden]
--
--
Pedro Arias
Materials Science and Engineering
University of California, Los Angeles
pedro.arias89@gmail.com
512-351-5425

Abdulfattah Abdulslam <aabdulsl@mymail.mines.edu>

Help please

ABBAS EBNONNASIR <aebnonna@ucla.edu> Sat, Mar 17, 2018 at 11:18 PM
To: Abdulfattah Abdulslam <aabdulsl@mymail.mines.edu>

To Whom It May Concern:

I, Abbas Ebnonnasir, hereby give permission to Adbdulfattah Abdulslam to use the theory and modelling sections of the main text and supplementary information of the manuscript nl-2018-00966x entitled "Bifurcation and Orientation-Dependence of Corrugation of 2-D Hexagonal Boron Nitride on Palladium" submitted to Nano Letters on 3/12/2018. In addition, I also give permission to use the experimental figure 4c as motivation for the computational modelling.

Sincerely,
Abbas

On Sat, Mar 17, 2018 at 11:15 AM, Abdulfattah Abdulslam <aabdulsl@mymail.mines.edu> wrote:
[Quoted text hidden]

Abdulfattah Abdulslam <aabdulsl@mymail.mines.edu>

permission to use material in thesis

Cristian Ciobanu <cciobanu@mines.edu> Sat, Mar 17, 2018 at 12:26 PM
To: Abdulfattah Abdulslam <aabdulsl@mymail.mines.edu>, Suneel Kodambaka <kodambaka@ucla.edu>
Cc: Pedro Arias <pedro.arias89@gmail.com>, Abbas Ebnonnasir <aebnonna@ucla.edu>

I, Cristian Ciobanu, hereby give permission to Adbdulfattah Abdulslam to use the theory and modelling sections of the main text and supplementary information of the manuscript nl-2018-00966x entitled "Bifurcation and Orientation-Dependence of Corrugation of 2-D Hexagonal Boron Nitride on Palladium" submitted to Nano Letters on 3/12/2018. In addition, I also give permission to use the experimental figure 4c as motivation for the computational modelling.

Cristian V. Ciobanu, PhD
Fellow of the Institute of Physics (UK)
Professor, Dept of Mechanical Engineering
and Materials Science Program
Colorado School of Mines
Phone: 303-384-2119
Fax: 303-273-3602
Email: cciobanu@mines.edu
http://www.mines.edu/~cciobanu

REFERENCES CITED

[1] Andre K Geim and Konstantin S Novoselov. The rise of graphene. *Nature Materials*, 6(3):183–191, 2007.

[2] LD Landau. Zur theorie der phasenumwandlungen ii. *Phys. Z. Sowjetunion*, 11:26–35, 1937.

[3] Rudolf Peierls. Quelques propriétés typiques des corps solides. In *Annales de l'institut Henri Poincaré*, volume 5, pages 177–222, 1935.

[4] J George Bednorz and K Alex Müller. Possible high t c superconductivity in the balacuo system. In *Ten Years Of Superconductivity: 1980–1990*, pages 267–271. Springer, 1986.

[5] Sheneve Z Butler, Shawna M Hollen, Linyou Cao, Yi Cui, Jay A Gupta, Humberto R Gutiérrez, Tony F Heinz, Seung Sae Hong, Jiaxing Huang, Ariel F Ismach, et al. Progress, challenges, and opportunities in two-dimensional materials beyond graphene. *ACS Nano*, 7(4):2898–2926, 2013.

[6] Yoichi Kamihara, Hidenori Hiramatsu, Masahiro Hirano, Ryuto Kawamura, Hiroshi Yanagi, Toshio Kamiya, and Hideo Hosono. Iron-based layered superconductor: Laofep. *Journal of Catalysisf the American Chemical Society*, 128(31):10012–10013, 2006.

[7] JA Wilson and AD Yoffe. The transition metal dichalcogenides discussion and interpretation of the observed optical, electrical and structural properties. *Advances in Physics*, 18(73):193–335, 1969.

[8] Jannik C Meyer, Andre K Geim, MI Katsnelson, KS Novoselov, TJ Booth, and S Roth. The structure of suspended graphene sheets. *Nature*, 446(7131):60–63, 2007.

[9] Mildred S Dresselhaus and G Dresselhaus. Intercalation compounds of graphite. *Advances in Physics*, 51(1):1–186, 2002.

[10] Masukazu Hirata, Takuya Gotou, Shigeo Horiuchi, Masahiro Fujiwara, and Michio Ohba. Thin-film particles of graphite oxide 1:: High-yield synthesis and flexibility of the particles. *Carbon*, 42(14):2929–2937, 2004.

[11] Sasha Stankovich, Dmitriy A Dikin, Geoffrey HB Dommett, Kevin M Kohlhaas, Eric J Zimney, Eric A Stach, Richard D Piner, SonBinh T Nguyen, and Rodney S Ruoff. Graphene-based composite materials. *Nature*, 442(7100):282–286, 2006.

[12] Min-Feng Yu, Oleg Lourie, Mark J Dyer, Katerina Moloni, Thomas F Kelly, and Rodney S Ruoff. Strength and breaking mechanism of multiwalled carbon nanotubes under tensile load. *Science*, 287(5453):637–640, 2000.

[13] Claire Berger, Zhimin Song, Tianbo Li, Xuebin Li, Asmerom Y Ogbazghi, Rui Feng, Zhenting Dai, Alexei N Marchenkov, Edward H Conrad, Phillip N First, et al. Ultrathin epitaxial graphite: 2d electron gas properties and a route toward graphene-based nanoelectronics. *The Journal of Physical Chemistry B*, 108(52):19912–19916, 2004.

[14] Yuanbo Zhang, Yan-Wen Tan, Horst L Stormer, and Philip Kim. Experimental observation of the quantum hall effect and berry's phase in graphene. *Nature*, 438(7065): 201–204, 2005.

[15] Ruben Mas-Balleste, Cristina Gomez-Navarro, Julio Gomez-Herrero, and Felix Zamora. 2d materials: to graphene and beyond. *Nanoscale*, 3(1):20–30, 2011.

[16] Alexander A Balandin, Suchismita Ghosh, Wenzhong Bao, Irene Calizo, Desalegne Teweldebrhan, Feng Miao, and Chun Ning Lau. Superior thermal conductivity of single-layer graphene. *Nano Letters*, 8(3):902–907, 2008.

[17] KSA Novoselov, Andre K Geim, SVb Morozov, Da Jiang, MIc Katsnelson, IVa Grigorieva, SVb Dubonos, and AAb Firsov. Two-dimensional gas of massless dirac fermions in graphene. *Nature*, 438(7065):197–200, 2005.

[18] Alfonso Reina, Xiaoting Jia, John Ho, Daniel Nezich, Hyungbin Son, Vladimir Bulovic, Mildred S Dresselhaus, and Jing Kong. Large area, few-layer graphene films on arbitrary substrates by chemical vapor deposition. *Nano Letters*, 9(1):30–35, 2008.

[19] AL Vázquez De Parga, F Calleja, BMCG Borca, MCG Passeggi Jr, JJ Hinarejos, F Guinea, and R Miranda. Periodically rippled graphene: growth and spatially resolved electronic structure. *Physical Review Letters*, 100(5):056807, 2008.

[20] S Marchini, S Günther, and J Wintterlin. Scanning tunneling microscopy of graphene on Ru (0001). *Physical Review B*, 76(7):075429, 2007.

[21] Hirokazu Ueta, Morihiko Saida, Chikara Nakai, Yoichi Yamada, Masahiro Sasaki, and Shigehiko Yamamoto. Highly oriented monolayer graphite formation on Pt (1 1 1) by a supersonic methane beam. *Surface Science*, 560(1-3):183–190, 2004.

[22] David E Starr, Eugene M Pazhetnov, Andrey I Stadnichenko, Andrey I Boronin, and Shamil K Shaikhutdinov. Carbon films grown on Pt (1 1 1) as supports for model gold catalysts. *Surface Science*, 600(13):2688–2695, 2006.

[23] DW Goodman and JT Yates Jr. Co isotopic mixing measurements on nickel: Evidence for irreversibility of co dissociation. *Journal of Catalysis*, 82(2):255–260, 1983.

[24] AG Starodubov, MA Medvetskii, AM Shikin, and VK Adamchuk. Intercalation of silver atoms under a graphite monolayer on Ni (111). *Physics of the Solid State*, 46 (7):1340–1348, 2004.

[25] NR Gall, EV Rutkov, and A Ya Tontegode. Interaction of silver atoms with iridium and with a two-dimensional graphite film on iridium: Adsorption, desorption, and dissolution. *Physics of the Solid State*, 46(2):371–377, 2004.

[26] Johann Coraux, Alpha T N Diaye, Carsten Busse, and Thomas Michely. Structural coherency of graphene on Ir (111). *Nano Letters*, 8(2):565–570, 2008.

[27] Congqin Miao, Churan Zheng, Owen Liang, and Ya-Hong Xie. Chemical vapor deposition of graphene. In *Physics and Applications of Graphene-experiments*. InTech, 2011.

[28] YI Zhang, Luyao Zhang, and Chongwu Zhou. Review of chemical vapor deposition of graphene and related applications. *Accounts of Chemical Research*, 46(10):2329–2339, 2013.

[29] Yumeng Shi, Christoph Hamsen, Xiaoting Jia, Ki Kang Kim, Alfonso Reina, Mario Hofmann, Allen Long Hsu, Kai Zhang, Henan Li, Zhen-Yu Juang, Li Lain-Jong Dress-Dresselhaus, Mi. S., and Jing Kong. Synthesis of few-layer hexagonal boron nitride thin film by chemical vapor deposition. *Nano Letters*, 10(10):4134–4139, 2010.

[30] Ki Kang Kim, Allen Hsu, Xiaoting Jia, Soo Min Kim, Yumeng Shi, Mario Hofmann, Daniel Nezich, Joaquin F Rodriguez-Nieva, Mildred Dresselhaus, Tomas Palacios, and Jing Kong. Synthesis of monolayer hexagonal boron nitride on cu foil using chemical vapor deposition. *Nano Letters*, 12(1):161–166, 2011.

[31] Seiichiro Matsumoto and Wenjun Zhang. Synthesis of boron nitride films by microwave plasma chemical vapor deposition in fluorine-containing gases. *Japanese Journal of Applied Physics*, 40(6A):L570, 2001.

[32] Li Song, Lijie Ci, Hao Lu, Pavel B Sorokin, Chuanhong Jin, Jie Ni, Alexander G Kvashnin, Dmitry G Kvashnin, Jun Lou, Boris I Yakobson, and Pluickel. M. Ajayan. Large scale growth and characterization of atomic hexagonal boron nitride layers. *Nano Letters*, 10(8):3209–3215, 2010.

[33] D Pacile, JC Meyer, C O Girit, and A Zettl. The two-dimensional phase of boron nitride: few-atomic-layer sheets and suspended membranes. *Applied Physics Letters*, 92(13):133107, 2008.

[34] Mark P Levendorf, Cheol-Joo Kim, Lola Brown, Pinshane Y Huang, Robin W Havener, David A Muller, and Jiwoong Park. Graphene and boron nitride lateral heterostructures for atomically thin circuitry. *Nature*, 488(7413):627–632, 2012.

[35] Jian-Hao Chen, Chaun Jang, Shudong Xiao, Masa Ishigami, and Michael S Fuhrer. Intrinsic and extrinsic performance limits of graphene devices on SiO2. *Nature Nanotechnology*, 3(4):206–209, 2008.

[36] Xuesong Li, Weiwei Cai, Jinho An, Seyoung Kim, Junghyo Nah, Dongxing Yang, Richard Piner, Aruna Velamakanni, Inhwa Jung, Emanuel Tutuc, Sanjay K. Banerjee, Ligi Colombo, and Rodney S. Ruoff. Large-area synthesis of high-quality and uniform graphene films on copper foils. *Science*, 324(5932):1312–1314, 2009.

[37] L Britnell, RV Gorbachev, R Jalil, BD Belle, F Schedin, A Mishchenko, T Georgiou, MI Katsnelson, L Eaves, SV Morozov, N. M. R. Peres, J. Leis, Geim A. K. ., Nov . Novoselov, and L. A. Ponomarenko. Field-effect tunneling transistor based on vertical graphene heterostructures. *Science*, 335(6071):947–950, 2012.

[38] Kin Fai Mak, Changgu Lee, James Hone, Jie Shan, and Tony F Heinz. Atomically thin MoS_2: a new direct-gap semiconductor. *Physical Review Letters*, 105(13):136805, 2010.

[39] Zongyou Yin, Hai Li, Hong Li, Lin Jiang, Yumeng Shi, Yinghui Sun, Gang Lu, Qing Zhang, Xiaodong Chen, and Hua Zhang. Single-layer MoS_2 phototransistors. *ACS Nano*, 6(1):74–80, 2011.

[40] Yi-Hsien Lee, Xin-Quan Zhang, Wenjing Zhang, Mu-Tung Chang, Cheng-Te Lin, Kai-Di Chang, Ya-Chu Yu, Jacob Tse-Wei Wang, Chia-Seng Chang, Lain-Jong Li, and Tsung-Wu Lin. Synthesis of large-area MoS_2 atomic layers with chemical vapor deposition. *Advanced Materials*, 24(17):2320–2325, 2012.

[41] Andres Castellanos-Gomez, Menno Poot, Gary A Steele, Herre SJ van der Zant, Nicolás Agraït, and Gabino Rubio-Bollinger. Elastic properties of freely suspended MoS_2 nanosheets. *Advanced Materials*, 24(6):772–775, 2012.

[42] Abbas Ebnonnasir, Badri Narayanan, Suneel Kodambaka, and Cristian V Ciobanu. Tunable MoS_2 bandgap in MoS_2-graphene heterostructures. *Applied Physics Letters*, 105(3):031603, 2014.

[43] Yongjie Zhan, Zheng Liu, Sina Najmaei, Pulickel M Ajayan, and Jun Lou. Large-area vapor-phase growth and characterization of MoS_2 atomic layers on a SiO_2 substrate. *Small*, 8(7):966–971, 2012.

[44] Shanshan Wang, Xiaochen Wang, and Jamie H Warner. All chemical vapor deposition growth of MoS_2: h-BN vertical van der waals heterostructures. *ACS Nano*, 9(5):5246–5254, 2015.

[45] Jaeho Jeon, Sung Kyu Jang, Su Min Jeon, Gwangwe Yoo, Yun Hee Jang, Jin-Hong Park, and Sungjoo Lee. Layer-controlled CVD growth of large-area two-dimensional mos 2 films. *Nanoscale*, 7(5):1688–1695, 2015.

[46] Patrick Vogt, Paola De Padova, Claudio Quaresima, Jose Avila, Emmanouil Frantzeskakis, Maria Carmen Asensio, Andrea Resta, Bénédicte Ealet, and Guy Le Lay. Silicene: compelling experimental evidence for graphenelike two-dimensional silicon. *Physical Review Letters*, 108(15):155501, 2012.

[47] Boubekeur Lalmi, Hamid Oughaddou, Hanna Enriquez, Abdelkader Kara, Sébastien Vizzini, Bénidicte Ealet, and Bernard Aufray. Epitaxial growth of a silicene sheet. *Applied Physics Letters*, 97(22):223109, 2010.

[48] Ruth E Roman and Steven W Cranford. Mechanical properties of silicene. *Computational Materials Science*, 82:50–55, 2014.

[49] Michel Houssa, Geoffrey Pourtois, VV Afanas' Ev, and Andre Stesmans. Can silicon behave like graphene? a first-principles study. *Applied Physics Letters*, 97(11):112106, 2010.

[50] Abdelkader Kara, Hanna Enriquez, Ari P Seitsonen, LC Lew Yan Voon, Sébastien Vizzini, Bernard Aufray, and Hamid Oughaddou. A review on silicene-new candidate for electronics. *Surface Science Reports*, 67(1):1–18, 2012.

[51] ND Drummond, Viktor Zolyomi, and VI Fal'Ko. Electrically tunable band gap in silicene. *Physical Review B*, 85(7):075423, 2012.

[52] ME Dávila, Lede Xian, S Cahangirov, Angel Rubio, and G Le Lay. Germanene: a novel two-dimensional germanium allotrope akin to graphene and silicene. *New Journal of Physics*, 16(9):095002, 2014.

[53] Linfei Li, Shuang-zan Lu, Jinbo Pan, Zhihui Qin, Yu-qi Wang, Yeliang Wang, Geng-yu Cao, Shixuan Du, and Hong-Jun Gao. Buckled germanene formation on Pt (111). *Advanced Materials*, 26(28):4820–4824, 2014.

[54] Shan Dong and Chang-Qing Chen. Stability, elastic properties, and electronic structure of germanane nanoribbons. *Journal of Physics: Condensed Matter*, 27(24):245303, 2015.

[55] Michel Houssa, Emilio Scalise, Kiroubanand Sankaran, Geoffrey Pourtois, VV AfanasEv, and Andre Stesmans. Electronic properties of hydrogenated silicene and germanene. *Applied Physics Letters*, 98(22):223107, 2011.

[56] Meng Ye, Ruge Quhe, Jiaxin Zheng, Zeyuan Ni, Yangyang Wang, Yakun Yuan, Geoffrey Tse, Junjie Shi, Zhengxiang Gao, and Jing Lu. Tunable band gap in germanene by surface adsorption. *Physica E: Low-dimensional Systems and Nanostructures*, 59: 60–65, 2014.

[57] Eugenie Samuel Reich et al. Phosphorene excites materials scientists. *Nature*, 506 (7486):19, 2014.

[58] Liangzhi Kou, Changfeng Chen, and Sean C Smith. Phosphorene: fabrication, properties, and applications. *The Journal of Physical Chemistry Letters*, 6(14):2794–2805, 2015.

[59] Jin Tao, Wanfu Shen, Sen Wu, Lu Liu, Zhihong Feng, Chao Wang, Chunguang Hu, Pei Yao, Hao Zhang, Wei Pang, et al. Mechanical and electrical anisotropy of few-layer black phosphorus. *ACS Nano*, 9(11):11362–11370, 2015.

[60] Han Liu, Adam T Neal, Zhen Zhu, Zhe Luo, Xianfan Xu, David Tománek, and Peide D Ye. Phosphorene: an unexplored 2d semiconductor with a high hole mobility. *ACS Nano*, 8(4):4033–4041, 2014.

[61] Yongqing Cai, Gang Zhang, and Yong-Wei Zhang. Layer-dependent band alignment and work function of few-layer phosphorene. *Scientific Reports*, 4, 2014.

[62] Abbas Ebnonnasir, Suneel Kodambaka, and Cristian V Ciobanu. Strongly and weakly interacting configurations of hexagonal boron nitride on nickel. *Surface Review and Letters*, 22(06):1550078, 2015.

[63] Sushobhan Joshi, David Ecija, Ralph Koitz, Marcella Iannuzzi, Ari P Seitsonen, Jurg Hutter, Hermann Sachdev, Saranyan Vijayaraghavan, Felix Bischoff, Knud Seufert, Johannes V. Barth, and Willi Auwärter. Boron nitride on Cu (111): an electronically corrugated monolayer. *Nano Letters*, 12(11):5821–5828, 2012.

[64] Munkhbayar Batmunkh, Munkhjargal Bat-Erdene, and Joseph G Shapter. Phosphorene and phosphorene-based materials–prospects for future applications. *Advanced Materials*, 2016.

[65] Apratim Khandelwal, Karthick Mani, Manohar Harsha Karigerasi, and Indranil Lahiri. Phosphorene–the two-dimensional black phosphorous: Properties, synthesis and applications. *Materials Science and Engineering: B*, 221:17–34, 2017.

[66] Vy Tran, Ryan Soklaski, Yufeng Liang, and Li Yang. Layer-controlled band gap and anisotropic excitons in few-layer black phosphorus. *Physical Review B*, 89(23):235319, 2014.

[67] Likai Li, Jonghwan Kim, Chenhao Jin, Guo Jun Ye, Diana Y Qiu, H Felipe, Zhiwen Shi, Long Chen, Zuocheng Zhang, Fangyuan Yang, et al. Direct observation of the layer-dependent electronic structure in phosphorene. *Nature Nanotechnology*, 12(1): 21, 2017.

[68] Vy Tran, Ryan Soklaski, Yufeng Liang, and Li Yang. Layer-controlled band gap and anisotropic excitons in few-layer black phosphorus. *Phys. Rev. B*, 89(6):235319, Jun 2014. doi: 10.1103/PhysRevB.89.235319. URL `https://link.aps.org/doi/10.1103/PhysRevB.89.235319`.

[69] Varrla Eswaraiah, Qingsheng Zeng, Yi Long, and Zheng Liu. Black phosphorus nanosheets: synthesis, characterization and applications. *Small*, 12(26):3480–3502, 2016.

[70] Fengnian Xia, Han Wang, and Yichen Jia. Rediscovering black phosphorus as an anisotropic layered material for optoelectronics and electronics. *Nature Communications*, 5:4458, 2014.

[71] Likai Li, Yijun Yu, Guo Jun Ye, Qingqin Ge, Xuedong Ou, Hua Wu, Donglai Feng, Xian Hui Chen, and Yuanbo Zhang. Black phosphorus field-effect transistors. *Nature Nanotechnology*, 9(5):372, 2014.

[72] Michele Buscema, Dirk J Groenendijk, Gary A Steele, Herre Sj Van Der Zant, and Andres Castellanos-Gomez. Photovoltaic effect in few-layer black phosphorus pn junctions defined by local electrostatic gating. *Nature Communications*, 5:4651, 2014.

[73] Qihang Liu, Xiuwen Zhang, LB Abdalla, Adalberto Fazzio, and Alex Zunger. Switching a normal insulator into a topological insulator via electric field with application to phosphorene. *Nano Letters*, 15(2):1222–1228, 2015.

[74] Jack R Brent, Nicky Savjani, Edward A Lewis, Sarah J Haigh, David J Lewis, and Paul O'Brien. Production of few-layer phosphorene by liquid exfoliation of black phosphorus. *Chemical Communications*, 50(87):13338–13341, 2014.

[75] Andres Castellanos-Gomez, Leonardo Vicarelli, Elsa Prada, Joshua O Island, KL Narasimha-Acharya, Sofya I Blanter, Dirk J Groenendijk, Michele Buscema, Gary A Steele, JV Alvarez, et al. Isolation and characterization of few-layer black phosphorus. *2D Materials*, 1(2):025001, 2014.

[76] Adrien Allard and Ludger Wirtz. Graphene on metallic substrates: suppression of the kohn anomalies in the phonon dispersion. *Nano Letters*, 10(11):4335–4340, 2010.

[77] Elena Voloshina and Yuriy Dedkov. Graphene on metallic surfaces: problems and perspectives. *Physical Chemistry Chemical Physics*, 14(39):13502–13514, 2012.

[78] GAKPA Giovannetti, PA Khomyakov, G Brocks, VM vd Karpan, J Van den Brink, and Paul J Kelly. Doping graphene with metal contacts. *Physical Revieweview Letters*, 101(2):026803, 2008.

[79] Jun Yan, Kristian S Thygesen, and Karsten W Jacobsen. Nonlocal screening of plasmons in graphene by semiconducting and metallic substrates: first-principles calculations. *Physical Review Letters*, 106(14):146803, 2011.

[80] Soon-Yong Kwon, Cristian V Ciobanu, Vania Petrova, Vivek B Shenoy, Javier Bareno, Vincent Gambin, Ivan Petrov, and Suneel Kodambaka. Growth of semiconducting graphene on palladium. *Nano Letters*, 9(12):3985–3990, 2009.

[81] Joshua B Smith, Daniel Hagaman, and Hai-Feng Ji. Growth of 2d black phosphorus film from chemical vapor deposition. *Nanotechnology*, 27(21):215602, 2016.

[82] Ziming Zhang, Deng-Hui Xing, Jun Li, and Qingfeng Yan. Hittorf's phosphorus: the missing link during transformation of red phosphorus to black phosphorus. *CrystEngComm*, 19(6):905–909, 2017.

[83] KG Keong, W Sha, and S Malinov. Crystallisation kinetics and phase transformation behaviour of electroless nickel–phosphorus deposits with high phosphorus content. *Journal of Alloys and Compounds*, 334(1-2):192–199, 2002.

[84] Samira Bagheri, Negar Mansouri, and Ermia Aghaie. Phosphorene: a new competitor for graphene. *International Journal of Hydrogen Energy*, 41(7):4085–4095, 2016.

[85] Gene Siegel, Cristian V Ciobanu, Badri Narayanan, Michael Snure, and Stefan C Badescu. Heterogeneous pyrolysis: a route for epitaxial growth of hbn atomic layers on copper using separate boron and nitrogen precursors. *Nano Letters*, 17(4):2404–2413, 2017.

[86] B. Predel. *Numerical Data and Functional Relationships in Science and Technology*, volume 5 of *5d*. Springer-Verlag Berlin Heidelberg, Berlin, Heidelberg, 1994.

[87] J Scott Bunch, Scott S Verbridge, Jonathan S Alden, Arend M Van Der Zande, Jeevak M Parpia, Harold G Craighead, and Paul L McEuen. Impermeable atomic membranes from graphene sheets. *Nano Letters*, 8(8):2458–2462, 2008.

[88] Georg Kresse and Jürgen Furthmüller. Efficient iterative schemes for ab initio total-energy calculations using a plane-wave basis set. *Physical Review B*, 54(16):11169, 1996.

[89] Georg Kresse and Jürgen Furthmüller. Efficiency of ab-initio total energy calculations for metals and semiconductors using a plane-wave basis set. *Computational Materials Science*, 6(1):15–50, 1996.

[90] John P Perdew, Kieron Burke, and Matthias Ernzerhof. Generalized gradient approximation made simple. *Physical Review Letters*, 77(18):3865, 1996.

[91] Stefan Grimme. Semiempirical gga-type density functional constructed with a long-range dispersion correction. *Journal of Computational Chemistry*, 27(15):1787–1799, 2006.

[92] Menno Bokdam, Geert Brocks, Mikhail I Katsnelson, and Paul J Kelly. Schottky barriers at hexagonal boron nitride/metal interfaces: A first-principles study. *Physical Review B*, 90(8):085415, 2014.

[93] Graeme Henkelman, Blas P Uberuaga, and Hannes Jónsson. A climbing image nudged elastic band method for finding saddle points and minimum energy paths. *The Journal of Chemical Physics*, 113(22):9901–9904, 2000.

[94] Graeme Henkelman and Hannes Jónsson. Improved tangent estimate in the nudged elastic band method for finding minimum energy paths and saddle points. *The Journal of Chemical Physics*, 113(22):9978–9985, 2000.

[95] Hannes Jónsson, Greg Mills, and Karsten W Jacobsen. Nudged elastic band method for finding minimum energy paths of transitions. In *Classical and quantum dynamics in condensed phase simulations*, pages 385–404. World Scientific, 1998.

[96] B.N. Jariwala, O.S. Dewey, P. Stradins, C.V. Ciobanu, and S. Agarwal. In situ gas-phase hydrosilylation of plasma-synthesized silicon nanocrystals. *ACS Applied Materials and Interfaces*, 3(8):3033–3041, 2011.

[97] B.N. Jariwala, C.V. Ciobanu, and S. Agarwal. Atomic hydrogen interacions with amorphous carbon thin films. *Journal of Applied Physics*, 106(7):073305, 2009.

[98] B.N. Jariwala, N.J. Kramer, M.C. Petcu, D.C. Bobela, M.C.M. van den Sanden, P. Stradins, C.V. Ciobanu, and S. Agarwal. Surface hydride composition of plasma-synthesized si nanoparticles. *Journal of Physical Chemistry C*, 115(42):20375–20379, 2011.

[99] Toyosei Kawasaki, Takashi Ichimura, Hiroshi Kishimoto, Ade Asneil Akbar, Takashi Ogawa, and Chuhei Oshima. Double atomic layers of graphene/monolayer h-bn on ni (111) studied by scanning tunneling microscopy and scanning tunneling spectroscopy. *Surface Review and Letters*, 9(03n04):1459–1464, 2002.

[100] C Oshima, A Itoh, E Rokuta, T Tanaka, K Yamashita, and T Sakurai. A hetero-epitaxial-double-atomic-layer system of monolayer graphene/monolayer h-BN on Ni (111). *Solid State Communications*, 116(1):37–40, 2000.

[101] C Oshima, N Tanaka, A Itoh, E Rokuta, K Yamashita, and T Sakurai. A heteroepitaxial multi-atomic-layer system of graphene and h-BN. *Surface Review and Letters*, 7(05n06):521–525, 2000.

[102] ME Medina, A Galano, and JR Alvarez-Idaboy. Site reactivity in the free radicals induced damage to leucine residues: a theoretical study. *Physical Chemistry Chemical Physics*, 17(7):4970–4976, 2015.

[103] T Bligaard, Jens Kehlet Nørskov, Søren Dahl, J Matthiesen, Claus H Christensen, and J Sehested. The brønsted–evans–polanyi relation and the volcano curve in heterogeneous catalysis. *Journal of Catalysis*, 224(1):206–217, 2004.

[104] Ashildur Logadottir, Thomas Holm Rod, Jens Kehlet Nørskov, Bjørk Hammer, Søren Dahl, and CJH Jacobsen. The brønsted–evans–polanyi relation and the volcano plot for ammonia synthesis over transition metal catalysts. *Journal of Catalysis*, 197(2): 229–231, 2001.

[105] Shantanu Roy, Stefan Goedecker, and Vladimir Hellmann. Bell-evans-polanyi principle for molecular dynamics trajectories and its implications for global optimization. *Physical Review E*, 77(5):056707, 2008.

[106] Min Wang, Minwoo Kim, Dorj Odkhuu, Noejung Park, Joohyun Lee, Won-Jun Jang, Se-Jong Kahng, Rodney S Ruoff, Young Jae Song, and Sungjoo Lee. Catalytic transparency of hexagonal boron nitride on copper for chemical vapor deposition growth of large-area and high-quality graphene. *ACS Nano*, 8(6):5478–5483, 2014.

[107] Robert Laskowski, Peter Blaha, Thomas Gallauner, and Karlheinz Schwarz. Single-layer model of the hexagonal boron nitride nanomesh on the Rh (111) surface. *Physical Review Letters*, 98(10):106802, 2007.

[108] R. Cortes, D.P. Acharya, C.V. Ciobanu, E. Sutter, and P. Sutter. Graphene on ru(0001) moire corrugation studied by scanning tunneling microscopy on au/graphene/ru(0001) heterostructures. *Journal of Physical Chemistry C*, 117(40):20675–20680, 2013.

[109] Ariel Ismach, Harry Chou, Domingo A Ferrer, Yaping Wu, Stephen McDonnell, Herman C Floresca, Alan Covacevich, Cody Pope, Richard Piner, Moon J Kim, Robert M. Wallace, Luigi Colombo, and Rodney S Ruoff. Toward the controlled synthesis of hexagonal boron nitride films. *Acs Nano*, 6(7):6378–6385, 2012.

[110] Roland Haubner, Matthias Wilhelm, Ronald Weissenbacher, and Benno Lux. Boron nitridesproperties, synthesis and applications. In *High Performance Non-Oxide Ceramics II*, pages 1–45. Springer, 2002.

[111] Kenji Watanabe, Takashi Taniguchi, and Hisao Kanda. Direct-bandgap properties and evidence for ultraviolet lasing of hexagonal boron nitride single crystal. *Nature Materials*, 3(6):404, 2004.

[112] Cory R Dean, Andrea F Young, Inanc Meric, Chris Lee, Lei Wang, Sebastian Sorgenfrei, Kenji Watanabe, Takashi Taniguchi, Phillip Kim, Kenneth L Shepard, and J Hone. Boron nitride substrates for high-quality graphene electronics. *Nature Nanotechnology*, 5(10):722, 2010.

[113] Alexander S Mayorov, Roman V Gorbachev, Sergey V Morozov, Liam Britnell, Rashid Jalil, Leonid A Ponomarenko, Peter Blake, Kostya S Novoselov, Kenji Watanabe, Takashi Taniguchi, and Geim A. K. Micrometer-scale ballistic transport in encapsulated graphene at room temperature. *Nano Letters*, 11(6):2396–2399, 2011.

[114] Gang Shi, Yuranan Hanlumyuang, Zheng Liu, Yongji Gong, Weilu Gao, Bo Li, Junichiro Kono, Jun Lou, Robert Vajtai, Pradeep Sharma, and Pulickel M. Ajayan. Boron nitride–graphene nanocapacitor and the origins of anomalous size-dependent increase of capacitance. *Nano Letters*, 14(4):1739–1744, 2014.

[115] Ji-Hoon Park, Jin Cheol Park, Seok Joon Yun, Hyun Kim, Dinh Hoa Luong, Soo Min Kim, Soo Ho Choi, Woochul Yang, Jing Kong, Ki Kang Kim, et al. Large-area monolayer hexagonal boron nitride on pt foil. *Acs Nano*, 8(8):8520–8528, 2014.

[116] Peter Sutter, Jayeeta Lahiri, Peter Albrecht, and Eli Sutter. Chemical vapor deposition and etching of high-quality monolayer hexagonal boron nitride films. *ACS Nano*, 5(9): 7303–7309, 2011.

[117] AB Preobrajenski, AS Vinogradov, May Ling Ng, E Ćavar, Rasmus Westerström, Anders Mikkelsen, Edvin Lundgren, and Nils Mårtensson. Influence of chemical interaction at the lattice-mismatched h-BN/ Rh (111) and h-BN/ Pt (111) interfaces on the overlayer morphology. *Physical Review B*, 75(24):245412, 2007.

[118] Sabina Caneva, Robert S Weatherup, Bernhard C Bayer, Barry Brennan, Steve J Spencer, Ken Mingard, Andrea Cabrero-Vilatela, Carsten Baehtz, Andrew J Pollard, and Stephan Hofmann. Nucleation control for large, single crystalline domains of monolayer hexagonal boron nitride via si-doped fe catalysts. *Nano Letters*, 15(3): 1867–1875, 2015.

[119] Chuhei Oshima and Ayato Nagashima. Ultra-thin epitaxial films of graphite and hexagonal boron nitride on solid surfaces. *Journal of Physics: Condensed Matter*, 9 (1):1, 1997.

[120] Zhao Jiang, Pei Qin, and Tao Fang. Mechanism of ammonia decomposition on clean and oxygen-covered Cu (1 1 1) surface: A dft study. *Chemical Physics*, 445:59–67, 2014.

[121] Yang Gao, Wencai Ren, Teng Ma, Zhibo Liu, Yu Zhang, Wen-Bin Liu, Lai-Peng Ma, Xiuliang Ma, and Hui-Ming Cheng. Repeated and controlled growth of monolayer, bilayer and few-layer hexagonal boron nitride on pt foils. *Acs Nano*, 7(6):5199–5206, 2013.

[122] Majharul Haque Khan, Zhenguo Huang, Feng Xiao, Gilberto Casillas, Zhixin Chen, Paul J Molino, and Hua Kun Liu. Erratum: Synthesis of large and few atomic layers of hexagonal boron nitride on melted copper. *Scientific Reports*, 5, 2015.

[123] Soo Min Kim, Allen Hsu, Min Ho Park, Sang Hoon Chae, Seok Joon Yun, Joo Song Lee, Dae-Hyun Cho, Wenjing Fang, Changgu Lee, Tomás Palacios, Mildred Dresselhaus, Ki Kang Kim, Young Hee Lee, and Kong Jing. Synthesis of large-area multilayer hexagonal boron nitride for high material performance. *Nature Communications*, 6: 8662, 2015.

[124] Mingsheng Xu, Daisuke Fujita, Hongzheng Chen, and Nobutaka Hanagata. Formation of monolayer and few-layer hexagonal boron nitride nanosheets via surface segregation. *Nanoscale*, 3(7):2854–2858, 2011.

[125] A Nagashima, N Tejima, Y Gamou, T Kawai, and C Oshima. Electronic structure of monolayer hexagonal boron nitride physisorbed on metal surfaces. *Physical Review Letters*, 75(21):3918, 1995.

[126] M Morscher, M Corso, T Greber, and J Osterwalder. Formation of single layer h-BN on Pd (111). *Surface Science*, 600(16):3280–3284, 2006.

[127] Martina Corso, Thomas Greber, and Jürg Osterwalder. h-BN on Pd (110): a tunable system for self-assembled nanostructures? *Surface Science*, 577(2):L78–L84, 2005.

[128] Martina Corso, Willi Auwärter, Matthias Muntwiler, Anna Tamai, Thomas Greber, and Jürg Osterwalder. Boron nitride nanomesh. *Science*, 303(5655):217–220, 2004.

[129] Andrii Goriachko, Yunbin He, Marcus Knapp, Herbert Over, Martina Corso, Thomas Brugger, Simon Berner, Juerg Osterwalder, and Thomas Greber. Self-assembly of a hexagonal boron nitride nanomesh on Ru (0001). *Langmuir*, 23(6):2928–2931, 2007.

[130] Fabrizio Orlando, Rosanna Larciprete, Paolo Lacovig, Ilan Boscarato, Alessandro Baraldi, and Silvano Lizzit. Epitaxial growth of hexagonal boron nitride on Ir (111). *The Journal of Physical Chemistry C*, 116(1):157–164, 2011.

[131] AB Preobrajenski, AS Vinogradov, and Nils Mårtensson. Monolayer of h-BN chemisorbed on Cu (111) and Ni (111): The role of the transition metal 3d states. *Surface Science*, 582(1):21–30, 2005.

[132] Y Murata, E Starodub, BB Kappes, CV Ciobanu, NC Bartelt, KF McCarty, and S Kodambaka. Orientation-dependent work function of graphene on Pd (111). *Applied Physics Letters*, 97(14):143114, 2010.

[133] Y Murata, S Nie, A Ebnonnasir, E Starodub, BB Kappes, KF McCarty, CV Ciobanu, and S Kodambaka. Growth structure and work function of bilayer graphene on Pd (111). *Physical Review B*, 85(20):205443, 2012.

[134] Robert Laskowski, Peter Blaha, and Karlheinz Schwarz. Bonding of hexagonal BN to transition metal surfaces: An ab initio density-functional theory study. *Physical Review B*, 78(4):045409, 2008.

[135] B Wang, M-L Bocquet, S Marchini, S Günther, and J Wintterlin. Chemical origin of a graphene moiré overlayer on Ru (0001). *Physical Chemistry Chemical Physics*, 10 (24):3530–3534, 2008.

[136] Eryin Wang, Guorui Chen, Guoliang Wan, Xiaobo Lu, Chaoyu Chen, Jose Avila, Alexei V Fedorov, Guangyu Zhang, Maria C Asensio, Yuanbo Zhang, and Shuyun Zhou. Electronic structure of transferred graphene/h-BN van der waals heterostructures with nonzero stacking angles by nano-ARPES. *Journal of Physics: Condensed Matter*, 28(44):444002, 2016.

[137] Gerd Binnig, Heinrich Rohrer, Ch Gerber, and Edmund Weibel. Surface studies by scanning tunneling microscopy. *Physical Review Letters*, 49(1):57, 1982.

[138] Gerd Binnig and Heinrich Rohrer. Scanning tunneling microscopy. *Surface Science*, 126(1-3):236–244, 1983.

[139] J Tersoff and DR Hamann. Theory and application for the scanning tunneling microscope. *Physical Review Letters*, 50(25):1998, 1983.

[140] Jerry Tersoff and DR Hamann. Theory of the scanning tunneling microscope. In *scanning tunneling microscopy*, pages 59–67. Springer, 1985.

[141] L Petersen, PT Sprunger, Ph Hofmann, Erik Lægsgaard, BG Briner, M Doering, H-P Rust, AM Bradshaw, Flemming Besenbacher, and EW Plummer. Direct imaging of the two-dimensional fermi contour: Fourier-transform STM. *Physical Review B*, 57 (12):R6858, 1998.

[142] Zhao Y Rong and Pieter Kuiper. Electronic effects in scanning tunneling microscopy: Moiré pattern on a graphite surface. *Physical Review B*, 48(23):17427, 1993.

[143] Marcella Iannuzzi and Juerg Hutter. Comparative study of the nature of chemical bonding of corrugated graphene on Ru (0001) and Rh (111) by electronic structure calculations. *Surface Science*, 605(15-16):1360–1368, 2011.

[144] Ralph Koitz, Ari P Seitsonen, Marcella Iannuzzi, and Jürg Hutter. Structural and electronic properties of a large-scale moiré pattern of hexagonal boron nitride on Cu (111) studied with density functional theory. *Nanoscale*, 5(12):5589–5595, 2013.

[145] Martin Schwarz, Alexander Riss, Manuela Garnica, Jacob Ducke, Peter S Deimel, David A Duncan, Pardeep Kumar Thakur, Tien-Lin Lee, Ari Paavo Seitsonen, Johannes V Barth, Francesco Allegretti, and Willi Auwärter. Corrugation in the weakly interacting hexagonal-BN/Cu (111) system: Structure determination by combining noncontact atomic force microscopy and x-ray standing waves. *ACS Nano*, 11(9): 9151–9161, 2017.

[146] NI Verbitskiy, AV Fedorov, G Profeta, A Stroppa, L Petaccia, B Senkovskiy, A Nefedov, Ch Wöll, D Yu Usachov, DV Vyalikh, L V Yashina, Eliseev A A, T Pichler, and A Grüneis. Atomically precise semiconductorgraphene and hBN interfaces by Ge intercalation. *Scientific Reports*, 5:17700, 2015.

[147] Simon Berner, Martina Corso, Roland Widmer, Oliver Groening, Robert Laskowski, Peter Blaha, Karlheinz Schwarz, Andrii Goriachko, Herbert Over, Stefan Gsell, Matthias Schreck, and Greber Thomas Sachdev, HermaSachdev. Boron nitride nanomesh: Functionality from a corrugated monolayer. *Angewandte Chemie International Edition*, 46(27):5115–5119, 2007.

[148] SJ Haigh, A Gholinia, R Jalil, S Romani, L Britnell, DC Elias, KS Novoselov, LA Ponomarenko, AK Geim, and R Gorbachev. Cross-sectional imaging of individual layers and buried interfaces of graphene-based heterostructures and superlattices. *Nature Materials*, 11(9):764, 2012.

[149] Branden B Kappes, Abbas Ebnonnasir, Suneel Kodambaka, and Cristian V Ciobanu. Orientation-dependent binding energy of graphene on palladium. *Applied Physics Letters*, 102(5):051606, 2013.

[150] Qiang Zhang, Yuxuan Chen, Chendong Zhang, Chi-Ruei Pan, Mei-Yin Chou, Changgan Zeng, and Chih-Kang Shih. Bandgap renormalization and work function tuning in $MoSe_2$/hBN/Ru (0001) heterostructures. *Nature Communications*, 7:13843, 2016.

[151] V Swamy, Surendra K Saxena, Bo Sundman, and J Zhang. A thermodynamic assessment of silica phase diagram. *Journal of Geophysical Research: Solid Earth*, 99(B6): 11787–11794, 1994.

[152] Kristina Spektor, Johanna Nylen, Emil Stoyanov, Alexandra Navrotsky, Richard L Hervig, Kurt Leinenweber, Gregory P Holland, and Ulrich Häussermann. Ultrahydrous stishovite from high-pressure hydrothermal treatment of SiO_2. *Proceedings of the National Academy of Sciences*, 108(52):20918–20922, 2011.

[153] JI Pankove and ML Tarng. Amorphous silicon as a passivant for crystalline silicon. *Applied Physics Letters*, 34(2):156–157, 1979.

[154] V Zuzaniuk and R Prins. Synthesis and characterization of silica-supported transition-metal phosphides as hdn catalysts. *Journal Of Catalysis*, 219(1):85–96, 2003.

[155] F.C. Chuang, C.V. Ciobanu, V.B. Shenoy, C.Z. Wang, and K.M. Ho. Finding the reconstructions of semiconductors surfaces via a genetic algorithm. *Surface Science*, 573(2):L375–L381, 2004.

[156] C.V. Ciobanu and C. Predescu. Reconstruction of silicon surfaces: a stochastic optimization problem. *Physical Review B*, 70(8):085321, 2004.

[157] C.V. Ciobanu, V.B. Shenoy, C.Z. Wang, and K.M. Ho. Structure and stability of of the si(105) structure. *Surface Science*, 544(2-3):L715–L721, 2003.

[158] F.C. Chuang, C.V. Ciobanu, C. Predescu, C.Z. Wang, and K.M. Ho. Structure of si(114) determined by global optimization methods. *Surface Science*, 578(1-3):183–195, 2005.

[159] C.V. Ciobanu, F.C. Chuang, and D.E. Lytle. On the structure of the si(103) surface. *Applied Physics Letters*, 91(17):171909, 2007.

[160] C.V. Ciobanu, B.N. Jariwala, T.E.B. Davies, and S. Agarwal. Roughness and structural motifs on the si(103) surface. *Computational Materials Science*, 45(1):150–157, 2009.

[161] C.V. Ciobanu, C.Z. Wang, and K.M. Ho. Global optimization of 2-dimensional nanoscale structures: a brief review. *Materials and Manufacturing Processes*, 24(2): 109–118, 2009.

[162] C.V. Ciobanu, C.Z. Wang, and K.M. Ho. *Atomic structure prediction of nanostructures, clusters, and surfaces*. Wiley-VCH, 2013.

[163] T.L. Chan, C.V. Ciobanu, F.C. Chuang, N. Lu, C.Z. Wang, and K.M. Ho. Magic structures of h-passivated <110> silicon nanowires. *Nano Letters*, 6(2):277–281, 2006.

[164] N. Lu, C.V. Ciobanu, T.L. Chan, F.C. Chuang, C.Z. Wang, and K.M. Ho. The structure of ultrathin h-passivated [112] silicon nanowires. *Journal of Physical Chemistry C*, 111(22):7933–7937, 2007.

[165] R.M. Briggs and C.V. Ciobanu. Evolutionary approach for finding the atomic structure of steps on stable crystal surfaces. *Physical Review B*, 75(19):195415, 2007.

[166] T.E.B. Davies, D.P. Mehta, J.L. Rodriguez-Lopez, G.H. Gilmer, and C.V. Ciobanu. A variable-number genetic algorithm for growth of 1-dimensional nanostructures into their global minimum configuration under radial confinement. *Materials and Manufacturing Processes*, 24(3):265–273, 2009.

[167] Bing Yang, William E Kaden, Xin Yu, Jorge Anibal Boscoboinik, Yulia Martynova, Leonid Lichtenstein, Markus Heyde, Martin Sterrer, Radosław Włodarczyk, Marek Sierka, et al. Thin silica films on Ru (0001): monolayer, bilayer and three-dimensional networks of [SiO_4] tetrahedra. *Physical Chemistry Chemical Physics*, 14(32):11344–11351, 2012.

[168] Jonas Weissenrieder, Sarp Kaya, J-L Lu, H-J Gao, Shamil Shaikhutdinov, H-J Freund, Marek Sierka, Tanya K Todorova, and Joachim Sauer. Atomic structure of a thin silica film on a Mo(112) substrate: a two-dimensional network of SiO_4 tetrahedra. *Physical Review Letters*, 95(7):076103, 2005.

[169] Marek Sierka, Tanya K Todorova, Sarp Kaya, Dario Stacchiola, Jonas Weissenrieder, Junling Lu, Hongjun Gao, Shamil Shaikhutdinov, Hans-Joachim Freund, and Joachim Sauer. Interplay between theory and experiment in the quest for silica with reduced dimensionality grown on a Mo (1 1 2) surface. *Chemical Physics Letters*, 424(1-3): 115–119, 2006.

[170] Enlai Gao, Bo Xie, and Zhiping Xu. Two-dimensional silica: Structural, mechanical properties, and strain-induced band gap tuning. *Journal of Applied Physics*, 119(1): 014301, 2016.

[171] Michael N Blonsky, Houlong L Zhuang, Arunima K Singh, and Richard G Hennig. Ab initio prediction of piezoelectricity in two-dimensional materials. *ACS Nano*, 9(10): 9885–9891, 2015.

[172] Gaoxue Wang, GC Loh, Ravindra Pandey, and Shashi P Karna. Novel two-dimensional silica monolayers with tetrahedral and octahedral configurations. *The Journal of Physical Chemistry C*, 119(27):15654–15660, 2015.

[173] Yang Xue, Yun-Sheng Ye, Fang-Yan Chen, Hao Wang, Chao Chen, Zhi-Gang Xue, Xing-Ping Zhou, Xiao-Lin Xie, and Yiu-Wing Mai. A simple and controllable graphene-templated approach to synthesise 2d silica-based nanomaterials using water-in-oil microemulsions. *Chemical Communications*, 52(3):575–578, 2016.

[174] Xiaona Li, Jianwen Liang, Zhiguo Hou, Yongchun Zhu, Yan Wang, and Yitai Qian. Coordination complex pyrolyzation for the synthesis of nanostructured geo 2 with high lithium storage properties. *Chemical Communications*, 50(90):13956–13959, 2014.

[175] D Matioszek, W-S Ojo, A Cornejo, N Katir, M El Ezzi, M Le Troedec, Hervé Martinez, H Gornitzka, A Castel, C Nayral, et al. From rational design of organometallic precursors to optimized synthesis of core/shell Ge/GeO_2 nanoparticles. *Dalton Transactions*, 44(16):7242–7250, 2015.

[176] Pinshane Y Huang, Simon Kurasch, Anchal Srivastava, Viera Skakalova, Jani Kotakoski, Arkady V Krasheninnikov, Robert Hovden, Qingyun Mao, Jannik C Meyer, Jurgen Smet, David A Muller, and Ute Kaiser. Direct imaging of a two-dimensional silica glass on graphene. *Nano Letters*, 12(2):1081–1086, 2012.

[177] Torbjörn Björkman, Simon Kurasch, Ossi Lehtinen, Jani Kotakoski, Oleg V Yazyev, Anchal Srivastava, Viera Skakalova, Jurgen H Smet, Ute Kaiser, and Arkady V Krasheninnikov. Defects in bilayer silica and graphene: common trends in diverse hexagonal two-dimensional systems. *Scientific reports*, 3:3482, 2013.

[178] D. Kim, Y.H. Jin, K.W. Jeon, Kim S., Kim S.J., Han O.H., D.K. Seo, and J.C. Park. Blue-silica by eu2+ activator occupied in interstitial sites. *RSC Advances*, 5:74790–74801, 2015.

[179] P. Kroll. Modelling and simulation of amorphous silicon oxycarbide. *Journal of Materials Chemistry*, 13(7):1657–1668, 2003.

[180] Leonid Lichtenstein, Markus Heyde, Stefan Ulrich, Niklas Nilius, and Hans-Joachim Freund. Probing the properties of metal–oxide interfaces: silica films on mo and ru supports. *Journal of Physics: Condensed Matter*, 24(35):354010, 2012.

[181] Peter E Blöchl. Projector augmented-wave method. *Physical Review B*, 50(24):17953, 1994.

[182] D.C. Wallace. *Thermodynamics of crystals*. Wiley, New york, 1972.

[183] JF Nye. Physical properties of crystals: their representation by tensors and matrices. 1985.

[184] SS Chen, QH Li, YH Liu, and ZQ Xue. A meshless local natural neighbour interpolation method for analysis of two-dimensional piezoelectric structures. *Engineering Analysis with Boundary Elements*, 37(2):273–279, 2013.

[185] A Sakhaee-Pour. Elastic properties of single-layered graphene sheet. *Solid State Communications*, 149(1):91–95, 2009.

[186] Konstantin N Kudin, Gustavo E Scuseria, and Boris I Yakobson. C 2 f, bn, and c nanoshell elasticity from ab initio computations. *Physical Review B*, 64(23):235406, 2001.

[187] BT KeLly. Physics of graphite (applied science, london, 1981). *J. Tersoff, Phys. Rev. Lett*, 57:440, 1986.